DISTRIBUTED FORMATION CONTROL IN SWARM ROBOTICS

A thesis submitted to the University of Manchester
for the degree of Doctor of Philosophy
in the Faculty of School of Engineering

2023

Kefan Wu
Department of Electrical and Electronic Engineering

Contents

Word count 22693 (errors:4) words

List of Tables

List of Figures

The University of Manchester

Kefan Wu
Doctor of Philosophy
Distributed formation control in swarm robotics
November 28, 2023

Inspired by natural swarm collective behaviours such as colonies of bees and schools of fish, coordination strategies in swarm robotics have received significant attention in recent years. Distributed control on formation aims to coordinate a team of robots to form a desired geometric pattern through local information, which is a hot topic in swarm intelligence. The main objective of this thesis is to construct formation algorithms combined with bearing measurements for multi-robot systems and provide applications in real robotic scenarios.

First, we establish a basic formation framework based on edge and bearing measurements for networked multi-robot systems. The edge-based and bearing-based protocols are combined in controller design to maximise the advantages of both methods. We discuss the robustness of the mixed controller for both leaderless and leader-follower cases by Lyapunov approach. Simulation case studies are also presented to verify the effectiveness of the theoretical results.

Furthermore, a bearing-only collision-free formation coordination strategy is proposed for networked heterogeneous robots, where each robot only measures the relative bearings of its neighbours to achieve cooperation. Different from many existing studies that can only guarantee global asymptotic stability, a gradient-descent control protocol is designed to make the robots achieve a target formation within a given finite time. The stability of the multi-robot system is guaranteed via Lyapunov theory, and the convergence time can be defined by users. The exogenous disturbances in the system and actuator faults in the controller are also considered in convergence analysis. Then, the proposed finite-time bearing-only protocol is extended to linear time-invariant systems. Numerical simulations and lab-based experiments using unmanned ground vehicles are conducted to validate the effectiveness of these proposed strategies.

Moreover, we explore the bearing-only formation for nonlinear multi-agent systems. A compensation function is established in the controller to eliminate the effect of the unknown nonlinear items in the system. This compensation function is also based on bearing measurements, which ensures that the overall controller is bearing-only. By using the Lyapunov techniques, the formation tracking error will converge to zero exponentially under the proposed bearing-only algorithm. Moreover, we investigate the performance of the protocol for moving leaders, where the formation tracking error can be restricted in a bounded set. Finally, the simulation results are presented to validate the feasibility of the proposed algorithm for both fixed and moving leaders.

Finally, an SDP-based robust formation-containment coordination is proposed for swarm robotic systems with input saturation. A novel control protocol and an implementation algorithm are proposed that enable the leaders to achieve the desired formation via SDP techniques. The followers then converge into the convex hull formed by the leaders simultaneously. Both single-integrator dynamics and double-integrator

dynamics are considered in the controller design. We conduct the simulations to verify the formation-containment algorithm and analyse some of the factors that affected the formation-containment performance. The proposed algorithm is also applied to a real-world scenario by performing an experiment using multiple mobile robots.

Declaration

No portion of the work referred to in the thesis has been submitted in support of an application for another degree or qualification of this or any other university or other institute of learning.

Copyright Statement

i. The author of this thesis (including any appendices and/or schedules to this thesis) owns certain copyright or related rights in it (the "Copyright") and s/he has given The University of Manchester certain rights to use such Copyright, including for administrative purposes.

ii. Copies of this thesis, either in full or in extracts and whether in hard or electronic copy, may be made **only** in accordance with the Copyright, Designs and Patents Act 1988 (as amended) and regulations issued under it or, where appropriate, in accordance with licensing agreements which the University has from time to time. This page must form part of any such copies made.

iii. The ownership of certain Copyright, patents, designs, trade marks and other intellectual property (the "Intellectual Property") and any reproductions of copyright works in the thesis, for example graphs and tables ("Reproductions"), which may be described in this thesis, may not be owned by the author and may be owned by third parties. Such Intellectual Property and Reproductions cannot and must not be made available for use without the prior written permission of the owner(s) of the relevant Intellectual Property and/or Reproductions.

iv. Further information on the conditions under which disclosure, publication and commercialisation of this thesis, the Copyright and any Intellectual Property and/or Reproductions described in it may take place is available in the University IP Policy, in any relevant Thesis restriction declarations deposited in the University Library, and the University Library's regulations.

Abbreviations

MAS Multi-Agent Systems

MRS Multi-Robot Systems

UAV Unmanned Aerial Vehicle

LTI Linear Time-Invariant

SVD Singular Value Decomposition

SDP Semidefinite Programming

GD Gradient-Descent

FTBO Finite-Time Bearing-Only

Symbols

$\mathbb{R}$ Set of real numbers

$\mathbb{R}^+$ Set of positive real numbers

$\mathbb{R}^n$ Set of real vectors of dimension n

$\mathbb{R}^{m\times n}$ Set of real matrices of size $m \times n$

$\mathbf{0}_n$ A column vector of size n with all entries equal to zero

$\mathbf{0}_{m\times n}$ A $m \times n$ matrix with all zeros

$\mathbf{1}_n$ A column vector of size n with all entries equal to one

$\mathcal{G}$ Graph

$\mathcal{A}$ Adjacency matrix

$\mathcal{L}$ Laplacian matrix

$\mathcal{B}$ Bearing Laplacian matrix

H Incidence matrix of the oriented graph

$\mathbf{diag}\{x_1, \cdots, x_n\}$ A diagonal matrix with diagonal entries x_1 to x_n

$\mathbf{max}\{\cdot\}$ Maximum elements

$\mathbf{min}\{\cdot\}$ Minimum elements

$\|\cdot\|$ Euclidean norm of a vector or the spectral norm of a matrix

A^T Transpose of matrix A

A^{-1} Inverse of matrix A

I_n Identity matrix with n dimensions

$\otimes$ Kronecker product

$f : \mathbb{X} \to \mathbb{Y}$ Function f with domain $\mathbb{X}$ and range $\mathbb{Y}$

Publications

[1] **K. Wu**, J. Hu, Z. Ding, and F. Arvin, "Finite-Time Fault-Tolerant Formation Control for Distributed Multi-Vehicle Networks With Bearing Measurements," **IEEE Transactions on Automation Science and Engineering**, 2023.

[2] **K. Wu**, J. Hu, B. Lennox, and F. Arvin, "Mixed controller design for multi-vehicle formation based on edge and bearing measurements," **2022 European Control Conference (ECC)**, 1666-1671, London, UK, 2022.

[3] **K. Wu**, J. Hu, B. Lennox, and F. Arvin, "Finite-time bearing-only formation tracking of heterogeneous mobile robots with collision avoidance," **IEEE Transactions on Circuits and Systems II: Express Briefs**, 68(10), 3316-3320, 2021.

[4] **K. Wu**, J. Hu, B. Lennox, and F. Arvin, "SDP-based robust formation-containment coordination of swarm robotic systems with input saturation," **Journal of Intelligent & Robotic Systems**, 102, 1-16, 2021.

[5] **K. Wu**, J. Hu, Z. Ding, and F. Arvin, "Distributed Bearing-Only Formation Control for Heterogeneous Nonlinear Multi-Robot Systems," **IFAC World Congress 2023**.

[6] **K. Wu**, J. Hu, Z. Li, Z. Ding, and F. Arvin, "Distributed Collision-Free Bearing-Based Coordination in Multi-UAV Networks with Actuator Faults and Time Delays," Submitted to **IEEE Transactions on Intelligent Transportation Systems**.

Acknowledgements

First of all. I would like to express my great thanks to my supervisor Dr. Farshad Arvin, for his continuous support and friendly help during my Ph.D. study. Dr. Arvin is a top academic in the field of swarm robotics who provided professional guidance for me over the past three years. In my mind, he is also an outstanding teacher with responsibility and patience. It is my great honour to be a Ph.D. student under his supervision.

I would also like to thank my supervisor Prof. Zhengtao Ding for his supervision in the theoretical part. Prof. Ding is a true master in the field of control systems who reaches a very high level in control theory. I always feel confident about my publication after discussing with him.

I am also very grateful to Dr. Junyan Hu who gave me many great suggestions for my research. Besides, I also thank all my friends and colleagues in Control System Group and Robotic Group.

Last but not least. I owe my deepest appreciation to my family, especially my father Zulei Wu, and my mother Zhouqing Xia, for their continuous unconditional love and support throughout my life.

To my beloved mother and father

Chapter 1

Introduction

1.1 Background and Motivation

Swarm robotics mainly focuses on coordination control mechanisms within a group of homogeneous or heterogeneous robots by following collective and decentralised decision-making approaches inspired by nature [3]. There are many swarm behaviours such as aggregation [4], foraging [5], collective motion and flocking [6], all of which have been successfully implemented using real mobile robots. There are also many potential real-world applications for swarm robotic systems, such as self-assembly [7], autonomous shepherding [8], exploration of unknown environments [9]. Moreover, swarm robotics is able to be implemented in agriculture [10, 11]. Fig.1.1 illustrates a scenario in precision agriculture by using the formation-containment approach in swarm systems. All these applications require carefully designed controllers to deal with the limitations imposed by the physical environments.

Formation in swarm robotics refers to the coordinated arrangement of individual robots within a swarm to achieve a desired spatial configuration or pattern. The concept of formation control draws inspiration from natural phenomena, such as bird flocks, fish schools, and insect swarms, where individual entities align and maintain relative positions to exhibit collective behaviours. Cooperative formation control for multi-robot systems (MRS) involves designing algorithms and control strategies that enable the robots to organise themselves spatially while performing a task. This technique can be implemented in many scenarios. For example, in surveillance and monitoring tasks

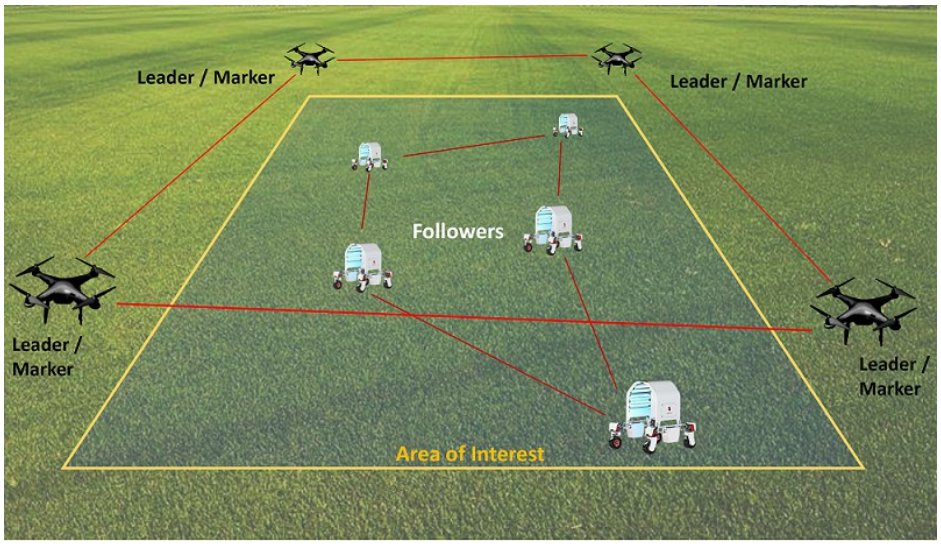

Figure 1.1: A scenario in precision agriculture where leaders mark an area of interest using formation control. Followers then directly interact with plants, and follow the formation-containment algorithm.

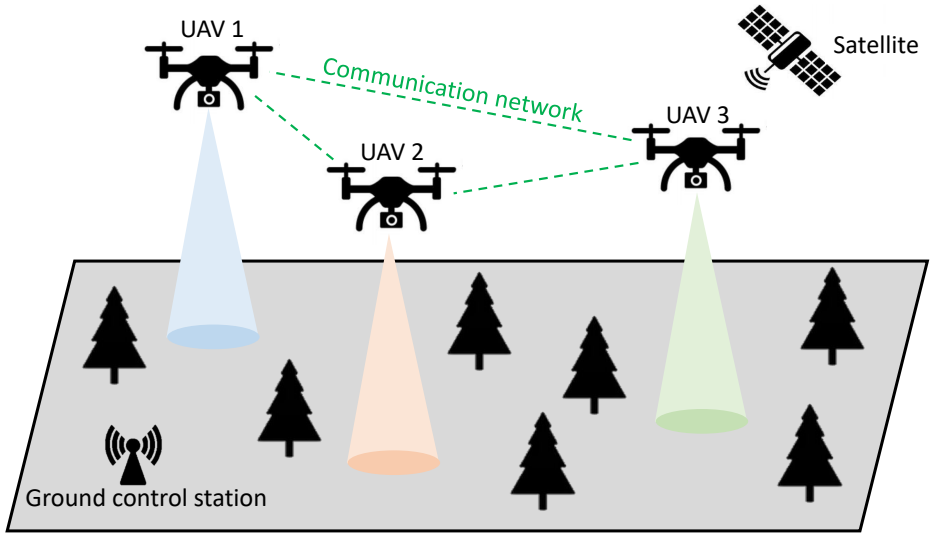

Figure 1.2: A cooperative target search task using three networked UAVs in the forest.

[12], robots can form patterns to cover a given area effectively. In search and rescue missions [13], the formation can be used to explore hazardous or inaccessible regions collaboratively. In autonomous vehicle platooning [14], the formation can optimise coordination and synchronisation among robots for tasks like assembly or transportation. An illustrative example is shown in Fig. 1.2, where a network of unmanned aerial vehicles (UAVs) are performing a cooperative target search mission in the forest environment by maintaining a triangle formation.

The traditional way to tackle the distributed formation problem is based on position measurements. Position-based formation protocol focuses on regulating the relative positions between neighbouring robots rather than relying on global or absolute coordinate systems. Each robot determines its position with respect to its neighbouring robots or a reference point in the formation [15]. This approach enables scalability as robots can adapt to changes in swarm size without relying on a centralised global coordinate system. As an example, the authors in [16] discussed the scalability of the formation algorithm for multi-UAV systems. However, as the swarm grows larger, the complexity of maintaining the desired formation pattern and ensuring coordination among a large number of robots can become more demanding. To overcome such limitations, the research in formation-containment control has attracted increasing attention over the past decade. The robots can be divided into leaders and followers. The formation-containment protocol enables the leaders to form a desired configuration, and simultaneously, the followers converge to the convex hull spanned by the leaders. Fig.1.1 illustrates an application of the formation-containment protocol in agriculture.

Another limitation of the position-based method is that it heavily relies on accurate perception and sensing of neighbouring robots' positions, which requires high-quality sensory outputs that may not be easily fulfilled in extreme environments. Hence, bearing-only formation control is proposed to deal with such issue. Only the neighbouring bearings of robots are required to realise the desired goal by implementing bearing-only protocols. During the hardware implementation, the bearing information can be detected by wireless vision-based sensors [17]. It is noticeable that exchanging signal may not accessible because the camera is a passive sensor [18]. Whereas, the relative bearing of the robot is a unit vector generated from a relative position vector by normalising its length, which can be obtained the onboard cameras based on vision-based techniques [19, 20]. Therefore, the design of bearing-only control shows the promising capacity to achieve multi-robot formation tasks by using onboard sensors. Some preliminary results on bearing-based formation such as bearing rigidity theory have been developed in the last decade. Nevertheless, there are still many issues to be considered when implementing bearing-only formation control techniques

on real-world MRS, e.g., dealing with nonlinear dynamics to ensure the convergence and stability of the whole system.

Another important indicator of performance is the settling time of the cooperation task. As a result, the finite-time control techniques (see [21–23] and the references therein) have been extensively explored in multi-agent systems (MAS). A typical method to deal with the finite-time convergence is based on signum functions. The finite-time protocols proposed in [24–26] were based on this approach. However, the convergence time is affected by the initial states. The authors in [27–29] further explored fixed-time strategies, where the settling time is independent to the initial state. Nevertheless, the designed control inputs are not smooth as they contain signum functions and fractional power feedback. Besides, in order to provide reliable performance in real-world applications, the uncertainties such as unknown disturbances and actuator faults in the robot dynamics should also be taken into consideration. In other words, how to design finite-time bearing-only (FTBO) formation control with smooth control inputs, exogenous disturbances, and actuator faults remains an open problem.

1.2 Thesis Organisation

This thesis is organised as follows:

Chapter 2: Literature Review and Main Objectives

In this chapter, we first introduce some previous works related to traditional formation techniques, cooperative formation-containment protocols, and bearing-based coordination techniques. After that we list the main objectives of the thesis

Chapter 3: Preliminaries

In this chapter, some related preliminaries including matrix theory, graph theory, bearing measurement, and Lyapunov stability theory are introduced.

Chapter 4: Basic Formation Framework Based on Bearing Measurements

In this chapter, a basic formation framework based on edge and bearing measurements is proposed for networked MRS. Although conventional edge-based controllers have been widely used in many formation tasks, the tracking accuracy may not be guaranteed in some extreme environments as it depends on the quality of the sensors and requires the exact position data of each robot. To overcome this limitation, we combine the edge-based controller with a bearing-based method where only relative bearings among the robots are required. Depending on the sensing-ability of the robotic platform, this mixed control method can provide an efficient solution to maximise the tracking performance. Both leaderless and leader-follower cases are considered in the protocol design. The stability of the networked MRS under the proposed mixed formation approach is ensured by Lyapunov theory. Finally, we present simulation results to verify the effectiveness of the theoretical results.

Chapter 5: Finite-Time Bearing-Only Formation Control

This chapter addresses a bearing-only formation tracking problem in robotic networks. In contrast to traditional position-based coordination strategies, the bearing-only coordinated movements of the robots only rely on the neighbouring bearing information. This feature can be utilised to reduce the sensing requirements in the hardware implementation. A GD protocol is first developed to achieve the desired coordination within a prespecified settling time. After that, the unknown disturbances are considered in the robotic dynamics, and then the bound of formation tracking error is guaranteed by the Lyapunov approach. In case of damage to the actuators (e.g., motors) in some of the robots during the task, fault-tolerant analysis of the proposed controller is provided to ensure the success of the task in extreme environments. Finally, numerical simulations and lab-based experiments using unmanned ground vehicles are conducted to validate the effectiveness of the proposed strategy.

Chapter 6: Formation-Containment Protocol and Application

In this chapter, formation-containment controller design for single-integrator and double-integrator swarm robotic systems with input saturation is investigated. The swarm system contains two types of robots – *leaders* and *followers*. A novel control protocol and an implementation algorithm are proposed that enable the leaders to achieve the

desired formation via semidefinite programming (SDP) techniques. The followers then converge into the convex hull formed by the leaders simultaneously. In contrast to conventional consensus-based formation control methods, the relative formation reference signal is not required in real-time data transmission, which provides greater feasibility for implementation on hardware platforms. The effectiveness of the proposed formation-containment control algorithm is demonstrated with both numerical simulations and experiments using real robots that utilise the miniature mobile robot, Mona.

Chapter 7: Conclusion

This chapter summarises the thesis and discusses future research.

Appendix A: Extension of the FTBO protocol to the LTI Systems with Exogenous Disturbance

In this appendix, we further explore the robustness of the finite-time bearing-only protocol for the LTI systems with exogenous disturbances, which can be applied to a wider range of robotic platforms.

Appendix B: Bearing-Only Formation Control for Nonlinear Systems

In this appendix, we address the bearing-only formation tracking problem for heterogeneous nonlinear MRS. In contrast to position and distance-based formation algorithms, the robots can only measure the bearing information from their neighbours to achieve cooperation while the state information is unavailable. This characteristic is able to be implemented in the hardware to reduce the requirements of the sensors. We construct a compensation function in the proposed controller to eliminate the effect of the unknown nonlinear terms in the system. This compensation function is also based on bearing measurements, which guarantees that the overall controller is bearing-only. The stability of the proposed formation tracking strategy can be ensured by Lyapunov techniques. Moreover, we analyse the performance of the protocol for moving leaders, where the formation tracking error can be restricted in a bounded set. Finally, the simulation results are presented to validate the feasibility of the proposed algorithm for both fixed and moving leaders.

Chapter 2

Literature Review and Main Objectives

2.1 Literature Review

2.1.1 Traditional Formation Techniques

Formation in robotic networks has received great attention from robotics and automation communities. Motivated by commonly observed collective behaviours of animals, distributed control on formation tasks aims to coordinate a team of unmanned vehicles to form a desired geometric pattern through local information [30]. During the past decade or so, many control mechanisms have been proposed, and valuable results have been obtained that relate to formation control in swarm systems. Among all the distributed formation control methods proposed in the last decade, one of the major approaches to deal with multi-robot formation problems is based on position measurement [31]. As an example, a cooperative control was proposed in [32] for vehicle formation. The authors used algebraic graph theory to model the communication network and then related its topology to formation stability. The eigenvalues of the graph Laplacian matrix were used to prove the Nyquist criterion to determine the effect of the communication topology on formation stability. The results showed that the information flow can thus be rendered highly robust to changes in the graph, enabling tight formation control despite limitations in intervehicle communication capability. The distributed motion coordination among a group of nonholonomic ground robots

was studied in [33]. The authors used a consensus approach to design vision-based control laws for parallel and balanced circular formations. These control protocols were distributed in the sense that they require information only from the neighbours. In [34], the problem of distributed and global stabilisation of rigid formations in the plane for a group of mobile agents was studied. The authors proposed a constructive perturbation method with the conventional gradient control law. They also proved that the control protocol stabilised the desired rigid formation in a global sense for all initial conditions except the case when a pair of communicating agents happened to have the same initial location. Lin et al. in [35] proposed a distributed formation law via complex Laplacian matrix. After that, the authors in [36] discussed the formation problem for leader-follower networks with variable formation size. A complex Laplacian-based method was used to describe the shape of the formation. In [37], the formation-keeping issue was considered for a group of autonomous agents in their local coordinates. The rooted graphs were adopted in the controller design. The formation protocol for the double-integrator swarm system was discussed in [38]. A consensus-based approach was utilised in formation design. The authors also presented the necessary and sufficient conditions for the multi-UAV systems to achieve time-varying formations. Both simulation and experiment were provided to validate the main results. Based on their proposed method, multiple leaders and switching interaction topologies were considered in [39] and [40], respectively. Moreover, Rao et al. in [41] proposed a phase-based formation protocol for self-propelled vehicles. A distributed estimation and formation control problem was addressed in [42] with guaranteed performance. Hu et al. in [43] investigated the cooperative control of heterogeneous vehicle platoons using the adaptive formation control technique. Automatic cruise control was achieved via vehicle-to-vehicle communication. Bio-inspired formation control for UAV swarms was analysed in [44], where multiple leaders and switching topology were considered in the control system design. Another standard way to solve the formation issue is based on distance measurements. For example, Distance-based formations for multiple robot localisation in MAS were studied in [45]. The authors proposed distributed formation control for multi-vehicle systems. The control was derived from a potential function based on an undirected infinitesimally

rigid graph that specifies the target formation. A sufficient condition for local asymptotical stability of the equilibrium manifold was studied in this paper. They also pointed out the drawbacks of the method – it assumes two-way sensor capability of the robots. The simulation results also showed that the theory can be only applied to undirected sensor graphs not to more general directed sensor graphs. In another work, distance-based multi-robot formation control was explored in [46] by utilizing the goal assignment. The authors in [47] developed nonlinear gradient control laws for nonlinear MRS with distance-based formation. This work investigated the relationship between the cycle space of the formation graph and the resulting equilibria of cyclic formations.

It is noticeable that the uncertainties (such as disturbance, actuator faults, etc.) in the system could not be ignored when considering the formation design. For instance, in [12], a distributed, adaptive, and nonlinear control protocol was proposed to achieve the group formation tracking for linear MAS having a directed communication topology with uncertainties. The control protocol used only relative state information and, thus, avoids direct computation of the graph Laplacian matrix. The results can be applied in swarm robotics, especially in multi-target surveillance operations where the targets (considered as leaders) may be placed far apart and sometimes the targets may keep on changing their positions due to an external disturbance. Robust formation control of MAS with uncertain dynamics was analysed in [48], where the leader's nonzero control input was also considered in the controller design. Distributed formation law for unmanned underwater vehicles was studied in [49] and this protocol is robust to disturbances and parametric uncertainties in the system. In another study, Hu et al. [50] proposed a novel formation control protocol for multiple mobile robots based on negative imaginary dynamics with modelling uncertainties. The article [51] has laid a major contribution in the area of fault-tolerant formation control design, where an event-triggered control scheme was developed for autonomous surface vehicles under malicious attacks. A fault-tolerant formation protocol was proposed for wheeled mobile robots in [52]. The authors in [53] employed the radial basis function neural networks and sliding-mode PID controller to deal with the fault-tolerant issue for heterogeneous vehicular platoons.

Safety is another significant indicator for multi-robot tasks. Hence, the obstacles and collision issues should also be taken into consideration during the formation process. As an example, a semianalytic approach was proposed in [54] to address the collision-free formation reconfiguration issue. In [55], a connectivity-preserving controller was developed to tackle the collision-free formation problem for nonholonomic-wheeled mobile robots. Liu et al. [56] studied collision-avoidance formation law for elliptical agents with dynamic mapping. In [57], the fuzzy formation problem was considered for swarm robotic cyber-physical systems. A robust orthogonal firefly algorithm was implemented to achieve collision-free formation. The collision-free formation tracking problem with communication constraints for second-order MAS was explored in [58]. The authors designed a potential function-based mechanism in formation protocol to avoid collision between agents. In another research, the authors in [59] investigated formation tracking problems in complex obstacle-laden environments. A built-in obstacle avoidance mechanism based on repulsive potentials was applied in the controller to deal with the collisions. Sui et al. in [60] utilised the deep reinforcement learning method to deal with collisions during the formation task.

The settling time of the cooperation task is also an important performance indicator. Therefore, the finite-time control techniques have been extensively explored in MAS (see [61–65] and the references therein). A distributed finite-time protocol was designed in [66] for quadrotor formation. In [67], a novel adaptive fuzzy fast finite-time formation strategy was developed for second-order MAS. The finite time rigidity-based formation issue was considered in [68]. The authors first designed a distributed velocity estimator to estimate the desired group velocity in finite time. After that, a finite-time formation manoeuvring controller is proposed for each agent to achieve the target formation in finite time. In another work, a finite-time formation algorithm was proposed in [69] for marine surface vehicle formation. In [70], the constraints of the sensors were taken into consideration for nonholonomic multi-robot formation. A finite-time vision-based formation tracking protocol was proposed for each robot to meet the requirements of visibility and performance constraints. H^{∞} time-varying formation tracking problem was studied in [71] for heterogeneous nonlinear MAS. Two kinds of distributed finite-time observers are designed for each follower. However, in

the aforementioned literature, the convergence time is related to the initial state of each agent. Hence, the research on fixed-time formation [72–75] has also attracted much attention in the past decade. A fixed-time formation protocol was proposed in [65] for MRS. Both simulation and experiment were displayed to verify the theoretical results. In [76], a fixed-time leader-follower formation algorithm was developed for autonomous underwater vehicles with an event-trigger scheme. The authors in [77] studied the formation tracking problem for wheeled mobile robots with prescribed performance. A novel fixed-time protocol was presented to achieve the formation tracking. A fast fixed-time formation tracking algorithm was designed in [78] for networked autonomous surface vehicles. The settling time is independent of the initial conditions in these works. However, the designed control inputs are not smooth as they contain signum functions and fractional power feedback. How to generate a smooth formation protocol with a prescribed settling time remains an open problem.

2.1.2 Cooperative Formation-Containment Protocols

In the existence of multiple leaders, the containment problem should be analysed where the followers can move into the convex hull formed by the states of the leaders. For example, in [79], a hybrid stop-go control strategy was discussed. The authors developed a hybrid Stop-Go policy for the leaders in a multi-agent containment scenario by exploiting the theory of partial difference equations. They also analysed the Non-Zenoness, liveness and convergence of the resulting system. The results illustrated that the followers in a connected interaction graph will always converge to locations in the leader-polytope for stationary leaders. In another study, the authors in [80] explored a distributed containment control for double-integrator systems with both stationary and dynamic leaders. For moving leaders, the author also considered two cases – leaders with an identical velocity and leaders with nonidentical velocities. They proposed several distributed containment algorithms for each scenario. Furthermore, a finite-time containment control under a fixed directed network topology was also proposed in this research. Both simulation and experimental results on a multi-robot platform showed the effectiveness of the theoretical results. In [81, 82], directed interaction topologies in containment problem were considered for high-order LTI systems. The time delays in a swarm system were studied in [83], and containment analysis and

design problems for high-order LTI singular swarm systems with time delays on directed graphs were discussed. The authors presented a sufficient condition to achieve containment for a time-delayed singular swarm system by linear matrix inequality. Then, containment problems were converted into the asymptotically stable problems of multiple low-dimensional time-delayed systems. They also proposed changing variable methods to determine the gain matrix in the protocols. The simulation results showed the effectiveness of the theoretical results. In [84], the model-free containment problem was investigated for MAS. A distributed containment protocol was proposed based on reinforcement learning method. Moreover, the time-vary actuator faults were also considered and a fault-tolerance controller was design to compensate for the influence of actuator faults. In another work, a double constrained containment protocol was designed for smart manufacturing in [85]. The authors developed a cloud decision-making center in the three-layer control framework to realise collaborative manufacturing. Both nonlinearities and velocity constraints were considered in the controller design. The authors in [86] explored the fixed-time containment problem for stochastic nonlinear MAS with event-trigger scheme. Based on e back-stepping technique and adaptive fuzzy protocol, the containment errors can converge to zero in fixed-time. Furthermore, the predefined-time containment issue was explored in [87]. In [88], a novel distributed bipartite containment control law was designed for high-order nonlinear MAS. The unknown and time-varying powers in the systems was also taken into the consideration. The bipartite containment observer and dynamic gain compensator were designed to tackle such issue. The authors in [89] discussed adaptive containment strategy for second-order nonlinear MAS with external disturbances. A fully distributed containment protocol was designed without global information. Furthermore, the proposed controller was independent to the bound of the disturbances. In other work, the adaptive bipartite containment issue was addressed for the nonaffine fractional-order MAS in [90]. A neural network approach was develop in the controller design to estimate the ideal input signal.

It was assumed that there was no interaction between the leaders in the aforementioned research studies. However, it is possible for the leaders to transmit information

to other leaders to accomplish complex tasks, like formation control in real-world scenarios, such as agri-robotics. In these applications, it is desired that not only the followers can converge to the convex hull spanned by the leaders, but the leaders can also converge to the desired formation, which is formed as formation-containment problems [91]. In [92, 93], formation-containment problems for first-order swarm systems with undirected interaction topologies and switching interaction topologies were studied. Hu et al. in [2] established adaptive formation-containment algorithms were proposed to coordinate multiple mobile robots. In another work, the authors in [94] proposed the formation-containment protocols for leaders to reach the predefined time-varying formation and followers to converge to the convex hull formed by the states of leaders. Then, they transformed the formation-containment into asymptotic stability problems and presented the sufficient conditions for swarm systems to achieve formation containment. They also proposed the necessary and sufficient conditions for swarm systems to achieve containment and time-varying formation. The simulation results showed the effectiveness of the theoretical results. After that, output formation-containment analysis problems for swarm systems with high-order linear dynamics and directed topologies were studied in [95]. In [96], a distributed adaptive finite-time control solution to the formation–containment problem for multiple networked systems with uncertain nonlinear dynamics and directed communication constraints was studied. The authors integrated the special topology feature of the new constructed symmetrical matrix to deal with the technical difficulty in the asymmetrical Laplacian matrix under single-way directed communication. They established an adaptive distributed control scheme for leaders by fractional power feedback of the local error and a distributed adaptive control scheme which was independent to leaders for followers to ensure that the system can achieve the formation-containment in finite time. The simulation results showed the effectiveness of our control protocols. In [97], The authors discussed time-varying group formation-containment problem for linear MAS with unknown control input. The formation leaders can follow the trial of the tracking leaders with unpredictable trajectories to reach the target formation, and then the followers converge to the convex hull spanned by leaders. In another work, the satellite formation-containment problem was studied in [98]. Both collision avoidance and bounded uncertainty suppression were taken into consideration. The

time-varying output formation-containment was addressed in [99]. The formation-containment protocol were designed for both homogeneous and heterogeneous MAS. In [100], a data driven formation-containment protocol was developed for multiple spacecrafts with switching topology. A distributed observer was designed to decrease the affect of the switching topology. Based on reinforcement learning approach, the optimal strategy can be generated through relative motion data and system inputs. The adaptive observer-based formation-containment issue was discussed in [101]. The proposed controller was able to deal with the undesirable chattering from the tracking leader's nonzero input. In another research, the adaptive fixed-time fuzzy formation-containment protocol was designed in [102] for Euler-Lagrange systems. However, in the aforementioned works, the formation reference signal from the neighbours was required before designing the control protocol, which means that some global information is required. Hence, the formation-containment objectives cannot be achieved by only using range & bearing sensors in a real implementation, such as [103].

2.1.3 Bearing-Based Coordination Techniques

In the aforementioned research studies, one of the constraints is that the relative position between every neighbouring robot should be detectable, which requires high-quality sensors in real-world implementations. Hence, the tracking accuracy of this method may not be guaranteed in some extreme environments. To overcome these limitations, bearing-only control techniques have been explored by researchers in recent years (see [104–106]). Only the neighbouring bearings of vehicles are required to realise the desired goal by implementing bearing-only protocols. During the hardware implementation, the bearing information can be detected by wireless vision-based sensors [107, 108]. Therefore, the design of bearing-only control shows the promising capacity to achieve multi-vehicle formation tasks by using onboard sensors. There are two main methods in bearing-only cooperative control, the first is controlling the bearing angles. In this regard, the distributed bearing-only triangular formation control of three mobile agents moving in the plane was discussed in [109]. They proposed the control laws using only the locally measured bearings and established a convergence result that guarantees global asymptotic convergence of the formation to the desired

formation shape. The simulation results showed the effectiveness of our control protocols. The second strategy is coordinating the bearing vectors [110, 111]. The authors in [112] focused on the problem of bearing-based network localisation, which aims to localise all the nodes in a static network given the locations of a subset of nodes termed anchors and inter-node bearings measured in a common reference frame. The bearing Laplacian matrix was proposed to guarantee the uniqueness of the target formation up to a global translation, rotation, and scaling of the agents' positions, which is a strong method to verify whether the target formation is infinitesimally bearing rigid and then examine the uniqueness of the target formation. In [113], the controller synthesis problem for distributed bearing-only formation control was studied. The author proposed the gradient-descent bearing-only control laws, which is favourable from the stability analysis point of view. These protocols allowed proof of global asymptotic convergence, and extensions for including distance measurements, leaders and collision avoidance. They also provided simulations and comparisons with other state-of-the-art algorithms to verify the effectiveness of their strategies. Zhao et al. in [114] studied the problem of bearing-only formation tracking control in MAS. The authors proposed new bearing-only formation control protocols to i) various dynamics of the system, including single-integrator, double-integrator, and unicycle models, and ii) moving target formation. Compared to the position measurement, The proposed control laws can minimise the requirements on the sensing ability of the agents, which is an important step towards the application of bearing-only formation control in practical tasks. They also discussed the sophisticated collision avoidance strategies in the system. The simulation and real experimental results showed the effectiveness of the theoretical results. Since exogenous disturbances may appear in the dynamics of the vehicles, the coordination problems become more challenging. , An integral term was also introduced in [114] in the protocol to handle the exogenous disturbance. In another work, the bearing-only formation control in the presence of the exogenous disturbance was considered in [115]. The authors designed the gradient-descent bearing-only formation protocol with the exogenous disturbance for an undirected formation topology in an arbitrary dimensional space. They presented the robust stability analysis by Lyapunov approach and showed that the formation error can exponentially converge to a bounded set with bounded exogenous disturbance. The numerical simulation example

was also provided to verify the effectiveness of the algorithm. In the follow-up study [116], the upper bound of the tracking error was computed and then the correlation between system factors was discussed. However, in the aforementioned works, only global asymptotic stability can be ensured, which means that the target geometric pattern cannot be formed within a finite time period.

It is noticeable that convergence time is also a significant performance indicator in formation tasks. Hence, the finite-time control protocols have also been widely discussed in the bearing-based formation (see [117–119] and the references therein). The authors in [120] proposed a finite-time protocol for cyclic formation based on bearing measurements. In [118], two types of bearing-only formation laws were designed to achieve the target formation in finite time. In another work, the authors in [121] develop the FTBO scheme based on global orientations estimation. Chen et al. in [122] discussed the finite-time circumnavigation issue by implementing a bearing-only approach. However, the finite time is related to initial states and the control input may not be smooth because such controllers contain fractional power feedback and signum functions. In [1]. The authors proposed the bearing-only formation protocol to achieve target formations in finite time for both leaderless and leader-follower cases. Unlike using the signum functions to suppress relative bearing errors, the convergence time is all determined by initial conditions. Under such control laws, the convergence time can be arbitrarily chosen by users and the derivative of the control input is continuous. The simulation and real experimental results showed the effectiveness of the theoretical results. After that, the authors in [123] designed a bearing-only protocol for second-order systems with predefined convergence time. In the above works, a time-varying scaling function was applied in the controller to ensure that the settling time can be selected by our users.

2.2 Main Objectives

Motivated by the advancements and challenges in formation problems. In this thesis, we aim to develop several advanced formation algorithms based on bearing measurements and formation-containment protocols with application to real robotic platforms. The main objectives of the thesis can be summarised as:

Objective 1: Basic Bearing-Based Formation for Linear Systems:

- Constructing a formation framework based on edge and bearing measurements.
- Exploring the stability of the controller for leaderless and leader-follower cases.
- Running the simulations in Matlab.

Objective 2: Finite-Time Bearing-Only Formation for Linear Systems:

- Proposing a gradient-descent (GD) bearing-only formation strategy with predefined settling time.
- Presenting a sufficient condition to avoid the collisions between each robot.
- Discussing the robustness of FTBO protocol with exogenous disturbances and actuator faults.
- Extending the results to linear time-invariant (LTI) system.
- Running the simulations in Matlab and implementing the algorithm to Mona robots.

Objective 3: Bearing-Only Formation for Nonlinear Systems:

- Developing a novel compensation function based on bearing measurements to deal with the nonlinearity.
- Discussing the stability of the controller for fixed and moving leaders.
- Running the simulations in Matlab.

Objective 4: Formation-Containment Protocol and Application:

- Designing new formation-containment protocols for single-integrator and double-integrator systems.
- Verifying the robustness of formation-containment protocol with input saturation.
- Running the simulations in Matlab and implementing the algorithm to Mona robots.

To sum up, four objectives are studied in this thesis. Objective 1 aims to study the basic bearing-based formation for linear systems, a formation framework is established in this work. Then, we consider the settling time in Objective 2. This objective aims to explore the finite-time bearing-only formation for linear systems. We propose a GD bearing-only protocol with predefined settling time and discuss the robustness of the FTBO strategy with exogenous disturbances and actuator faults. Moreover, the nonlinearity is considered in Objective 3. We design a novel compensation function based on bearing measurements to deal with the nonlinearity, and the designed controller is still bearing-only. Finally, we focus on the formation-containment protocol and application in Objective 4. The novel formation-containment algorithms are developed and implemented in Mona robots in this work.

Chapter 3

Preliminaries

3.1 Matrix Theory

In this section, we give the basic definition and some properties of the Kronecker product that will be used throughout the thesis.

Definition 3.1. *[124] The Kronecker product of matrices $P \in \mathbb{R}^{j\times k}$ and $Q \in \mathbb{R}^{m\times n}$ is defined as*

$$P \otimes Q = \begin{bmatrix} p_{11}Q & \cdots & p_{1m}Q \\ \vdots & \ddots & \vdots \\ p_{j1}Q & \cdots & p_{jk}Q \end{bmatrix} \in \mathbb{R}^{np\times mq},$$

and it has following properties:

$$P \otimes (Q + S) = P \otimes Q + P \otimes S$$
$$(cP) \otimes Q = P \otimes (cQ) = cP \otimes Q$$
$$(R \otimes S)(Q \otimes Z) = RQ \otimes PS$$
$$(P \otimes Q)^{-1} = P^{-1} \otimes Q^{-1}$$
$$(P \otimes Q)^{T} = P^{T} \otimes Q^{T}$$

where W, P, Q, and Z are the matrices with compatible dimensions for multiplication.

3.2 Graph Theory

Considering n networked mobile agents (which include n_l leaders and n_f followers) in $\mathbb{R}^d$ ($n \geq 2$, $d \geq 2$ and $n_l + n_f = n$). Denote the position of the ith agent as p_i. The

configuration of the agents can be denoted as $p = \mathrm{col}(p_1, \cdots, p_n)$. Let the undirected graph $\mathcal{G} = (\mathcal{V}, \mathcal{E})$ denote the communication among the agents. $\mathcal{V}_l = \{v_1, \ldots, v_{n_l}\}$ denoted leaders' set, and $\mathcal{V}_f = \{v_{n_l+1}, \ldots, v_n\}$ denotes followers' set, respectively, and $\mathcal{V} = \mathcal{V}_l \cup \mathcal{V}_f$. The edge set is denoted by $\mathcal{E} \subseteq \mathcal{V} \times \mathcal{V}$. The edge $(i, j) \in \mathcal{E}$ indicates that agent i can obtain the relative bearing from agent j, such that agent j is a neighbour of i. Let $\mathcal{N}_i = \{j \in \mathcal{V} : (i, j) \in \mathcal{E}\}$ be the neighbor set of agent i. Since the graph is undirected, we have $(i, j) \in \mathcal{E} \Leftrightarrow (j, i) \in \mathcal{E}$. The adjacency matrix of $\mathcal{G}$ can be written as $\mathcal{A} = [a_{ij}] \in \mathbb{R}^{n \times n}$, where $a_{ij} > 0$ if $(i, j) \in \mathcal{E}$ and $a_{ij} = 0$, otherwise. Hence, the Laplacian matrix of $\mathcal{G}$ can be defined as $\mathcal{L} = \mathcal{D} - \mathcal{A}$, where $\mathcal{D} = \mathrm{diag}\{\mathrm{d}_{11}, \cdots, \mathrm{d}_{\mathrm{nn}}\} \in \mathbb{R}^{\mathrm{n} \times \mathrm{n}}$ and $d_{ii} = \sum_{j \neq i} a_{ij}$. It is obvious that $\mathcal{L}$ is positive semi-define for undirected topology and $\mathcal{L}\mathbf{1}_n = 0$, where $\mathbf{1}_n = [1, \cdots, 1]^\top$ [125].

3.3 Basic Notations

In this section, we introduce some basic notations about formation scale and bearing measurements.

3.3.1 Formation Scale

Definition 3.2. *The scale of the formation in the system is defined as*

$$\boldsymbol{s}(t) = \sqrt{\frac{1}{n}\sum_{i=1}^{n} \|p_i(t) - \bar{p}(t)\|^2} = \frac{\|p(t) - \boldsymbol{1}_n \otimes \bar{p}(t)\|}{\sqrt{n}} ,$$

where $\bar{p}(t) = \frac{1}{n}(\boldsymbol{1}_n \otimes I_d)^\top p(t)$ *denotes the centroid of the formation.*

We note that it is complicated to analysis the stability of the formation system with increasing formation scale. Hence, we should propose the assumption to ensure the boundness of the formation scale for later stability analysis in some cases.

3.3.2 Bearing Measurements

The relative *edge vector* and *bearing vector* of p_j with respect to p_i can be defined as

$$e_{ij} := p_j - p_i, \quad g_{ij} := \frac{e_{ij}}{\|e_{ij}\|} ,$$

where $\|\cdot\|$ denotes the Euclidean norm of a vector or the spectral norm of a matrix. The spectral norm of the matrix $A \in \mathbb{R}^{n\times n}$ is defined as $\|A\| = \sqrt{\lambda_{\max}(A^T A)}$, where $\lambda_{\max}(\cdot)$ represents the maximum eigenvalue.

Oriented graphs are widely used in bearing-based formation research. Specifically, an orientation of an undirected graph is the assignment of a direction to each edge. An oriented graph is an undirected graph together with an orientation [125]. Denote m as the number of the undirected edges and n as the number of the agent. Let the edge (i, j) correspond to the kth ($k \in \{1, 2, \cdots, m\}$) directed edge in oriented graph. For kth directed edge, we can redefine the edge and bearing vector as

$$e_k := e_{ij} = p_j - p_i, \quad g_k := \frac{e_k}{\|e_k\|}.$$

Let $H \in \mathbb{R}^{m\times n}$ be the incidence matrix of the oriented graph (undirected graph $\mathcal{G}$ with orientation), $[H]_{ki}$ denotes the entry of H which is defined as

$$[H]_{ki} = \begin{cases} 1, & i \text{ is the head of } k, \\ -1, & i \text{ is the tail of } k \\ 0, & \text{otherwise.} \end{cases}$$

Based on the definition of H, we can conclude that $e = \mathrm{col}(e_1, \cdots, e_m) = \bar{H}p$, where $\bar{H} = H \bigotimes I_d$.

Define

$$P_{g_{ij}} := I_d - g_{ij} g_{ij}^{\mathrm{T}} \in \mathbb{R}^{d\times d},$$

It is obvious that $P_{g_{ij}} \geq 0$, $P_{g_{ij}}^2 = P_{g_{ij}}$, and $\mathrm{Null}(P_{g_{ij}}) = \mathrm{span}\{g_{ij}\}$. Then, we can imply that $\forall x \in \mathbb{R}^d, x$ is parallel to g_{ij} if and only if $P_{g_{ij}} x = 0$. This property is significant to design the controller via bearing measurement [112, 126]. Then we can obtain the time derivative of g_{ij} as follow:

$$\dot{g}_{ij} = \frac{P_{g_{ij}}}{\|e_{ij}\|} \dot{e}_{ij}.$$

It can be seen that $g_{ij}^\top \dot{g}_{ij} = e_{ij}^\top \dot{g}_{ij} = g_k^\top \dot{g}_k = e_k^\top \dot{g}_k = 0$ due to the fact that $P_{g_{ij}} g_{ij} = 0$.

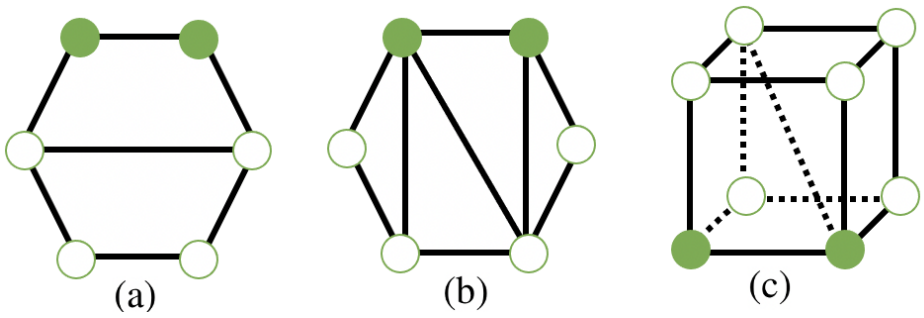

Figure 3.1: Examples of non-unique target formation (a) and unique target formation (b and c) determined by bearing vectors.

Let $p^* = \mathrm{col}(p_1^*, \cdots, p_n^*)$ and $g^* = \mathrm{col}(g_1^*, \cdots, g_m^*)$ denote configuration and bearing vector of the goal formation $(\mathcal{G}, p^*)$. The *bearing Laplacian matrix* $\mathcal{B} \in \mathbb{R}^{dn\times dn}$ is introduced to characterise the properties of a formation. The block of $\mathcal{B}$ can be written as [112]

$$[\mathcal{B}]_{ij} = \begin{cases} \mathbf{0_{d\times d}}, & i \neq j,\ (i,j) \notin \mathcal{E}, \\ -P_{g_{ij}^*}, & i \neq j,\ (i,j) \in \mathcal{E}, \\ \sum_{k\in\mathcal{N}_i} P_{g_{ik}^*}, & i = j,\ i \in \mathcal{V}. \end{cases}$$

It is easy to see that $\mathcal{B} \geq 0$, $\mathcal{B}\mathbf{1}_{dn} = \mathcal{B}p^* = 0$, and $\mathcal{B} = \bar{H}^\top \mathrm{diag}(P_{g_k^*})\bar{H}$. The partition of $\mathcal{B}$ by leaders and followers is shown as

$$\mathcal{B} = \begin{bmatrix} \mathcal{B}_{ll} & \mathcal{B}_{lf} \\ \mathcal{B}_{lf}^\top & \mathcal{B}_{ff} \end{bmatrix} \tag{3.1}$$

where $\mathcal{B}_{ff} \in \mathbb{R}^{dn_f\times dn_f}$ and $\mathcal{B}_{ll} \in \mathbb{R}^{dn_l\times dn_l}$. In this thesis, it is necessary to ensure that the target formation is unique. Hence, we present the following result.

Lemma 3.1. *[112] The desired formation can be uniquely determined by the bearing vectors* $\{g_{ij}^*\}_{(i,j)\in\mathcal{E}}$ *and the states of the fixed leaders* $\{p_i^*\}_{i\in\mathcal{V}_l} \Leftrightarrow \mathcal{B}_{ff}$ *is full rank.*

For a better understanding of the construction of the desired formation, an illustrative example is provided in Fig. 3.1, where the leaders are denoted by solid circles and the followers are denoted by hollow circles. The interaction topology shown in Fig. 3.1 (a) cannot guarantee the uniqueness of the target formation. However, the target formation can be determined uniquely by implementing the interaction topologies in Fig. 3.1 (b) and (c).

The following lemmas reveal some significant properties of the edge and bearing vectors:

Lemma 3.2. *[114]: If there is no collision between the agents, we have*

$$p^\top \bar{H}^\top (g^* - g) \leq 0 \tag{3.2}$$

$$(p^*)^\top \bar{H}^\top (g^* - g) \geq 0 \tag{3.3}$$

$$(p - p^*)^\top \bar{H}^\top (g^* - g) \leq 0 \tag{3.4}$$

where the equalities hold if and only if $g = g^*$.

Lemma 3.3. *[114]: If there is no collision between the agents, we have*

$$p^\top \mathcal{B} p \leq 2p^\top \bar{H}^\top (g - g^*) \max_k \|e_k\| \tag{3.5}$$

3.4 Lyapunov Stability Theory

In this section, we introduce some basic Lyapunov stability theories which will be applied to further stability analysis of the error systems. The main reference of this section is [127].

Considering a nonlinear system

$$\dot{x}(t) = f(x, t) \tag{3.6}$$

where $x \in \mathcal{U} \subset \mathbb{R}^n$ stands for the state and $\mathcal{U} \subset \mathbb{R}^n$ is a domain with $x = 0$ as an interior point. $f : \mathcal{U} \subset \mathbb{R}^n \times [0, +\infty) \to \mathbb{R}^n$ denotes a continuous function with $f(0, t) = 0$.

Definition 3.3. *(**Lyapunov stability**, [127]). The equilibrium point* $x = 0$ *of the system* (3.6) *is said to be Lyapunov stable if for any given constant* $R \in \mathbb{R}^+$ *there exists a constant* r *such that* $\|x(t)\| < R$, $\forall t > 0$ *if* $\|x(0)\| < r$. *Otherwise, the equilibrium point is unstable.*

Definition 3.4. *(**Asymptotic stability**, [127]). The equilibrium point* $x = 0$ *of the system* (3.6) *is said to be asymptotically stable if it is Lyapunov stable and furthermore* $\lim_{t\to\infty} x(t) = 0$.

Definition 3.5. *(**Global asymptotic stability**, [127]). If the asymptotic stability defined in Definition 3.4 holds for any initial state in $\mathbb{R}^n$, the equilibrium point is said to be globally asymptotically stable.*

Definition 3.6. *(**Exponential stability**, [127]). The equilibrium point $x = 0$ of the system (3.6) is said to be exponentially stable if there exist two positive real numbers a and b such that the following inequality holds:*

$$\|x(t)\| < a\|x(0)\|e^{-bt},$$

for $t > 0$ in some neighbourhood $\mathcal{U} \subset \mathbb{R}^n$ containing the equilibrium point.

Definition 3.7. *(**Global exponential stability**, [127]). If the exponential stability defined in Definition 3.6 holds for any initial state in $\mathbb{R}^n$, the equilibrium point is said to be globally exponential stable.*

Definition 3.8. *(**Positive definition function**, [127]). A function $V(x) \in \mathcal{U} \subset \mathbb{R}^n$ is said to be locally positive definite if $V(x) > 0$ for $x \in \mathcal{U}$ except at $x = 0$ where $V(x) = 0$. If $\mathcal{U} = \mathbb{R}^n$, i.e., the above property holds for the entire state space, $V(x)$ is said to be globally positive definite.*

Definition 3.9. *(**Lyapunov function**, [127]). If in $\mathcal{U} \in \mathbb{R}^n$ containing the equilibrium point $x = 0$, the function $V(x)$ is positive definite and has continuous partial derivatives, and if its time derivative along any state trajectory of system (3.6) is non-positive, i.e.,*

$$\dot{V}(x) \leq 0,$$

then $V(x)$ is a Lyapunov function.

Definition 3.10. *(**Radially unbounded function**, [127]). A positive definite function $V(x) : R^n \to \mathbb{R}$ is said to be radially unbounded if $V(x) \to \infty$ as $\|x\| \to \infty$.*

Theorem 3.1. *(**Lyapunov theorem for global stability**, [127]). For system (3.6) with $\mathcal{U} \in \mathbb{R}^n$ if there exists a function $V(x) : R^n \to \mathbb{R}$ with first order derivatives such that*

- *$V(x)$ is positive definite*
- *$\dot{V}(x)$ is negative definite*

- $V(x)$ *is radially unbounded*

then the equilibrium point $x = 0$ *is globally asymptotically stable.*

Definition 3.11. *(**Positively invariant set**, [127]). A set* M *is a positively invariant set with respect to* (3.6) *if*

$$x(0) \in M \Rightarrow x(t) \in M, \ \ \forall t \geq 0.$$

Theorem 3.2. *(**LaSalle's invariance principle**, [127]). Let* $\omega \in \mathcal{U}$ *be a compact set that is positively invariant with respect to* (3.6)*. Let* $V : \mathcal{U} \to \mathbb{R}$ *be a continuously differentiable function such that* $\dot{V}(x) \leq 0$ *in* $\mathcal{U}$*. Let* $\mathcal{O}$ *be the set of all points in* $\mathcal{U}$ *where* $\dot{V} = 0$*. Let* M *be the largest invariant set in* $\mathcal{O}$*. Then every solution starting in* $\mathcal{O}$ *approaches* M *as* $t \to \infty$*.*

Chapter 4

Basic Formation Framework Based on Bearing Measurements

4.1 Introduction

Compared to traditional formation techniques, bearing-only formation control can minimise the requirements on the sensing ability of robots, which is more practical to deal with onboard-sensor-based issues. In this chapter, we aim to deal with Objective 1 and propose a novel mixed formation protocol that contains both edge-based and bearing-based measurements, which helps maximise the utilisation of the sensing-ability of each unmanned robot. Based on the different scenarios of the formation missions, both leaderless and leader-follower cases are considered when designing the protocol and in both cases convergence of the controlled output can be guaranteed via Lyapunov theory. The main contributions of this chapter are as follows:

- A novel mixed formation control approach with edge and bearing measurements is proposed, which can be used to maximise the tracking performance based on the sensing-ability of each unmanned robot in a multi-robot team.
- Both leaderless and leader-follower cases are considered in this chapter. By using Lyapunov theory, all the unmanned robots can be proved to achieve the target formation asymptotically for leaderless case and exponentially for leader-follower case.

The remainder of the chapter is organised as follows. Section 4.2 presents the main

objective of the chapter. In Section 4.3, we propose the mixed formation protocols based on edge and bearing measurements for both leaderless and leader-follower cases and analyse the stability of the MRS. Section 4.4 provides simulation results to validate the theoretical results and Section 4.5 concludes the chapter.

4.2 Problem Descriptions

Suppose that the dynamics of the ith robot can be described by

$$\dot{p}_i(t) = u_i(t), \quad i \in \{1, 2, \cdots, n\}\,, \tag{4.1}$$

where $u_i(t) \in \mathbb{R}^p$ denotes the control input of ith robot. Suppose that the interaction topology between each robot is denoted by $\mathcal{G}$. The main problem to be solved is described as follows.

Problem: Design the formation protocols for each robot based on both edge vectors $\{e_{ij}\}_{j\in\mathcal{N}_i}$ and bearing vectors $\{g_{ij}\}_{j\in\mathcal{N}_i}$ such that all the robots will converge to the target formation.

To deal with the problem, we have the following assumptions.

Assumption 4.1. *There exists at least one spanning tree in the interaction topology $\mathcal{G}$.*

This assumption is universally used in networked formation problem since the configuration of the target formation can be guaranteed by edge vectors [125].

Assumption 4.2. *There is no collision during the formation task.*

This assumption guarantees that the bearing vector between any pair of neighbours is always well-defined during the formation construction, which has been commonly used in bearing-based control problems such as [114, 126].

4.3 Edge-based and bearing-based formation controller design for multi-robot systems

4.3.1 Formation Protocols for Leaderless Case

In this section, we design the formation protocol for each robot in the leaderless case. The control input of the ith robot can be written as

$$u_i(t) = u_i^e(t) + u_i^b(t), \quad i \in \{1, 2, \cdots, n\} , \tag{4.2}$$

where $u_i^e(t)$ and $u_i^b(t)$ denote the controller measured by edge vectors $\{e_{ij}\}_{j\in\mathcal{N}_i}$ and bearing vectors $\{g_{ij}\}_{j\in\mathcal{N}_i}$, which can be designed as

$$u_i^e(t) = \sum_{j\in\mathcal{N}_i} c_{ij}^e(e_{ij} - e_{ij}^*) , \tag{4.3}$$

$$u_i^b(t) = \sum_{j\in\mathcal{N}_i} c_{ij}^b(g_{ij} - g_{ij}^*) , \tag{4.4}$$

where c_{ij}^e and c_{ij}^b are positive control gains. The compact form of (4.2) can be written as

$$\dot{p} = -\hat{H}^\top \bar{C}_e(e - e^*) - \hat{H}^\top \bar{C}_b(g - g^*) , \tag{4.5}$$

where $\hat{H} = H \otimes I_p$, $\bar{C}_e = C_e \otimes I_p$ and $C_e = \mathrm{diag}\{\mathrm{c_{ij}^e}\}$; $\bar{C}_b = C_b \otimes I_p$ and $C_b = \mathrm{diag}\{\mathrm{c_{ij}^b}\}$. In order to analyse the convergence of the system (4.5), we have the following results

Lemma 4.1. *For any positive-definite diagonal matrix* $Q = \mathrm{diag}\{\mathrm{q_1}, \cdots, \mathrm{q_m}\} \in \mathbb{R}^{\mathrm{m}\times\mathrm{m}}$*, if Assumption 4.1 holds, we can obtain the following inequalities:*

$$p^\top \hat{H}^\top \bar{Q}(g - g^*) \geq 0 , \tag{4.6}$$

$$-(p^*)^\top \hat{H}^\top \bar{Q}(g - g^*) \geq 0 , \tag{4.7}$$

where $\bar{Q} = Q \otimes I_p$*. The equalities hold if and only if* $g - g^* = 0$*.*

Proof. According to the discussion in [114, Lemma 2] and $q_k > 0$, $\forall k \in \{1, 2, \cdots, m\}$, we have

$$\begin{aligned} p^\top \hat{H}^\top \bar{Q}(g - g^*) &= \sum_{k=1}^{m} q_k \|e_k\|(1 - g_k^\top g_k^*) \\ &= \frac{1}{2}\sum_{k=1}^{m} q_k \|e_k\| \|g_k - g_k^*\| \geq 0. \end{aligned} \tag{4.8}$$

Similarly, we can get

$$\begin{aligned} -(p^\top)^* \hat{H}^\top \bar{Q}(g - g^*) &= \sum_{k=1}^{m} q_k \|e_k^*\|(1 - g_k^\top g_k^*) \\ &= \frac{1}{2}\sum_{k=1}^{m} q_k \|e_k^*\| \|g_k - g_k^*\| \geq 0. \end{aligned} \tag{4.9}$$

This completes the proof. □

Lemma 4.2. *The equilibrium of system* (4.5) *satisfies* $e = e^*$*, that is to say* $\dot{p} = 0$ *if and only if* $e = e^*$*.*

Proof. Since $e = e^*$ contains $g = g^*$, the sufficient part is finished. Now, we only focus on the necessity part. By $\dot{p} = 0$, we have

$$\begin{aligned} (p - p^*)^\top \dot{p} = &-(p - p^*)\hat{H}^\top \bar{C}_b(g - g^*) \\ &- (e - e^*)^\top \bar{C}_e(e - e^*) \, . \end{aligned} \tag{4.10}$$

Consider that $-(e - e^*)^\top \bar{C}_e(e - e^*) \leq 0$ and the equality holds if and only if $e = e^*$. Combining with lemma 4.1, we have $(p - p^*)^\top \dot{p} \leq 0$ and the equality holds if $e = e^*$. Thus we complete the proof. □

Define the centroid of the formation as

$$\bar{p} = \frac{1}{n}\sum_{i=1}^{n} p_i = \frac{(\mathbf{1}_n \otimes I_p)p}{n},$$

The following Lemma holds.

Lemma 4.3. *For system* (4.1) *with the controller* (4.2)*, the centroid* $\bar{p}$ *is fixed under the protocols* (4.3) *and* (4.4) *during the formation task.*

Proof. By the definition of H, we have

$$\hat{H}(\mathbf{1}_n \otimes I_p) = H\mathbf{1}_n \otimes I_p = 0.$$

Then, we can imply that

$$\begin{aligned} \dot{\bar{p}} &= \frac{(\mathbf{1}_n \otimes I_p)\dot{p}}{n} \\ &= -\frac{(\hat{H}(\mathbf{1}_n \otimes I_p))^\top (\bar{C}_e(e - e^*) - \bar{C}_b(g - g^*))}{n} \\ &= 0. \end{aligned} \tag{4.11}$$

Now, we finish the proof. □

Next, we will analyse the stability of our formation protocols and present the following result.

Theorem 4.1. *If $\bar{p}^* = \bar{p}(0)$, under Assumptions 4.1 and 4.2, all the autonomous robots will converge to target formation p^* asymptotically by control protocols* (4.3) *and* (4.4)*.*

Proof. From lemma 4.3, we have that the centroid of the formation is fixed during the formation. Hence we can set the centroid of the target formation $\bar{p}^*$ as $\bar{p}(0)$, which is invariant. By combining with Assumption 4.1, we can imply that p^* can be uniquely determined by e^*. That is to say $e = e^* \Leftrightarrow p = p^*$. Let $\delta_p = p - p^*$, consider the following Lyapunov function

$$V = \frac{1}{2}\delta_p^\top \delta_p \, .$$

From (4.5), the derivative of V can be expressed as

$$\begin{aligned} \dot{V} &= \delta_p^\top \dot{\delta}_p = \delta_p^\top \dot{p} \\ &= -\delta_p^\top \hat{H}^\top \bar{C}_b (g - g^*) - \delta_p^\top \hat{H}^\top \bar{C}_e (e - e^*) \end{aligned} \tag{4.12}$$

According to Lemma 4.1, we have

$$\dot{V} = -(p - p^*)^\top \hat{H}^\top \bar{C}_b (g - g^*) - (e - e^*)^\top C_e (e - e^*) \leq 0 \tag{4.13}$$

and $\dot{V} = 0 \Leftrightarrow e = e^*$. Then, we can imply that the equilibrium of system (4.5) is stable. Hence, all the robots will converge to target formation p^* asymptotically by control protocols (4.3) and (4.4). □

4.3.2 Formation Protocols for Leader-follower Case

This section studies the formation protocol for leader-follower system. Suppose there are n_l stationary leaders ($\dot{p}_i = 0,\ \forall i \in \{1, 2, \cdots, n_l\}$) and n_f followers ($n_l + n_f = n$). The dynamics of the follower robots can be described as

$$\dot{p}_i(t) = u_i(t), \quad i \in \{n_l + 1, n_l + 2, \cdots, n\} \, , \tag{4.14}$$

where the controller $u_i(t) = u_i^e(t) + u_i^b(t)$ is still measured by edge vectors $\{e_{ij}\}_{j \in \mathcal{N}_i}$ and bearing vectors $\{g_{ij}\}_{j \in \mathcal{N}_i}$.

The partition of $\mathcal{B}$ and $\mathcal{L}$ according to the leaders and followers can be expressed as

$$\mathcal{B} = \begin{bmatrix} \mathcal{B}_{ll} & \mathcal{B}_{lf} \\ \mathcal{B}_{lf}^\top & \mathcal{B}_{ff} \end{bmatrix}, \mathcal{L} = \begin{bmatrix} \mathcal{L}_{ll} & \mathcal{L}_{lf} \\ \mathcal{L}_{lf}^\top & \mathcal{L}_{ff} \end{bmatrix}, \tag{4.15}$$

where $\mathcal{B}_{ll} \in \mathbb{R}^{pn_l \times pn_l}$ and $\mathcal{B}_{ff} \in \mathbb{R}^{pn_f \times pn_f}$, $\mathcal{L}_{ll} \in \mathbb{R}^{n_l \times n_l}$ and $\mathcal{L}_{ff} \in \mathbb{R}^{n_f \times n_f}$. The following assumption is presented to ensure the uniqueness of the target formation p^*.

Assumption 4.3. *The target formation p^* can be uniquely determined by the edge vectors $\{e_{ij}\}_{j\in\mathcal{N}_i}$ and the bearing vectors $\{g_{ij}\}_{j\in\mathcal{N}_i}$.*

From the Lemma 1 in [114], we can easily find that Assumption 4.3 holds if and only if $\mathcal{B}_{ff} > 0$. It also can be obtained that $\mathcal{L}_{ff} > 0$ by Assumption 4.1 ([128]). To analyse the stability of our formation protocols (4.3) and (4.4), we provide the following Lemma.

Lemma 4.4. *For any positive-definite diagonal matrix $Q = \mathrm{diag}\{\mathrm{q}_1, \cdots, \mathrm{q}_\mathrm{m}\} \in \mathbb{R}^{\mathrm{m}\times\mathrm{m}}$, the following inequality holds if Assumption 4.1 is satisfied*

$$p^\top \hat{H}^\top \bar{Q}(g - g^*) \geq \frac{\tilde{q} p^\top \mathcal{B} p}{2\max_k \|e_k\|}, \tag{4.16}$$

where $\bar{Q} = Q \otimes I_p$ and $\tilde{q} = \min\{q_1, \cdots, q_m\}$.

Proof. From [114, Lemma 3], we can get

$$p^\top \mathcal{B} p = \sum_{k=1}^{m} \|e_k\|^2 (1 + g_k^\top g_k^*)(1 - g_k^\top g_k^*). \tag{4.17}$$

Since $\tilde{q} \leq q_k$, $\forall k \in \{1, \cdots, m\}$ and $1 + g_k^\top g_k^* \leq 2$, we have

$$\begin{aligned} \tilde{q} p^\top \mathcal{B} p &\leq 2\max_k \|e_k\| \sum_{k=1}^{m} \tilde{q} \|e_k\| (1 - g_k^\top g_k^*) \\ &\leq 2\max_k \|e_k\| \sum_{k=1}^{m} q_k \|e_k\| (1 - g_k^\top g_k^*) \\ &= 2\max_k \|e_k\| p^\top \hat{H}^\top \bar{Q}(g - g^*). \end{aligned} \tag{4.18}$$

Hence, we can imply that (4.16) holds. □

The following Theorem is presented to reveal the convergence of the protocols (4.3) and (4.4) in leader-follower case.

Theorem 4.2. *Under Assumption 4.1, 4.2 and 4.3, all the robots will converge to target formation p^* exponentially if we apply the control protocols* (4.3) *and* (4.4) *for each follower robot.*

Proof. Let $p_l = [p_1^\top, \cdots, p_{n_l}^\top]^\top$ and $p_f = [p_{n_l+1}^\top, \cdots, p_n^\top]^\top$ denote the state of the leaders and followers, and $p = [p_l^\top, p_f^\top]^\top$. Substituting (4.3) and (4.4) into (4.14), the compact form of (4.14) can be rewritten as

$$\dot{p} = -\Gamma \bar{C}_e \hat{H}^\top (e - e^*) - \Gamma \bar{C}_b \hat{H}^\top (g - g^*) \,, \tag{4.19}$$

where $\Gamma = \begin{bmatrix} 0 & 0 \\ 0 & I_{pn_f} \end{bmatrix}$.

Let $\delta_p = p(t) - p^* = [0, \delta_{p_f}^\top]^\top$, we can imply that $\delta_p^\top \Gamma = \delta_p^\top$ because the leaders are fixed. Consider the following Lyapunov function candidate,

$$V = \frac{1}{2} \delta_p^\top \delta_p \,.$$

From (4.5) and the fact that $\delta_p^\top \Gamma = \delta_p^\top$, the derivative of V is shown as

$$\begin{aligned} \dot{V} &= \delta_p^\top \dot{\delta}_p = \delta_p^\top \dot{p} \\ &= -\delta_p^\top \Gamma \hat{H}^\top \bar{C}_b (g - g^*) - \delta_p^\top \Gamma \hat{H}^\top \bar{C}_e (e - e^*) \\ &= -\delta_p^\top \hat{H}^\top \bar{C}_b (g - g^*) - \delta_p^\top \hat{H}^\top \bar{C}_e (e - e^*) \end{aligned} \tag{4.20}$$

According to (4.6), (4.13), and the definition of Laplacian matrix $\mathcal{L}$, we have

$$\begin{aligned} \dot{V} &\leq -p^\top \hat{H}^\top \bar{C}_b (g - g^*) - \delta_p^\top \hat{H}^\top \bar{C}_e \hat{H} \delta_p \\ &= -p^\top \hat{H}^\top \bar{C}_b (g - g^*) - \delta_p^\top \hat{\mathcal{L}} \delta_p \\ &\leq 0 \end{aligned} \tag{4.21}$$

where $\hat{\mathcal{L}} = \mathcal{L} \otimes I_p$. We can conclude that $\mathcal{B} p^* = 0$ from the definition of $\mathcal{B}$. Let $\hat{\mathcal{L}}_{ff} = \mathcal{L}_{ff} \otimes I_p$, then, by Lemma 4.4, it follows that

$$\begin{aligned} \dot{V} &\leq -\frac{\tilde{q} p^\top \mathcal{B} p}{2 \max_k \|e_k\|} - \delta_{p_f}^\top \hat{\mathcal{L}}_{ff} \delta_{p_f} \\ &\leq -\frac{\tilde{q} \delta_p^\top \mathcal{B} \delta_p}{2 \max_k \|e_k\|} - \delta_{p_f}^\top \hat{\mathcal{L}}_{ff} \delta_{p_f} \\ &= -\frac{\tilde{q} \delta_{p_f}^\top \mathcal{B}_{ff} \delta_{p_f}}{2 \max_k \|e_k\|} - \delta_{p_f}^\top \hat{\mathcal{L}}_{ff} \delta_{p_f} \\ &\leq -(\frac{\tilde{q} \lambda_{\min}(\mathcal{B}_{ff})}{2\|e\|} + \lambda_{\min}(\hat{\mathcal{L}}_{ff})) \|\delta_p\|^2. \end{aligned} \tag{4.22}$$

From (4.13), we can indicate that $\delta_p(t) \leq \delta_p(0)$. Hence we can get

$$\begin{aligned} \|e\| &\leq \|\hat{H}\|\|p\| = \|\hat{H}\|\|p^* + \delta_p\| \\ &\leq \|\hat{H}\|(\|p^*\| + \|\delta_p\|) \\ &\leq \|\hat{H}\|(\|p^*\| + \|\delta_p(0)\|). \end{aligned} \tag{4.23}$$

This together with (4.22), we have

$$\begin{aligned} \dot{V} &\leq -(\frac{\tilde{q}\lambda_{\min}(\mathcal{B}_{ff})}{\|\hat{H}\|(\|p^*\| + \|\delta_p(0)\|)} + 2\lambda_{\min}(\hat{\mathcal{L}}_{ff}))V \\ &= -\alpha V. \end{aligned} \tag{4.24}$$

That is to say that all the robots will converge to target formation p^* exponentially with the exponential convergence rate $\alpha = \frac{\tilde{q}\lambda_{\min}(\mathcal{B}_{ff})}{\|\hat{H}\|(\|p^*\|+\|\delta_p(0)\|)} + 2\lambda_{\min}(\hat{\mathcal{L}}_{ff})$. □

Remark 4.1. *The control gains c_i^e and c_i^b represent the weights of the edge-based and bearing-based control effort. To deal with the sensors with low quality, the edge-based gain c_i^e could be selected smaller and the bearing-based gain c_i^b could be selected larger to reduce the affect of low accuracy measured by positions.*

4.4 Simulation Results

In this section, the performance of the formation protocols (4.3) and (4.4) is verified by MATLAB for both leaderless and leader-follower cases.

4.4.1 Simulation Case Study without Leaders

In this simulation, six mobile robots are deployed for the leaderless case. We set the shape of the target formation as a regular hexagon (linked by red solid lines in Fig 4.1).According to Remark 4.1, we can treat the parameters c_{ij}^e and c_{ij}^b as the proportion of edge-based and bearing-based controller. So we have $c_{ij}^e + c_{ij}^b = 1$. In order to verify that the proposed mixed protocol is effective this assignment of the parameters. The control gains c_{ij}^e and c_{ij}^b are selected arbitrarily from $(0, 1)$ and satisfy $c_{ij}^e + c_{ij}^b = 1$. In Fig 4.1, the initial positions of six robots (denoted by six different colours) are linked by blue dashed lines. Hence, we can calculate the centroid $\bar{p}(0)$, which will be set as the centroid of the target formation (denoted by the yellow star). The trajectories of

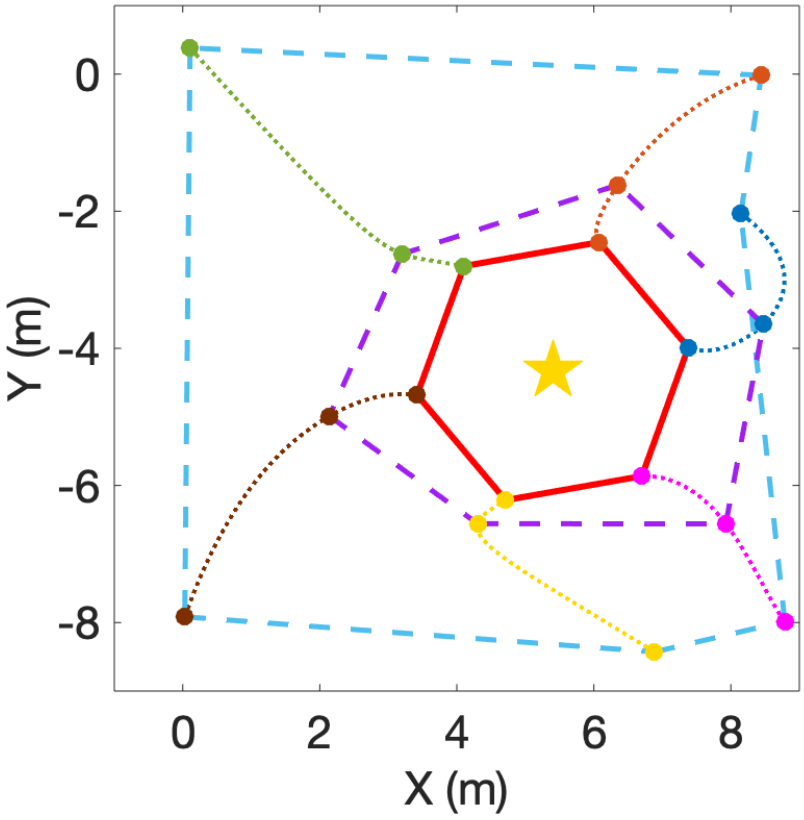

Figure 4.1: Trajectories of the six robots with a fixed centroid (yellow star).

six robots are shown by dashed lines with six different colours corresponding to each robot. Fig 4.2(a) and 4.2(b) show the control inputs of the six robots along the x-axis (u_x) and y-axis (u_y) during the task. In Fig 4.3, we can see that the bearing error ($\|g - g^*\|$), edge error ($\|e - e^*\|$) and the statement error ($\|p - p^*\|$) converge to zero within 15 seconds. It can be observed from these results that the control protocols (4.3) and (4.4) are effective at accomplishing the formation task.

In order to explore the performance of the mixed protocol with different proportion of edge-based and bearing-based controller, we design a simulation case study with four examples shown in Table 4.1. By implementing the proposed mixed protocol, the time variation of the formation errors are shown in Fig 4.4. It can be observed that the convergence rate will be increased for larger proportion of the edge-based controller, which is the advantage of the edge-based controller compare with bearing-based controller.

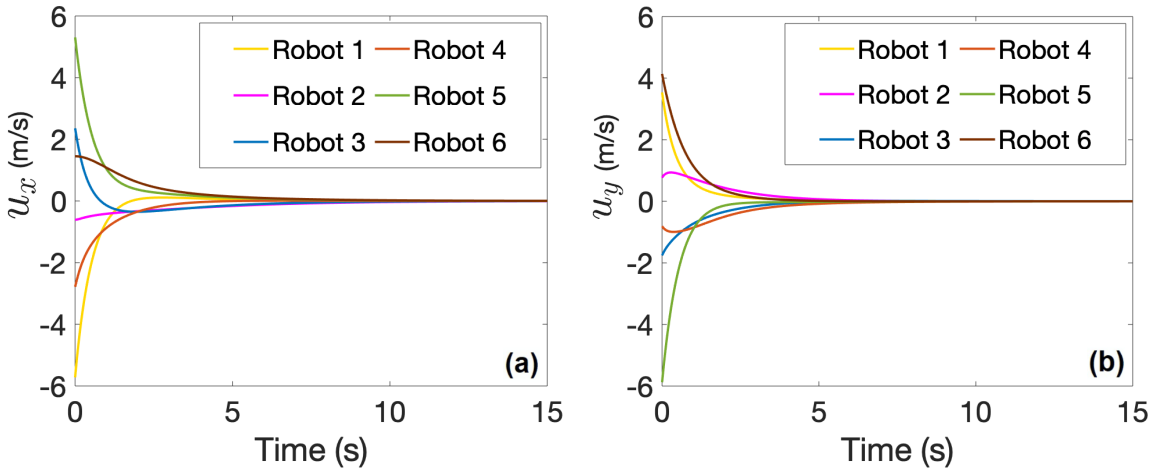

Figure 4.2: Control inputs of the six robots. (a) Along the X-axis (u_x). (b) Along the Y-axis (u_y).

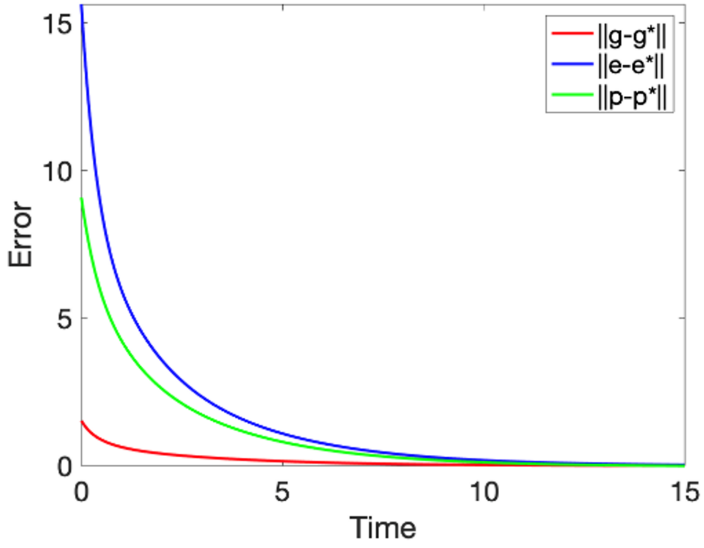

Figure 4.3: Time variation of the bearing error ($\|g - g^*\|$), edge error ($\|e - e^*\|$), and state error ($\|p - p^*\|$).

Table 4.1: Selection of c_{ij}^e and c_{ij}^b

	c_{ij}^e	c_{ij}^b
Example 1	0.1	0.9
Example 2	0.3	0.6
Example 3	0.7	0.2
Example 4	0.9	0.1

4.4.2 Simulation Case Study with Leaders

In this simulation, nine mobile robots (six followers and three stationary leaders) are deployed for the leader-follower case. The shape of the target formation is selected as four small squares, together with a large square (linked by red solid lines in Fig 4.5).

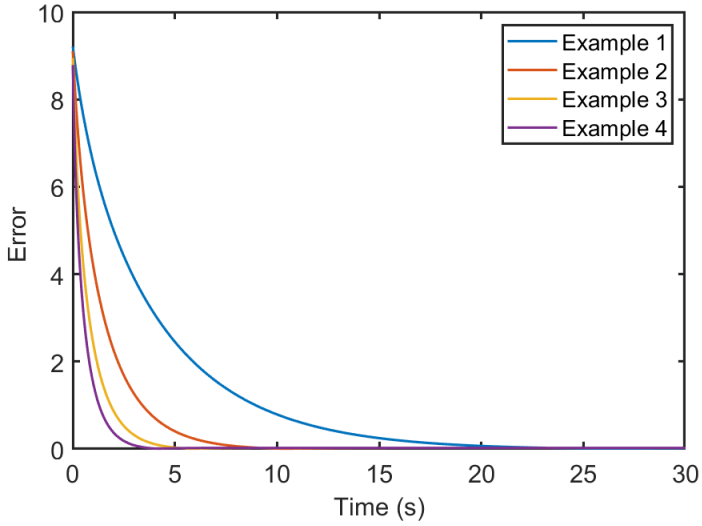

Figure 4.4: Time variation of the formation error .

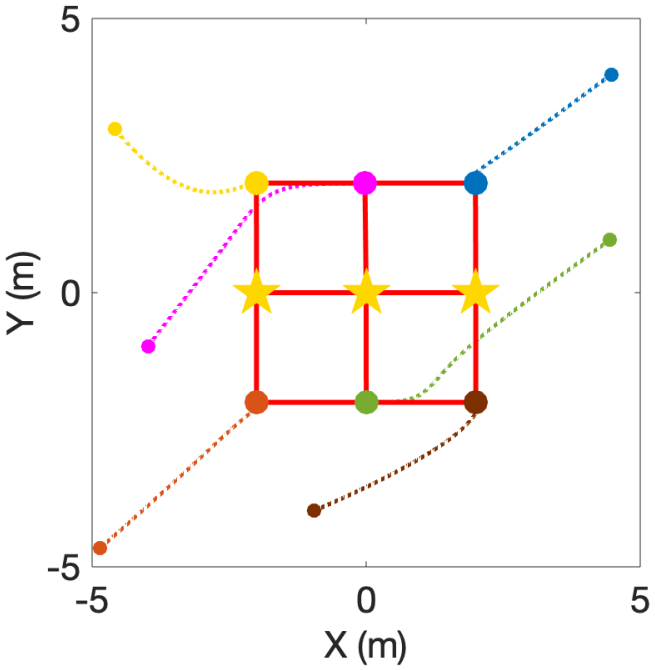

Figure 4.5: Trajectories of six follower robots with fixed leaders (yellow stars).

We choose the control gains c_{ij}^e and c_{ij}^b randomly from $(0, 1)$ and satisfy $c_{ij}^e + c_{ij}^b = 1$. In Fig 4.5, the initial positions of three leaders (denoted by three yellow stars) are $[-2, 0]$, $[0, 0]$, and $[2, 0]$. The yellow, pink, blue, brown, green, and orange dashed lines denote the trajectories of six follower robots from their initial states to target formation. The control inputs of six follower robots along the x-axis (u_x) and y-axis (u_y) are shown in Fig 4.6(a) and Fig 4.6(b), respectively. In Fig 4.7, we can see that the bearing error ($\|g - g^*\|$), edge error ($\|e - e^*\|$) and the statement error ($\|p - p^*\|$)

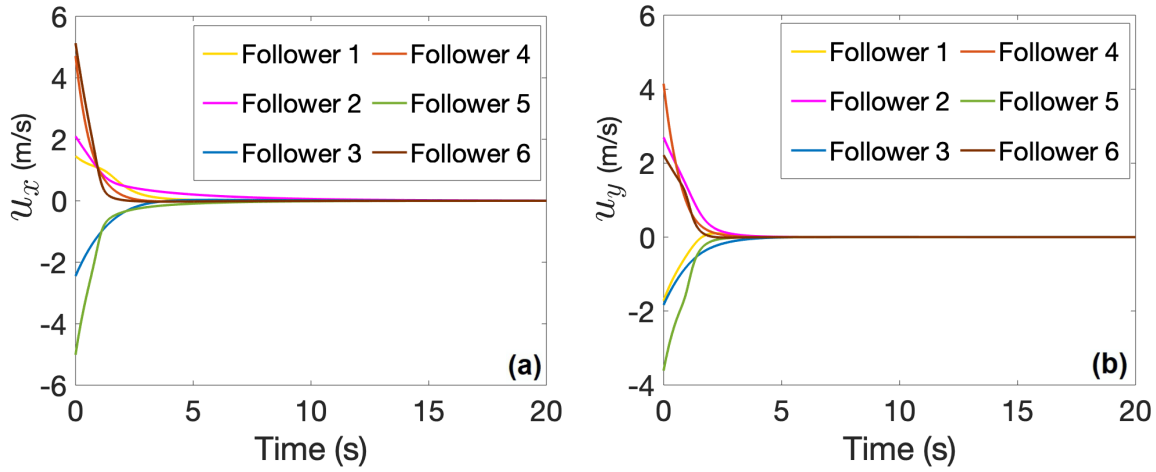

Figure 4.6: Control inputs of six follower robots. (a) Along the X-axis (u_x). (b) Along the Y-axis (u_y).

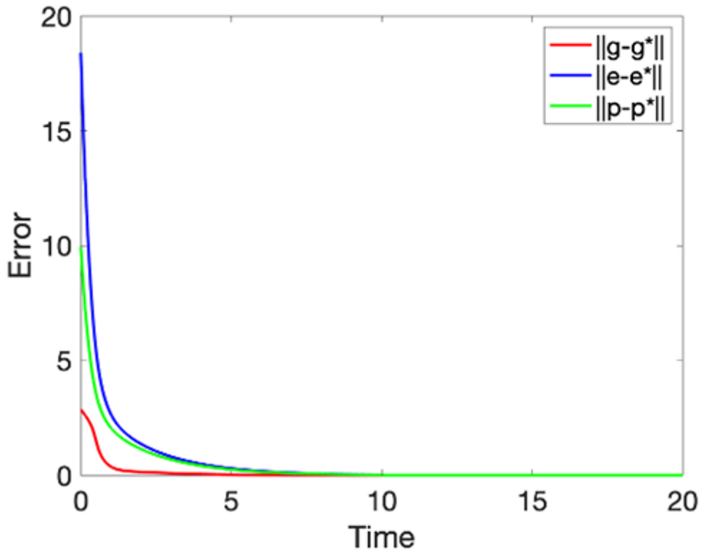

Figure 4.7: Time variation of the bearing error ($\|g - g^*\|$), edge error ($\|e - e^*\|$), and state error ($\|p - p^*\|$).

converges to zero. Hence, the control objective can be fulfilled under the proposed mixed formation protocol.

4.4.3 Comparison with Bearing-Only Protocol

To demonstrate the superior performance of the proposed mixed strategy, we make a comparison of the proposed controller with the bearing-only protocol proposed in [114]. For this comparison, nine mobile robots including six followers and three stationary leaders were deployed. We adopted the same target formation and the initial positions of three leaders in Section IV.B and ran 50 simulations for each controller

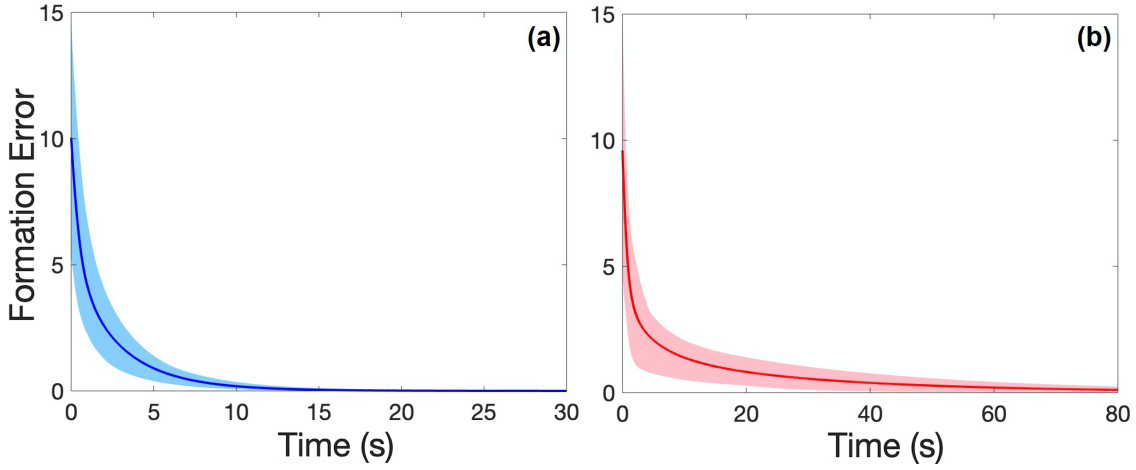

Figure 4.8: Controller performance of (a) mixed protocol, (b) bearing-only protocol.

with the initial positions of each follower chosen randomly from $[-4, 4] \times [-4, 4]$. The performances of the mixed and bearing-only protocols are displayed in Fig. 4.8(a) and 4.8(b), respectively. We utilise $\|p - p^*\|$ to define the formation error. The blue and red zones illustrate the results of 50 simulations and the dark blue and red solid lines represent the average result of the mixed protocol and bearing-only protocol. It can be concluded from the comparison that the convergence time of the mixed protocol ($T = 20$s) is shorter than the bearing-only protocol ($T = 80$s). Hence, the proposed mixed protocol can be used to increase the convergence rate of the formation and maximise the tracking performance based on the sensing-ability of each robot.

4.5 Summary

A novel mixed formation controller for MRS was proposed in this chapter via both edge-based and bearing-based measurements. Both leaderless and leader-follower cases were considered in the protocol design. The stability of the MRS can be guaranteed by choosing an appropriate Lyapunov function. Finally, the simulation results were demonstrated to validate the effectiveness of the proposed formation protocols. In the next stage, the convergence time of the bearing-based protocol will be taken into consideration.

Chapter 5

Finite-Time Bearing-Only Formation Control

5.1 Introduction

Settling time is an important factor during the formation process, which is not considered in Chapter 4. Hence, we explore a series of FTBO formation problems in this chapter for Objective 2. A novel GD bearing-only formation protocol is proposed for multi-robot networks with predefined convergence time. This bearing-based controller can minimise the sensing requirements of each robot compared with traditional position-based method (see [13, 31, 42]). Different from most works related to finite-time control strategies (see [64, 65]), the multi-robot formation can be accomplished within a given finite time that can be predefined by users by implementing the designed algorithm. Then, we present a sufficient condition to ensure that there is no collision between each robot. After that, the exogenous disturbance and the actuator failures are considered in the multi-robot system. Via Lyapunov stability analysis, a sufficient condition is presented to show that the formation error will converge to a bounded set if a bounded exogenous disturbance appears in the robot dynamics. Besides, we also extend the proposed results to deal with LTI dynamics, which is more practical compared to first-order and second-order systems that are often considered in the bearing-only coordination problems. Numerical simulations and lab-based experiments using wheeled robots are conducted to validate the effectiveness of the proposed strategy. The contribution of this chapter can be summarised as:

- A FTBO formation coordination protocol is proposed for multi-robot networks. In contrast to traditional position-based coordination strategies, the coordinated movement of each robot only requires the neighbouring bearings, which significantly reduces the sensing requirements.

- A novel GD coordination law is proposed to realise the desired geometric pattern within a prespecified converge time that can be selected by users. Different from most studies in the area of bearing-only control, the proposed method can also be used to deal with LTI dynamics.

- Exogenous disturbances and actuator faults are considered in the protocol design. It has been proved that the formation tracking error will converge to a bounded set for unknown exogenous disturbances and actuator faults.

The rest of the chapter proceeds as follows. Section 5.2 formulates the problem. In Section 5.3, the bearing-only control problem is handled by a Lyapunov approach and the bound of the formation tracking error is provided. The proposed results are extended to deal with actuator faults. Simulation results and hardware experiments are given in Section 5.4 to verify the feasibility of the proposed scheme. Section 5.5 concludes the chapter.

5.2 Problem Descriptions

In this chapter, we focus on developing a collaboration protocol for networked agents in the presence of exogenous disturbance. Thus the single-integrator dynamics of the robots are considered for simplicity. Let $\mathcal{V}_l$ and $\mathcal{V}_f$ be the set of leaders and followers. Suppose the leaders are fixed ($\dot{p}_i = 0$, $\forall i \in \mathcal{V}_l$), and the dynamics of the followers is

$$\dot{p}_i(t) = u_i(t) + \omega_i(t), \quad i \in \mathcal{V}_f. \tag{5.1}$$

where $\omega_i(t) \in \mathbb{R}^d$ is the exogenous disturbance of robot $i \in \mathcal{V}_f$.

Remark 5.1. *Although the dynamics of most robotic systems (e.g., wheeled mobile robots and quadrotor UAVs) are nonlinear and coupled, the input–output feedback linearisation technique [129] can be exploited to transform the dynamics of the robots to a single-integrator system at any operating point. This technique has been widely*

applied to mobile robots [130, 131]. Hence, this work particularly focuses on designing control protocols for multi-robot formation based on the linearised model with external disturbances.

Let $\delta_i = p_i - p_i^*$ and $\delta = \text{col}(\delta_1, \cdots, \delta_n)$ denote the formation error, the assumptions are given as follows:

Assumption 5.1. *The exogenous disturbance is upper-bounded i.e.,* $\|\omega_i(t)\| \leq f_i$, $\forall t \geq 0$, *where* f_i *is a positive constant.*

From Assumption 5.1, we can easily conclude that $\|\omega(t)\| \leq F = \sum_{i=n_{l+1}}^{n} f_i$, where $\omega(t) = \text{col}(\omega_{n_{l+1}}(t), \cdots, \omega_n(t))$.

Assumption 5.2. *In the single-integrator system with exogenous disturbance, the formation scale* $\boldsymbol{s}(t)$ *is upper-bounded. i.e.,* $\boldsymbol{s}(t) \leq \boldsymbol{s}_0$, $\forall\ t \geq 0$.

Assumption 5.3. *The target formation is unique, i.e.,* $\mathcal{B}_{ff} > 0$.

Assumption 5.4. *There is no collision between each robot during the task.*

From Assumption 5.4, we can deduce that there exists $\tau > 0$ such that $\|p_i - p_j\| > \tau$, $\forall i, j \in \mathcal{V}$ and $i \neq j$.

We now demonstrate the problem statement of this chapter in a precise form. Suppose the dynamics of each mobile robot with exogenous disturbances are guaranteed by system (5.1). To ensure superior performance of the formation tracking mission, the main objectives can be described as: i) Developing a novel finite-time controller for each robot $i \in \mathcal{V}_f$ based on bearing vectors $\{g_{ij}(t)\}_{j\in\mathcal{N}_i}$ and exploring the convergence of the formation error δ. ii) Discussing the robustness of the controller with exogenous disturbances. iii) Providing the fault-tolerant analysis of the finite-time protocol in the presence of actuator failures in the hardware.

Remark 5.2. *In order to transfer the main objectives into a stabilisation problem of bearing vectors* $\{g_{ij}^*\}_{(i,j)\in\mathcal{E}}$ *in finite time, we should link the target formation with the bearing vectors* $\{g_{ij}^*\}_{(i,j)\in\mathcal{E}}$. *Hence, we have the above Assumption 5.3, which is commonly used in bearing-only control problems (e.g., [1, 112, 114]).*

Remark 5.3. *Assumption 5.4 ensures that the bearing vector between any pair of neighbours is always well-defined during the formation construction, which has been*

commonly used in bearing-based control problems such as [114, 126]. The convergence analysis of the protocols proposed in the rest of the chapter is still valid without this assumption before collision occurs. Hence, we also provide the sufficient conditions to guarantee that the formation process is collision-free. With these conditions, Assumption 5.4 could be dropped.

5.3 Main Results

Formation tracking algorithms can be used effectively for swarm robots to converge to the desired pattern in a distributed manner. In this section, we first introduce a finite-time formation control protocol with bearing-only measurements. Then, we provide the stability analysis to guarantee the performance of the formation protocol under external disturbances and actuator faults. Thus it can be implemented safely by practitioners in extreme environments.

5.3.1 FTBO Protocol Design

In this section, we consider bearing-only formation tracking problem based on GD method to deal with the main objective without exogenous ($\omega_i = 0$). The coordinated protocol of each follower is designed as

$$u_i(t) = (a + b\frac{\dot{\mu}(t)}{\mu(t)}) \sum_{j\in\mathcal{N}_i} (g_{ij}(t) - g^*_{ij}(t)), \quad i \in \mathcal{V}_f. \tag{5.2}$$

where $a > 0$ and $b > 0$ are two gains, and $\mu : \mathbb{R}^+ \to \mathbb{R}^+$ is a time-varying scaling function defined as

$$\mu(t) = \begin{cases} \dfrac{T^h}{(T-t)^h} & t \in [0, T) \\ 1, & t \in [T, \infty), \end{cases} \tag{5.3}$$

where $h > 0$ is a parameter to be specified. By using the right-hand derivative of $\mu(t)$ at $t = T$ as $\dot{\mu}(T)$, we have

$$\dot{\mu}(t) = \begin{cases} \dfrac{h}{T}\mu^{(1+\frac{1}{h})}, & t \in [0, T) \\ 0, & t \in [T, \infty). \end{cases} \tag{5.4}$$

$\mu(t)$ is important in the controller since it ensures the bearing-only formation task can be finished in finite time T which can be predefined by users.

Let $g = \text{col}(g_1, \cdots, g_m)$ and $g^* = \text{col}(g_1^*, \cdots, g_m^*)$, in order to analyse the finite-time convergence of the system by GD method, we introduce the following lemmas.

Lemma 5.1. *[1] Suppose $z : \mathbb{R} \to \mathbb{R}_{\geq 0}$ is a continuously differentiable function, if*

$$\dot{z}(t) \leq -\eta z(t) - \xi \frac{\dot{\mu}(t)}{\mu(t)} z(t), \quad t \in [0, \infty) \tag{5.5}$$

where η and ξ are positive. Then, we conclude that $z(t) = 0$ if $t \geq T$ and

$$z(t) \leq e^{-\eta t} \mu^{-\xi} z(0), \quad t \in [0, T). \tag{5.6}$$

Lemma 5.2. *Let $\boldsymbol{a}$ and $\boldsymbol{b}$ be two unit vectors. If $\alpha_1 \geq \alpha_2 \geq 0$, then*

$$\|\alpha_1 \boldsymbol{a} - \alpha_2 \boldsymbol{b}\| \geq \alpha_2 \|\boldsymbol{a} - \boldsymbol{b}\|.$$

Proof. Let ϕ denote the angle between the unit vector $\mathbf{a}$ and $\mathbf{b}$, we have

$$\begin{aligned}
&\|\alpha_1 \mathbf{a} - \alpha_2 \mathbf{b}\|^2 - (\alpha_2 \|\mathbf{a} - \mathbf{b}\|)^2 \\
&= \alpha_1^2 - \alpha_2^2 - 2\alpha_1 \alpha_2 \cos\phi + 2\alpha_2^2 \cos\phi \\
&= (\alpha_1 - \alpha_2)(\alpha_1 + \alpha_2 - 2\alpha_2 \cos\phi) \\
&\geq 2\alpha_2(\alpha_1 - \alpha_2)(1 - \cos\phi) \geq 0.
\end{aligned}$$

This completes the proof. □

Let $u = \text{col}(u_{n_l+1}, \cdots, u_n)$, $e^* = \text{col}(e_1^*, \cdots, e_m^*)$, $\delta_i = p_i - p_i^*$, and $\delta = \text{col}(\delta_1, \cdots, \delta_n)$. The distributed FTBO controller design is shown in the following Theorem:

Theorem 5.1. *Under Assumption 5.3, if*

$$\|\delta(0)\| \leq \frac{1}{\sqrt{n}} \left(\min_{i,j \in \mathcal{V}} \|p_i^* - p_j^*\| - \gamma \right), \tag{5.7}$$

where $\gamma \in (0, \min_{i,j \in \mathcal{V}} \|p_i^* - p_j^*\|)$ is a constant, a collision-free path can be generated for each robot. The robots will converge to the target formation in finite time predefined by users under the protocol (5.2). Furthermore, let $\tilde{p}^* = p^* - \mathbf{1}_n \otimes \bar{p}$ and $\bar{p} = \sum_{i=1}^n p_i^*/n$ denote the centroid of the target formation, if

$$bh\lambda_{min}(\mathcal{B}_{ff}) > 2\|\bar{H}\|(\|\delta(0)\| + \|\tilde{p}^*\|), \tag{5.8}$$

the control input u is uniformly bounded and C^1 smooth for $t \in [0, \infty)$.

Proof. By implementing control protocol (5.2), the compact form of (5.1) can be expressed as

$$\dot{p} = (a + b\frac{\dot{\mu}}{\mu}) \begin{bmatrix} 0 & 0 \\ 0 & I_{dn_f} \end{bmatrix} \bar{H}^\top (g - g^*). \tag{5.9}$$

We choose the Lyapunov function as $V = \frac{1}{2}\|\delta\|^2$. The derivative of V along the system is

$$\begin{aligned} \dot{V} &= \delta^\top \dot{p} \\ &= -(a + b\frac{\dot{\mu}}{\mu})\delta^\top \begin{bmatrix} 0 & 0 \\ 0 & I_{dn_f} \end{bmatrix} \bar{H}^\top (g - g^*) \\ &= -(a + b\frac{\dot{\mu}}{\mu})\delta^\top \bar{H}^\top (g - g^*) \\ &= -(a + b\frac{\dot{\mu}}{\mu})(p - p^*)^\top \bar{H}^\top (g - g^*) \\ &\leq 0. \end{aligned} \tag{5.10}$$

The last inequality can be obtain from (3.4) from Lemma 3.2. Hence, we can imply that for any $t \geq 0$, $\|\delta(t)\| \leq \|\delta(0)\|$.

From (5.7), since

$$\begin{aligned} \|p_i(t) - p_j(t)\| &= \|(p_i(t) - p_i^*) - (p_j(t) - p_j^*) + (p_i^* - p_j^*)\| \\ &\geq \|p_i^* - p_j^*\| - \|p_i(t) - p_i^*\| - \|p_j(t) - p_j^*\| \\ &\geq \|p_i^* - p_j^*\| - \sum_{m=1}^{n} \|p_m(t) - p_m^*\| \\ &\geq \|p_i^* - p_j^*\| - \sqrt{n}\|p(t) - p^*\| \\ &\geq \|p_i^* - p_j^*\| - \sqrt{n}\|\delta(0)\|, \end{aligned} \tag{5.11}$$

we have $\|p_i(t) - p_j(t)\| \geq \gamma$, $\forall t > 0$ and $\forall i, j \in \mathcal{V}$.

According to Lemma 3.3 and the fact $\mathcal{B}p^* = 0$ and $\delta = [0, \delta_f^\top]$, it follows from (5.10)

that

$$\begin{aligned}\dot{V} &\leq -(a+b\frac{\dot{\mu}}{\mu})p^\top \bar{H}^\top (g-g^*)\\ &\leq -(a+b\frac{\dot{\mu}}{\mu})\frac{1}{2\max_k\|e_k\|}p^\top \mathcal{B}p\\ &= -(a+b\frac{\dot{\mu}}{\mu})\frac{1}{2\max_k\|e_k\|}\delta^\top \mathcal{B}\delta\\ &= -(a+b\frac{\dot{\mu}}{\mu})\frac{1}{2\max_k\|e_k\|}\delta_f^\top \mathcal{B}\delta_f\\ &\leq -(a+b\frac{\dot{\mu}}{\mu})\frac{\lambda_{\min}(\mathcal{B}_{ff})}{2\max_k\|e_k\|}\|\delta\|^2.\end{aligned} \tag{5.12}$$

Note that

$$\begin{aligned}\max_k\|e_k\| \leq \|e\| = \|\bar{H}p\| &= \|\bar{H}(p-p^*+p^*)\|\\ &\leq \|\bar{H}\delta\| + \|\bar{H}p^*\|\\ &= \|\bar{H}\delta\| + \|\bar{H}\tilde{p}^*\|\\ &\leq \|\bar{H}\|(\|\delta\| + \|\tilde{p}^*\|)\\ &\leq \|\bar{H}\|(\|\delta(0)\| + \|\tilde{p}^*\|).\end{aligned} \tag{5.13}$$

Combine (5.12) and (5.13), we obtain that

$$\begin{aligned}\dot{V} \leq & -\underbrace{\frac{a\lambda_{\min}(\mathcal{B}_{ff})}{\|\bar{H}\|(\|\delta(0)\| + \|\tilde{p}^*\|)}}_{\bar{a}}V - \underbrace{\frac{b\lambda_{\min}(\mathcal{B}_{ff})}{\|\bar{H}\|(\|\delta(0)\| + \|\tilde{p}^*\|)}}_{\bar{b}}\frac{\dot{\mu}}{\mu}V\\ = & -\bar{a}V - \bar{b}\frac{\dot{\mu}}{\mu}V.\end{aligned} \tag{5.14}$$

From Lemma 5.1, we have

$$\|\delta(t)\|\begin{cases}\leq e^{-\bar{a}t}\mu^{-\bar{b}}\|\delta(0)\|, & t\in[0,T)\\ = 0, & t\in[T,\infty).\end{cases} \tag{5.15}$$

That is to say $p\to p^*$ in finite time T. Then, we will prove that u remains uniformly bounded and C^1 smooth.

By (5.9), we have

$$\|u\| \leq (a+b\frac{\dot{\mu}}{\mu})\|\bar{H}^\top\|\|(g-g^*)\|, \tag{5.16}$$

From Lemma 5.2, (5.7) and (5.11), we have

$$\begin{aligned}\|e-e^*\|^2 = \sum_{i=1}^m \|g_i\|e_i\| - g_i^*\|e_i^*\|\|^2 &\geq \gamma^2\sum_{i=1}^m\|g_i-g_i^*\|^2\\ \geq \gamma^2\|g-g^*\|^2,\end{aligned} \tag{5.17}$$

then it follows

$$\|g-g^*\|^2 \leq \frac{1}{\gamma^2}\|e-e^*\|^2 \leq \frac{1}{\gamma^2}\|\bar{H}\|^2\|\delta(t)\|^2. \tag{5.18}$$

Combined (5.18) with (5.16), we have

$$\|g-g^*\| \begin{cases} \leq \frac{1}{\gamma}\|H\|\mu^{-\bar{b}}e^{-\bar{a}t}\|\delta(0)\|, & t\in[0,T) \\ \equiv 0, & t\in[T,\infty), \end{cases} \tag{5.19}$$

and

$$\|\frac{\dot{\mu}}{\mu}(g-g^*)\| \begin{cases} \leq \frac{1}{\gamma}\|H\|\frac{h}{T}\mu^{-(\bar{b}-\frac{1}{h})}e^{-\bar{a}t}\|\delta(0)\|, & \\ & t\in[0,T) \\ \equiv 0, & t\in[T,\infty), \end{cases} \tag{5.20}$$

from (5.8), we have $\bar{b}-\frac{1}{h}>0$, so we can obtain

$$\lim_{t\to T^-}\|\frac{\dot{\mu}}{\mu}(g-g^*)\| = 0. \tag{5.21}$$

By (5.15), (5.16), (5.19), (5.20), and (5.21), it can be concluded that

$$\lim_{t\to T^-}\|u\| = 0. \tag{5.22}$$

That is to say u is uniformly bounded and continuous on $[0,\infty)$.

Next, we focus on the derivative of u. Since

$$\begin{aligned} \frac{du}{dt} =& \frac{bh}{T^2}\mu^{\frac{2}{h}}\bar{H}^\top(g-g^*)+(a+b\frac{\dot{\mu}}{\mu})\bar{H}^\top\dot{g} \\ =& \frac{bh}{T^2}\mu^{\frac{2}{h}}\bar{H}^\top(g-g^*)+(a+b\frac{\dot{\mu}}{\mu})\bar{H}^\top P\bar{H}\dot{p} \\ =& [\frac{bh}{T^2}\mu^{\frac{2}{h}}\bar{H}^\top+(a+b\frac{\dot{\mu}}{\mu})^2\bar{H}^\top P\bar{H}\bar{H}^\top](g-g^*) \end{aligned} \tag{5.23}$$

where $P=\mathrm{diag}(\frac{P_{g_k}}{\|e_k\|})$. It is easily to see that $\frac{du}{dt}$ is continuous on $[0,T)$ and (T,∞). Furthermore $\|P\|$ is bounded, so there exist $\Lambda>0$ such that $\|\bar{H}^\top\|^2\|\bar{H}\|\|P\|<\Lambda$. Hence, from (5.23), we have

$$\begin{aligned} \left\|\frac{du}{dt}\right\| \leq& \frac{bh}{T^2}\mu^{\frac{2}{h}}\|\bar{H}^\top\|\|g-g^*\|+\Lambda(a+b\frac{\dot{\mu}}{\mu})^2\|g-g^*\| \\ =& [\Lambda a^2+2ab\Lambda\mu^{\frac{1}{h}}+(\Lambda b^2+\frac{bh}{T^2}\|\bar{H}^\top\|)\mu^{\frac{2}{h}}]\|g-g^*\| \end{aligned} \tag{5.24}$$

From (5.8), we have $\bar{b}-(2/h)>0$, similar to the analysis of (5.20), (5.21) and (5.24), we can imply that

$$\lim_{t\to T^-}\left\|\frac{du}{dt}\right\| = 0. \tag{5.25}$$

That is to say, du/dt is uniformly bounded and continuous on $[0, \infty)$. So it can be concluded that the control input u is uniformly bounded and C^1 smooth for $t \in [0, \infty)$. □

Remark 5.4. *We utilise the forward difference method to deal with* (5.9) *with our controller. Since there is only one loop in the forward difference algorithm and the iterations of this algorithm are proportional to the finite-time T that is selected by the user, the computational complexity of this algorithm is $O(T)$. Hence, the proposed algorithm can be realised in real time because it can ensure that the execution time increases linearly with the finite-time T.*

Remark 5.5. *The collision avoidance is considered in our protocol. We can observe that condition* (5.7) *is the sufficient condition to avoid collision from* (5.11). *If we select the initial positions of the follower robots properly to make the initial error satisfy* (5.7)*, the collision will not appear in the process of tracking. When the formation size in a real-world implementation becomes very large, some of the robots may have occlusion problems when using vision systems to determine their relative orientation. However, since the proposed controller is distributed, the interaction topology of the robot network can be changed to ensure that each robot is able to detect at least one neighbour and thus the formation can still be achieved.*

5.3.2 Robustness Analysis with Exogenous Disturbance

In this section, the robustness analysis of the proposed FTBO protocol with exogenous disturbance is considered.

Since there exist unknown exogenous disturbances in the system. The goal is to discuss the robustness of the FTBO controller (5.2). Before we show the main theorem and associate proof, the following lemma should be introduced:

Lemma 5.3. *Suppose $z : \mathbb{R} \to \mathbb{R}_{\geq 0}$ is a continuously differentiable function, if*

$$\dot{z}(t) \leq -az(t) - b\frac{\dot{\mu}(t)}{\mu(t)}z(t) + \varepsilon, \quad t \in [0, \infty) \tag{5.26}$$

where a, b, and ε are positive and $bh > 1$. Then, it follows that

$$z(t) \leq \begin{cases} \mu^{-b}e^{-at}z(0) + \epsilon(t), & t \in [0, T) \\ \varepsilon/a, & t \in [T, \infty) \end{cases} \tag{5.27}$$

where

$$\epsilon(t) = (\frac{T-t}{bh-1} - \frac{T\mu^{-b}}{bh-1})\varepsilon. \tag{5.28}$$

Proof. On one hand, if $t \in [0, T)$. Let $h(t) = \mu^b(t)z(t)$, we have

$$\dot{h} = \mu^b\dot{z} + b\mu^{b-1}\dot{\mu}z = \mu^b(\dot{z} + b\frac{\dot{\mu}}{\mu}z). \tag{5.29}$$

From (5.26), we can get

$$\begin{aligned} \dot{h} &\leq \mu^b(-az + \varepsilon) \\ &= -ah + \mu^b\varepsilon \end{aligned} \tag{5.30}$$

That is to say

$$\begin{aligned} h(t) &\leq e^{-at}(h(0) + \varepsilon\int_0^t \mu^b(\tau)e^{a\tau}d\tau) \\ &\leq e^{-at}h(0) + \varepsilon\int_0^t \mu^b(\tau)e^{a(\tau-t)}d\tau \\ &\leq e^{-at}h(0) + \varepsilon\int_0^t \mu^b(\tau)d\tau \end{aligned} \tag{5.31}$$

then it can be obtained that

$$\begin{aligned} z(t) &\leq \mu^{-b}(e^{-at}z(0) + \varepsilon\int_0^t \mu^b(\tau)d\tau) \\ &\leq \mu^{-b}(e^{-at}z(0) + (\frac{T^{bh}}{(bh-1)(T-t)^{bh-1}} - \frac{T}{bh-1})\varepsilon) \\ &= \mu^{-b}e^{-at}z(0) + \epsilon(t). \end{aligned} \tag{5.32}$$

On the other hand, if $t \in [T, +\infty)$, we have

$$\dot{z}(t) \leq -az(t) + \varepsilon \tag{5.33}$$

Hence, we can conclude that $z \leq \varepsilon/a$. This completes the proof. □

Now, we would like to give the following analysis of the robustness of the multi-robot network under the proposed control protocol.

Theorem 5.2. *Consider the single-integrator system with the exogenous disturbance. Under Assumption 5.1−5.4 and protocol* (5.2)*, let* $K = 2n\boldsymbol{s}_0$*, by choosing* $\gamma = \sqrt{K/a\lambda_{min}(\mathcal{B}_{ff})}$ *and*

$$bh\lambda_{min}(\mathcal{B}_{ff}) > 2K, \tag{5.34}$$

the formation error δ converges to the bound set $\mathcal{S}$

$$\mathcal{S} = \left\{ \delta : \|\delta\|^2 \leq \frac{4\gamma^2 F^2 K}{a\lambda_{\min}(\mathcal{B}_{ff})} \right\}.$$

in finite time. Furthermore, the control input u is C^1 smooth and uniformly bounded over the time interval $[0, \infty)$.

Proof. By implementing the protocol (5.2), the dynamics of (5.1) can be written in a compact form as

$$\dot{p} = (a + b\frac{\dot{\mu}}{\mu}) \begin{bmatrix} 0 & 0 \\ 0 & I_{dn_f} \end{bmatrix} \bar{H}^\top (g^* - g) + \omega. \tag{5.35}$$

The Lyapunov function can be constructed as $V = \frac{1}{2}\|\delta\|^2$. The derivative of V can be described as

$$\begin{aligned} \dot{V} &= \delta^\top \dot{p} \\ &= (a + b\frac{\dot{\mu}}{\mu})\delta^\top \begin{bmatrix} 0 & 0 \\ 0 & I_{dn_f} \end{bmatrix} \bar{H}^\top (g^* - g) + \delta^\top \omega \\ &= (a + b\frac{\dot{\mu}}{\mu})\delta^\top \bar{H}^\top (g^* - g) + \delta^\top \omega \\ &= (a + b\frac{\dot{\mu}}{\mu})(p - p^*)^\top \bar{H}^\top (g^* - g) + \delta^\top \omega. \end{aligned} \tag{5.36}$$

From Lemma 3.2 and 3.3, we can substitute (3.5) in (5.36). Since $\mathcal{B}p^* = 0$ and $\delta = [0, \delta_f^\top]$, we have

$$\begin{aligned} \dot{V} &= (a + b\frac{\dot{\mu}}{\mu})(p - p^*)^\top H^\top (g^* - g) + \delta^\top \omega \\ &\leq (a + b\frac{\dot{\mu}}{\mu}) p^\top H^\top (g^* - g) + \delta^\top \omega \\ &\leq -(a + b\frac{\dot{\mu}}{\mu}) \frac{1}{2\max_k \|e_k\|} p^\top \mathcal{B} p + \delta^\top \omega \\ &\leq -(a + b\frac{\dot{\mu}}{\mu}) \frac{\lambda_{\min}(\mathcal{B}_{ff})}{2\max_k \|e_k\|} \|\delta\|^2 + \delta^\top \omega. \end{aligned} \tag{5.37}$$

For all robots in the system, from Cauchy inequality, we have

$$\begin{aligned} n^2 \mathbf{s}(t)^2 &= n \sum_{k=1}^{n} \|p_k - \bar{p}\|^2 \\ &\geq (\|p_i - \bar{p}\| + \sum_{k \in \mathcal{V}, k \neq i}^{n} \|p_k - \bar{p}\|)^2 \\ &\geq \|p_i - \bar{p}\|^2 \end{aligned} \tag{5.38}$$

From (5.38) and Assumption 5.2, we can obtain

$$\begin{aligned}\|e_k\| &= \|p_i - p_j\| \\ &= \|(p_i - \bar{p}) - (p_j - \bar{p})\| \\ &\leq \|p_i - \bar{p}\| + \|p_j - \bar{p}\| \\ &\leq 2n\mathbf{s}(t) \leq 2n\mathbf{s}_0 = K.\end{aligned} \tag{5.39}$$

By average inequality, we have

$$\frac{\gamma^{-2}}{4}\|\delta\|^2 + \gamma^2\|\omega\|^2 \geq \|\delta^T\|\|\omega\| \geq \delta^T\omega. \tag{5.40}$$

Combine with (5.39), (5.37) can be written as

$$\begin{aligned}\dot{V} &\leq -(a + b\frac{\dot{\mu}}{\mu})\frac{\lambda_{\min}(\mathcal{B}_{ff})}{2K}\|\delta\|^2 + \delta^\top\omega \\ &\leq -(a + b\frac{\dot{\mu}}{\mu})(\frac{\lambda_{\min}(\mathcal{B}_{ff})}{2K}\|\delta\|^2) + \frac{\gamma^{-2}}{4}\|\delta\|^2 + \gamma^2\|\omega\|^2 \\ &\leq -(a + b\frac{\dot{\mu}}{\mu})(\frac{\lambda_{\min}(\mathcal{B}_{ff})}{2K} - \frac{\gamma^{-2}}{4a})\|\delta\|^2 + \gamma^2\|\omega\|^2\end{aligned} \tag{5.41}$$

By choosing

$$\gamma = \sqrt{\frac{K}{a\lambda_{\min}(\mathcal{B}_{ff})}} \tag{5.42}$$

and following Assumption 5.1, we have

$$\dot{V} \leq -(a + b\frac{\dot{\mu}}{\mu})\frac{\lambda_{\min}(\mathcal{B}_{ff})}{4K}V + \gamma^2F^2. \tag{5.43}$$

Therefore

$$\begin{aligned}\dot{V} \leq& -\frac{a\lambda_{\min}(\mathcal{B}_{ff})}{2K}V - \frac{b\lambda_{\min}(\mathcal{B}_{ff})}{2K}\frac{\dot{\mu}}{\mu}V + \gamma^2F^2 \\ =& -\bar{a}V - \bar{b}\frac{\dot{\mu}}{\mu}V + \gamma^2F^2,\end{aligned} \tag{5.44}$$

where $\bar{a} = \frac{a\lambda_{\min}(\mathcal{B}_{ff})}{2K}$ and $\bar{b} = \frac{b\lambda_{\min}(\mathcal{B}_{ff})}{2K}$.

In light of Lemma 5.3, we have

$$\|\delta(t)\|^2 \begin{cases} \leq \mu^{-\bar{b}}e^{-\bar{a}t}\|\delta(0)\|^2 + 2\bar{\epsilon}(t), & t \in [0, T) \\ \leq 2\gamma^2F^2/\bar{a}, & t \in [T, \infty) \end{cases} \tag{5.45}$$

where

$$\bar{\epsilon}(t) = (\frac{T - t}{\bar{b}h - 1} - \frac{T\mu^{-\bar{b}}}{\bar{b}h - 1})\gamma^2F^2. \tag{5.46}$$

Since

$$\lim_{t\to T^-} \mu^{-\bar{b}} = 0, \tag{5.47}$$

it is easily to get

$$\lim_{t\to T^-} \bar{\epsilon}(t) = 0. \tag{5.48}$$

From (5.47) and (5.48), it can be concluded that

$$\lim_{t\to T^-} \|\delta(t)\| = 0. \tag{5.49}$$

Hence, we can obtain that the formation error δ converges to the bound set $\mathcal{S}$ in finite time T from Lemma 5.3.

From (5.34), we have $\bar{b} - \frac{2}{h} > 0$. Similar to the proof in Theorem 5.1, we can conclude that $\|u\|$ and $\|du/dt\|$ are bounded. Moreover

$$\lim_{t\to T^-} \|u\| = \lim_{t\to T^-} \left\|\frac{du}{dt}\right\| = 0. \tag{5.50}$$

That is to say, the continuity and uniformly boundness of u and du/dt can be guaranteed on $[0, \infty)$. Hence we complete the proof. □

Following the analysis presented above, the procedure to construct the offline protocol u_i is given in Algorithm 1.

5.3.3 Fault-Tolerant Analysis

Based on the fact that actuator failures (e.g., the efficiency and the output bias) of the controller could not be ignored in some platforms. The fault-tolerant analysis of the proposed controller is discussed in this subsection. We explore the robustness of the controller (5.2) against the exogenous disturbances and the actuator failures.

The actuator failures u_i^f of each follower agent can be expressed as

$$u_i^f(t) = \rho_i(t)u_i(t) + \tilde{b}_i(t), \tag{5.51}$$

where $\rho_i(t) \in (0, 1]$ represents the unknown efficiency factor of the actuator channel, and $\tilde{b}_i(t) = [\tilde{b}_{i1}(t), \cdots, \tilde{b}_{id}(t)]^\top$ represents the unknown output bias of the actuator channel following [51, 52, 132]. For both time-varying $\rho_i(t)$ and $\tilde{b}_i(t)$, we have the following assumption

Algorithm 1 Finite-time bearing-only protocol design

1: Select n_l leader robots and n_f follower robots;
2: Set the target formation configuration p^* and compute the target bearing g^*;
3: Set the initial positions for fixed leaders and followers
4: Set the bidirectional communication graph and the oriented graph among each robot;
5: **if** Assumption 4 is satisfied **then**
6: Compute the edge vectors and bearing vectors for each connected robot;
7: Compute the bearing Laplacian matrix $\mathcal{B}$ as shown in (3.1);
8: **if** $\mathcal{B}_{ff} > 0$ **then**
9: Set the finite time T;
10: Select the positive control parameters a, b, and h;
11: **if** condition (5.8) holds **then**
12: Construct the control law u_i given in (6.1);
13: **else**
14: Back to step 9;
15: **end if**
16: **else**
17: Back to step 4;
18: **end if**
19: **else**
20: Back to step 3;
21: **end if**

Assumption 5.5. *The unknown efficiency factor and unknown output bias are bounded, and there exists a positive constant* $\rho*$ *and* $\tilde{b}^*$ *such that* $0 < \rho^* \leq \rho_i(t) \leq 1$ *and* $\|b_i(t)\| \leq \tilde{b}_i^*$.

From Assumption 5.5, we can easily conclude that $\|\tilde{b}(t)\| \leq \tilde{b}^* = \sum_{i=n_{l+1}}^{n} \tilde{b}_i^*$, where $\tilde{b}(t) = \text{col}(\tilde{b}_{n_{l+1}}(t), \cdots, \tilde{b}_n(t))$.

Suppose the leaders are fixed, the dynamics of the followers can be described as

$$\dot{p}_i(t) = u_i^f(t) + \omega_i \quad i \in \mathcal{V}_f. \tag{5.52}$$

Now, we would like to present the following result of the fault-tolerant analysis of the multi-robot network under the proposed control protocol.

Theorem 5.3. *Consider the single-integrator system with the exogenous disturbance and actuator failures. Under Assumption 5.1-5.5, let* $K = 2n\boldsymbol{s}_0$, *by choosing*

$$\gamma = \sqrt{K/\rho^* a \lambda_{min}(\mathcal{B}_{ff})}$$

and

$$\rho^* bh\lambda_{min}(\mathcal{B}_{ff}) > 2K, \tag{5.53}$$

the formation error δ *converges to the bound set* $\mathcal{S}$

$$\mathcal{S} = \left\{ \delta : \|\delta\|^2 \leq \frac{4\gamma^2(F+\tilde{b}^*)^2 K}{\rho^* a\lambda_{\min}(\mathcal{B}_{ff})} \right\}.$$

in a finite time.

Proof. By implementing the protocol (5.2), the compact form of (5.52) can be written as

$$\dot{p} = (a + b\frac{\dot{\mu}}{\mu}) \begin{bmatrix} 0 & 0 \\ 0 & \bar{\rho}(t) \end{bmatrix} \bar{H}^\top (g^* - g) + \omega + \tilde{b}(t). \tag{5.54}$$

Choosing Lyapunov function as $V = \frac{1}{2}\|\delta\|^2$. The derivative of V can be described as

$$\begin{aligned} \dot{V} &= \delta^\top \dot{p} \\ &= (a + b\frac{\dot{\mu}}{\mu})\delta^\top \begin{bmatrix} 0 & 0 \\ 0 & \bar{\rho}(t) \end{bmatrix} \bar{H}^\top (g^* - g) + \delta^\top(\omega + \tilde{b}(t)) \\ &\leq (a + b\frac{\dot{\mu}}{\mu})\rho^*(p - p^*)^\top \bar{H}^\top (g^* - g) + \delta^\top(\omega + \tilde{b}(t)). \end{aligned} \tag{5.55}$$

The last inequality can be obtained by Assumption 5.5. By average inequality, we have

$$\begin{aligned} \delta^\top(\omega + \tilde{b}(t)) &\leq \|\delta^\top\|(\|\omega\| + \|\tilde{b}(t)\|) \\ &\leq \|\delta^\top\|(\|\omega\| + \tilde{b}^*) \\ &\leq \frac{\gamma^{-2}}{4}\|\delta\|^2 + \gamma^2(\|\omega\| + \tilde{b}^*)^2 \end{aligned} \tag{5.56}$$

Choosing

$$\gamma = \sqrt{\frac{K}{\rho^* a\lambda_{\min}(\mathcal{B}_{ff})}} \tag{5.57}$$

According to (5.37)-(5.39), (5.41), and (5.43), we can get

$$\begin{aligned} \dot{V} \leq & -\frac{\rho^* a\lambda_{\min}(\mathcal{B}_{ff})}{2K} V - \frac{\rho * b\lambda_{\min}(\mathcal{B}_{ff})}{2K}\frac{\dot{\mu}}{\mu} V \\ & + \gamma^2(F + \tilde{b}^*)^2 \\ = & -a_f V - b_f \frac{\dot{\mu}}{\mu} V + \gamma^2(F + \tilde{b}^*)^2 \end{aligned} \tag{5.58}$$

with $a_f = \frac{\rho^* a\lambda_{\min}(\mathcal{B}_{ff})}{2K}$ and $b_f = \frac{\rho^* b\lambda_{\min}(\mathcal{B}_{ff})}{2K}$.

From Lemma 5.3, we have

$$\|\delta(t)\|^2 \begin{cases} \leq \mu^{b_f} e^{-a_f t}\|\delta(0)\|^2 + 2\epsilon_f(t), & t \in [0, T) \\ \leq 2\gamma^2(F + \tilde{b}^*)^2/a_f, & t \in [T, \infty) \end{cases} \tag{5.59}$$

where

$$\epsilon_f(t) = (\frac{T-t}{b_f h - 1} - \frac{T\mu^{-b_f}}{b_f h - 1})\gamma^2(F + \tilde{b}^*)^2. \tag{5.60}$$

Similar to the analysis in Theorem 5.1, we can find that the formation error δ converges to the bound set $\mathcal{S}$ in finite time T from Lemma 5.3. This completes the proof. □

Remark 5.6. *The performance of the finite-time controller is affected by the efficiency factor and the output bias of the actuator channel. The formation error is closer to zero for smaller output bias and larger control gain a, which can reduce the effect of the actuator failures. From* (5.59)*, it can be obtained that the decrease of $\|\delta\|$ is faster for larger a_f, b_f, and ρ^*. Hence, the convergence rate of the formation error is determined by the boundary of the efficiency factor.*

5.4 Simulation and Experimental Results

To verify the effectiveness of the obtained results, Matlab simulation results and hardware experimental results using real mobile robots are shown in this section.

5.4.1 Formation Tracking Performance without Exogenous Disturbances

In this section, a simulation case study performed in Matlab is presented to validate the feasibility of the control protocol (5.2) without exogenous disturbances. Four omnidirectional mobile robots (i.e., two fixed leaders and two followers) with single-integrator dynamics are used in the task. All the robots are expected to form a square-shaped target formation using bearing-only measurements. The predefined settling time is set as $T = 50$ s. In Fig. 5.1, the initial positions of the leaders (shown as green star and blue star) are $(1, 0)$ and $(5, 0)$, respectively. For the followers (marked by pink and yellow nodes), we choose their positions as $(-1.5, -2)$ and $(7.5, -1.5)$, which satisfy the conditions in Theorem 5.1. For the parameters, we set $a = 2$, $b = 5$, $h = 6$

Table 5.1: Selection of a, b, and h

	a	b	h
Example 1	1	1	1
Example 2	2	2	5
Example 3	2	4	8
Example 4	4	5	10

which satisfy the condition (5.8). The formations of the robots at $t = 0$ s, $t = 10$ s, and $t = 50$ s are linked by blue dash lines, purple dash lines, and red solid lines, respectively. The pink and the yellow dotted lines are the trajectories of the followers from $t = 0$ s to $t = 50$ s. Control inputs of the followers along the X and Y axes are illustrated in Fig. 5.2(a) and Fig. 5.2(b), respectively. It can be seen that the designed inputs are uniformly bounded and C^1 smooth as proved in Theorem 1. Fig. 5.3 shows that the formation tracking error $\|p - p^*\|$ reaches zero at $t = 50$ s. From the observed results, all the robots can form the target square formation within the given finite time T using bearing-only measurements.

In order to explore the performance of the finite-time convergence with different parameters, we design a simulation case study with four examples shown in Table 5.1. By implementing the proposed FTBO protocol, the time variation of the formation errors are shown in Fig 5.4. It can be observed that the finite-time convergence can not be achieved if the parameters are chosen from Example 1. Moreover, the formation error still can not converge to zero in the predefined settling time even though we increase the parameters shown in Example 2. However, when we increase the parameters such that they satisfy the conditions on Theorem 5.1, such as Example 3 and 4, The formation error will converge to zero in the finite-time. Furthermore, if we continue to increase the parameters (shown in Example 4), the formation error can also converge to zero in the finite time with a faster convergence rate compare with Example 3. Hence, the finite-time formation task can only be completed if the selection of the parameters satisfy the conditions on Theorem 5.1.

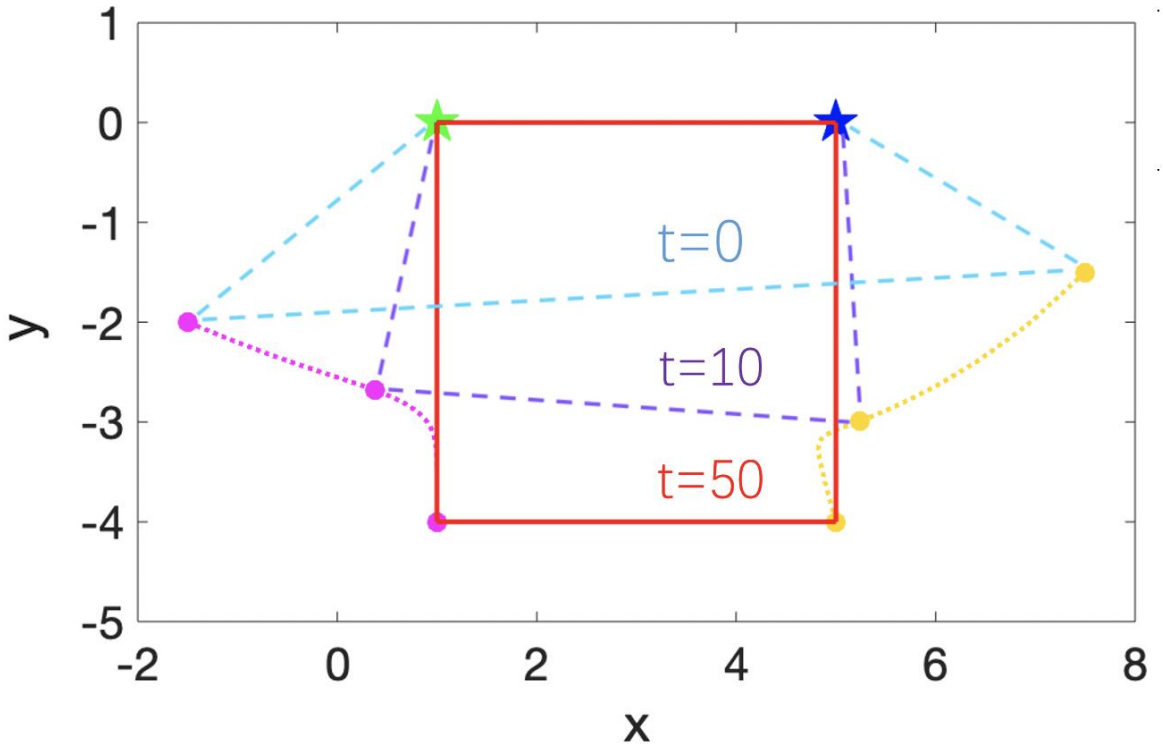

Figure 5.1: Positions of the robots at different time instants.

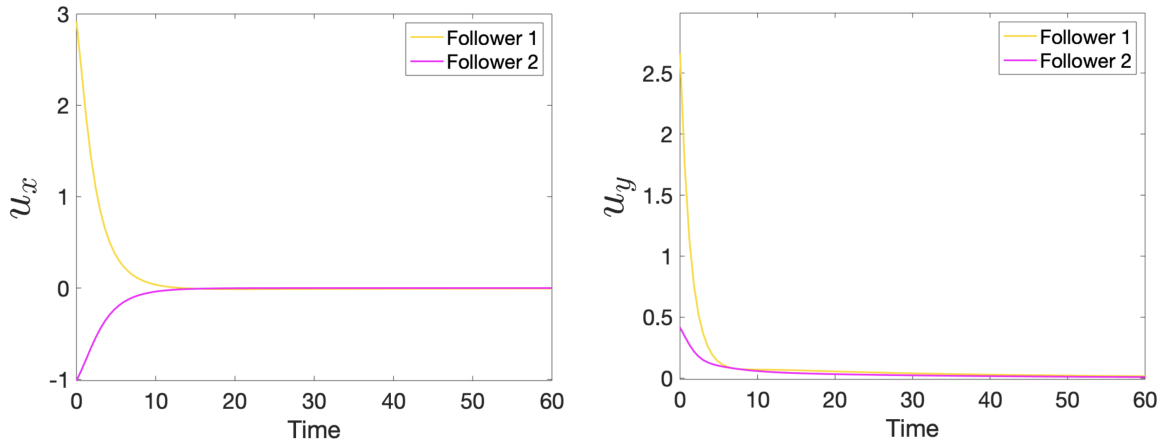

(a) (b)

Figure 5.2: Control inputs of the followers. (a) Along the X-axis. (b) Along the Y-axis.

5.4.2 Formation Tracking Performance with Exogenous Disturbances

We design the simulations to validate the effectiveness and the continuity of the FTBO controller with exogenous disturbance. Five UAVs, with two leaders and three followers, are used in this task. These UAVs aim to attain a pentagon shape desired formation

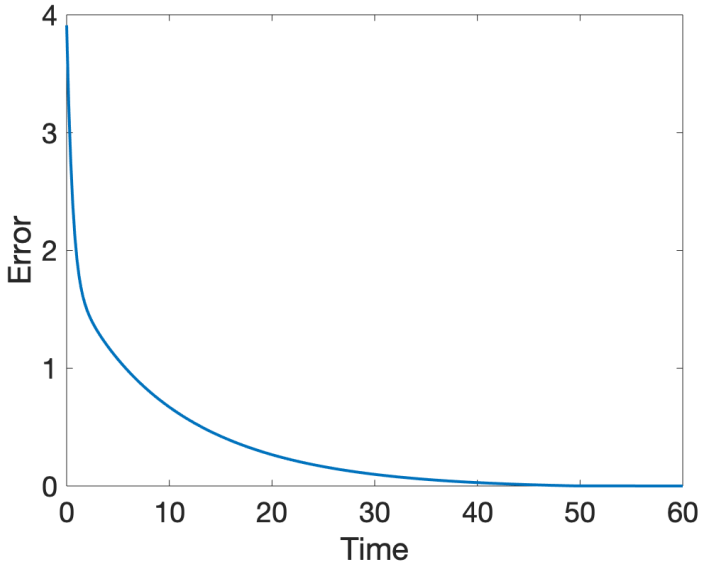

Figure 5.3: Time variation of the formation tracking error $\|p - p^*\|$.

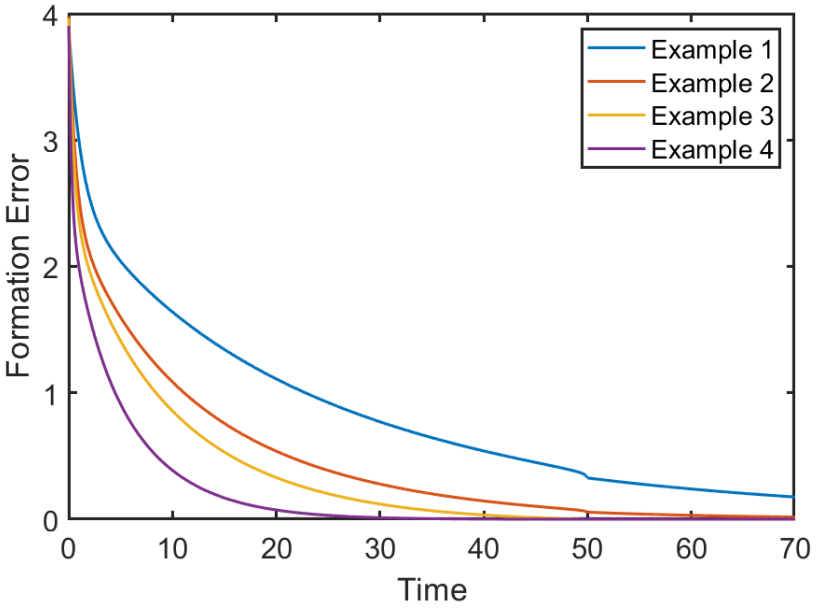

Figure 5.4: Time variation of the formation tracking error for four examples with different parameter shown in Table 5.1

in a 3D space via bearing-only measurements in the presence of unknown exogenous disturbances with the boundary 0.1. We set the predefined convergence time $T = 50$ s. The positions of the two fixed leaders (marked by blue and green squares) in the x-y-z plane are selected as $(2.5, 2, 0)$ and $(2.5, 5, 0)$, respectively. The initial positions of three followers are selected as $(2, 6, 4)$, $(4, 1, 3)$, and $(1, 3, 0.5)$ respectively. The interaction topology between each agent is represented by red solid lines in 5.5 (a). For the parameters, we first choose $a = 2$. After that, we can estimate the boundary of bh

according to (5.34) in Theorem 5.2 because K is related to a and initial state , and $\lambda_{min}(\mathcal{B}_{ff})$ can be determined by the interaction topology. Hence, we select $b = 8$ and $h = 5$ which satisfy the condition in Theorem 5.2.

By implementing Algorithm 1, the trajectories of the UAVs during the formation forming mission are shown in Fig. 5.5. We adopt the yellow, pink, and dark green dotted lines to denote the movements of the followers from $t = 0$ s to $t = 50$ s. The formations of the UAVs are captured at time instants $t = 0$ s, $t = 5$ s $t = 15$ s, and $t = 50$ s (From $(a) - (d)$ in Fig. 5.5), respectively. Fig. 5.6 shows the control actions of the followers during the mission. From the curves of the control inputs, it can be concluded that the controller can converge to zero in finite-time smoothly. Fig. 5.7 reveals that $\|\delta\|$ (represented by a blue solid line) will converge to a bound set at $t = 50$ s. The tracking errors of three followers are denoted by the yellow, pink, and dark green dash lines. As can be seen from all these figures, the bearing-only formation tracking task has been accomplished by the proposed finite-time protocol under unknown external disturbances.

5.4.3 Fault-Tolerant Formation Tracking with Different Parameters

In this section, four simulation case studies (with different efficiency factors and output bias) are conducted to explore the relationship between the fault parameters and the performances of the controller in the presence of the exogenous disturbance. The selection of ρ^* and $\bar{b}^*$ is presented in Table 5.2. $\rho_i(t)$ and $\tilde{b}_i(t)$ are generated randomly at any time t to satisfy Assumption 5 for each robot to simulate the unknown actuator failures. Twelve UAVs, with three leaders and nine followers, are used to complete the formation task within the finite-time $T = 50$ s. The interaction topology between these UAVs is shown in Fig. 5.8. These UAVs aim to attain the desired formation as two equilateral triangles in a 2D space via bearing-only measurements in the presence of unknown exogenous disturbances with boundary 0.1.

In order to satisfy the conditions in Theorem 5.3, we set the parameters as $a = 2$,

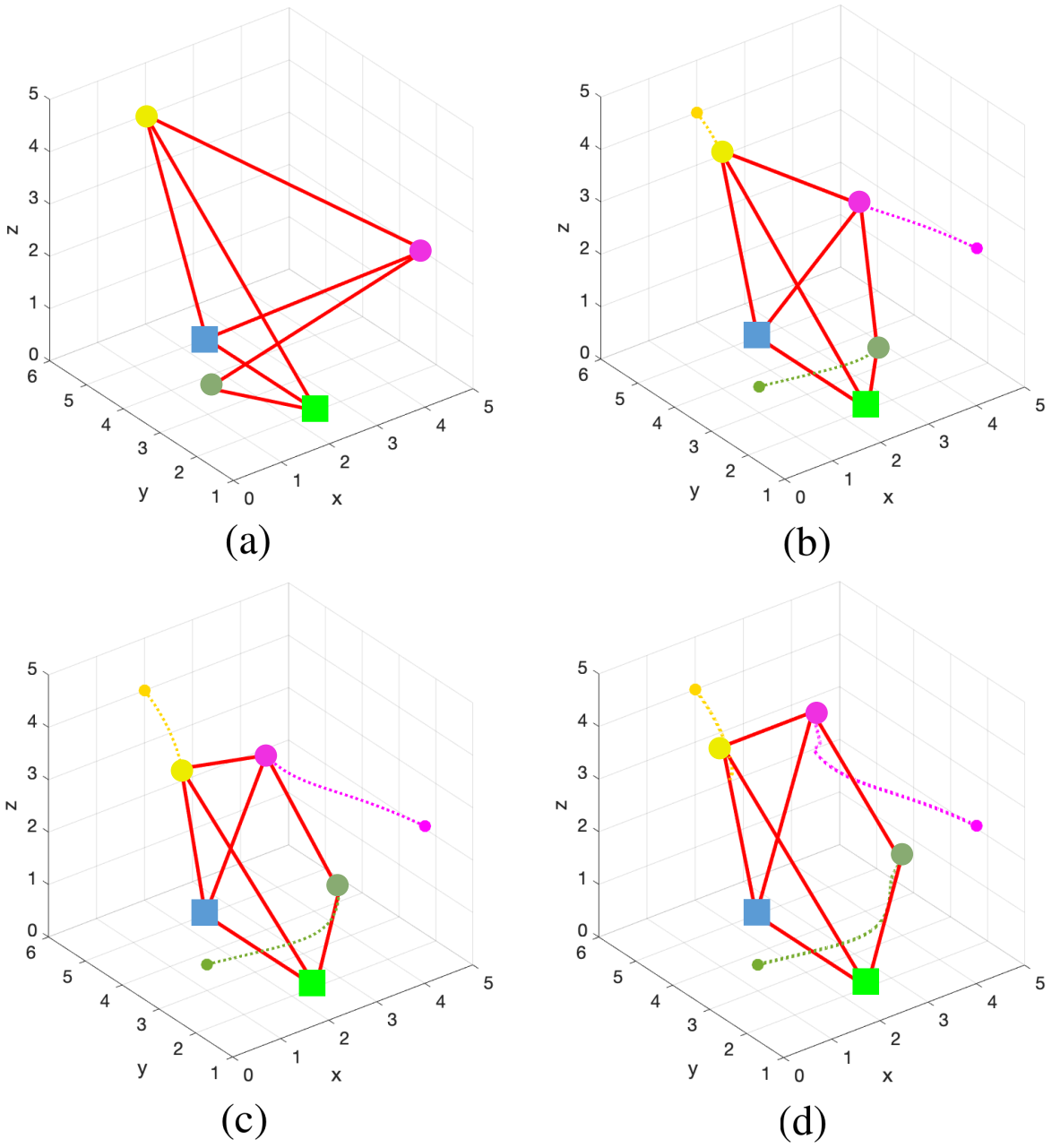

Figure 5.5: Trajectories of the networked UAVs at different time instants during the formation forming mission. (a) $t = 0$ s; (b) $t = 5$ s; (c)$t = 15$ s and (d) $t = 50$ s.

$b = 8$, and $h = 5$ for all the examples. By implementing the controller to (5.52), the trajectories and the tracking errors of the mobile robots during the formation forming mission are shown in Fig. 5.9 and Fig. 5.10 ($(a) - (d)$ represent the example 1-4). The positions of the three fixed leaders (marked by three yellow stars) are selected as $(-2, 0)$, $(0, 0)$, and $(2, 0)$, respectively. We select the same initial positions of the nine followers for all the examples. It can be concluded from (a), (b), and (d) in Fig. 5.9 that different efficiency factors (ρ^*) affect the performance slightly if the parameters a,

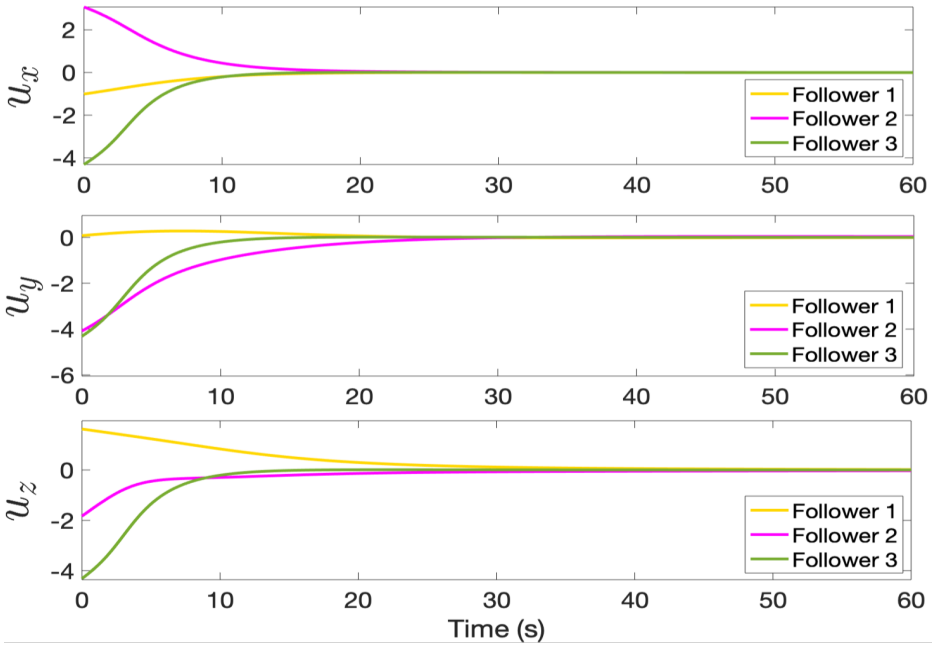

Figure 5.6: Control actions of the follower UAVs along the X-axis, Y-axis and Z-axis.

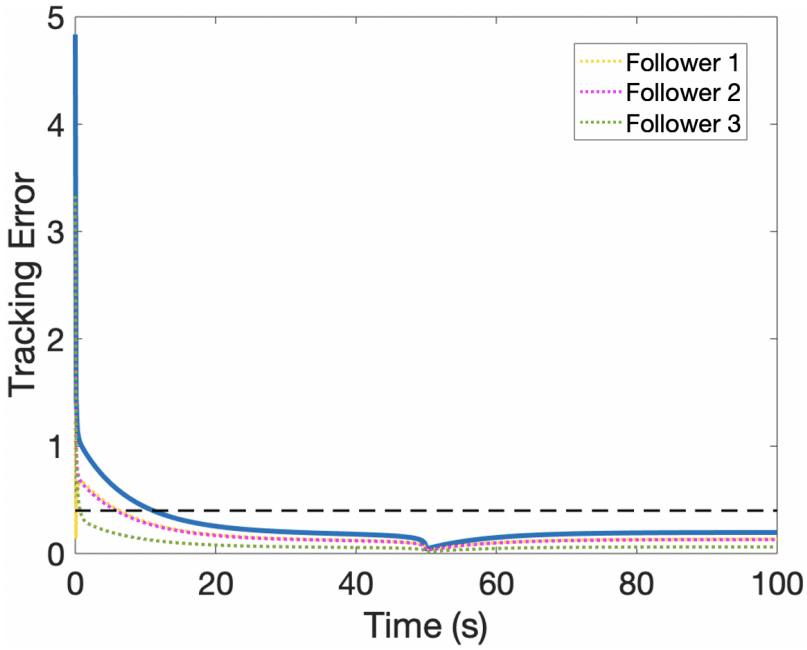

Figure 5.7: Time variation of the formation tracking error. The black dash line denotes the computed bound.

b, and h are chosen appropriately to satisfy the conditions in Theorem 5.3. We can also obtain that different efficiency factors can affect the convergence rate of some followers from (a), (b), and (d) in Fig. 5.10. From (b) and (c) in Fig. 5.9 and Fig. 5.10, we can conclude that the bound set $\mathcal{S}$ is expanded for large output bias $(\bar{b}^*)$. Hence, the tracking error will increase, and the final formation shape will be affected in a certain

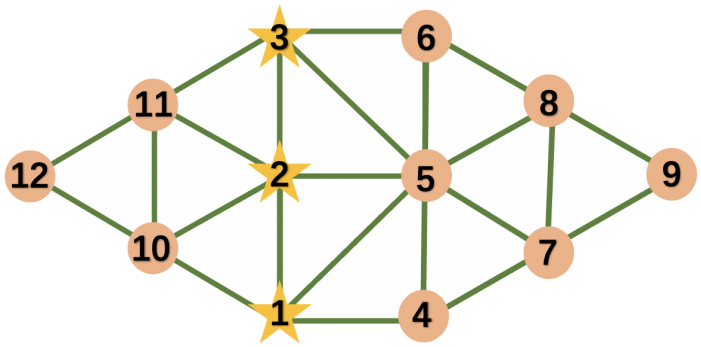

Figure 5.8: Interaction topology between each UAV. The three yellow stars (labelled by 1,2,3) are leaders, the nine circles (labelled from 4 to 12) are followers. The communication between each agent is denoted by green solid lines.

Table 5.2: Selection of ρ^* and $\bar{b}^*$

	ρ^*	$\bar{b}^*$
Example 1	0.8	0.05
Example 2	0.5	0.05
Example 3	0.5	0.2
Example 4	0.3	0.05

degree for large output bias. From all these figures and analyses, it can be concluded that the bearing-only fault-tolerant formation tracking task has been accomplished by the proposed finite-time protocol under unknown external disturbances.

5.4.4 Comparison and Discussion

In recent years, some bearing-based formation control methods have been developed in the literature. In [118, 120, 121], the signum functions were used in the designed protocols to ensure finite-time convergence. However, the controller becomes non-smooth, and the settling time depends on the initial state. To overcome this limitation, an improved bearing-based finite-time controller for double-integrator was considered in a recent work [123]. However, the position measurements are still required in the proposed algorithm, which increases the sensing requirements in the hardware implementation. Compared with those aforementioned works related to bearing-based control protocol design, the proposed FTBO protocol also facilitates robustness against exogenous disturbance and actuator faults.

To highlight the superior robust performance of the FTBO protocol proposed in this

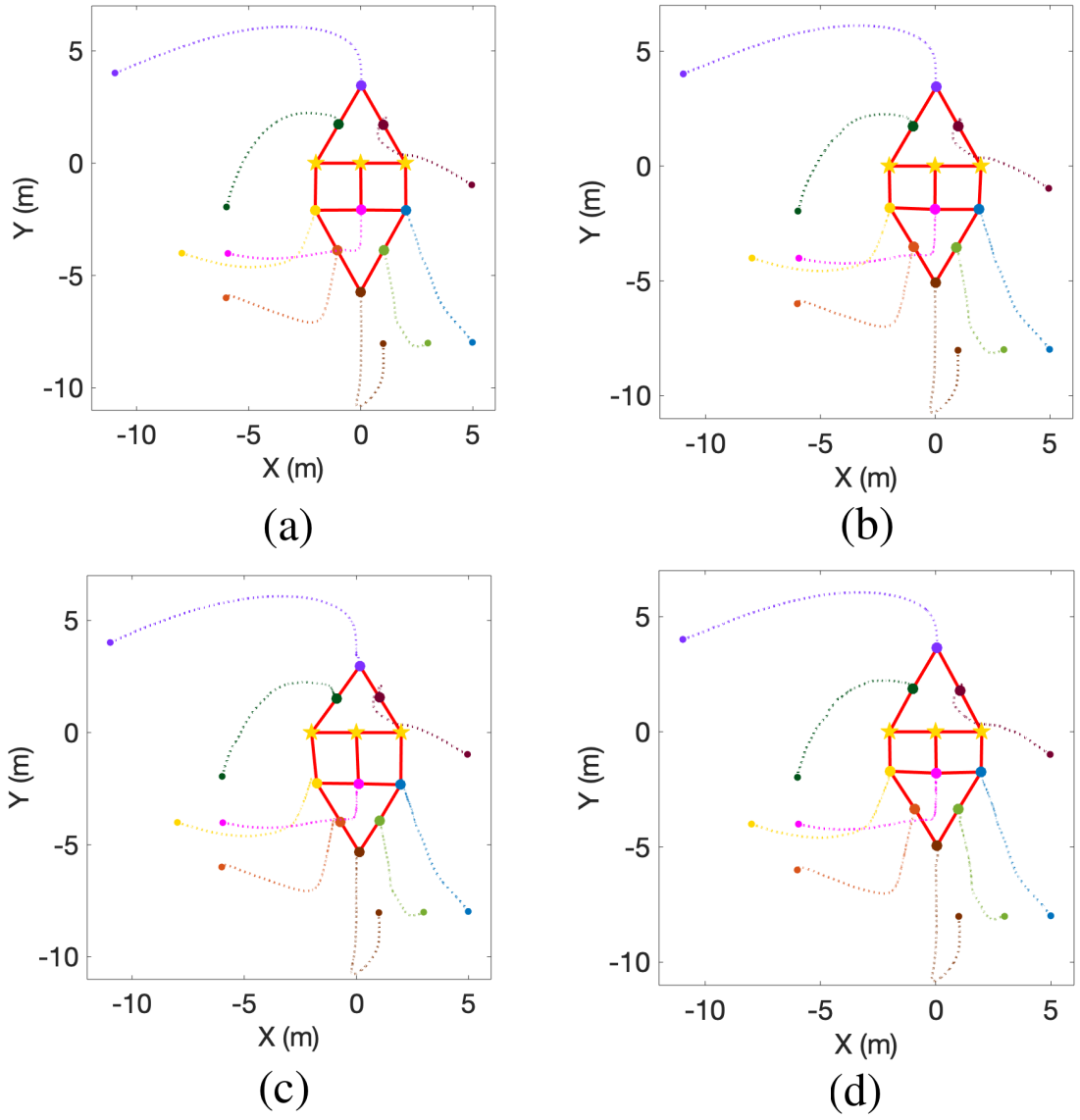

Figure 5.9: Trajectories of the followers for Example 1 (a), Example 2 (b), Example 3 (c), and Example 4 (d).

chapter, we make a comparison between the proposed controller and the conventional bearing-only method proposed in [1], which adopts the same scaling function $\mu(t)$ with different forms of the bearing-based scheme. According to the conventional results, the convergence rate of the traditional method relies on the initial formation error, which is possible to affect the performance of the controller under the exogenous disturbance and actuator failures. In this comparison, four UAVs, with two leaders and two followers, are used to attain the desired square formation via bearing-only measurements in the presence of unknown exogenous disturbances with a boundary of 0.05. The boundary of the efficiency factor (ρ^*) and the output bias ($\bar{b}^*$) are chosen as 0.3 and

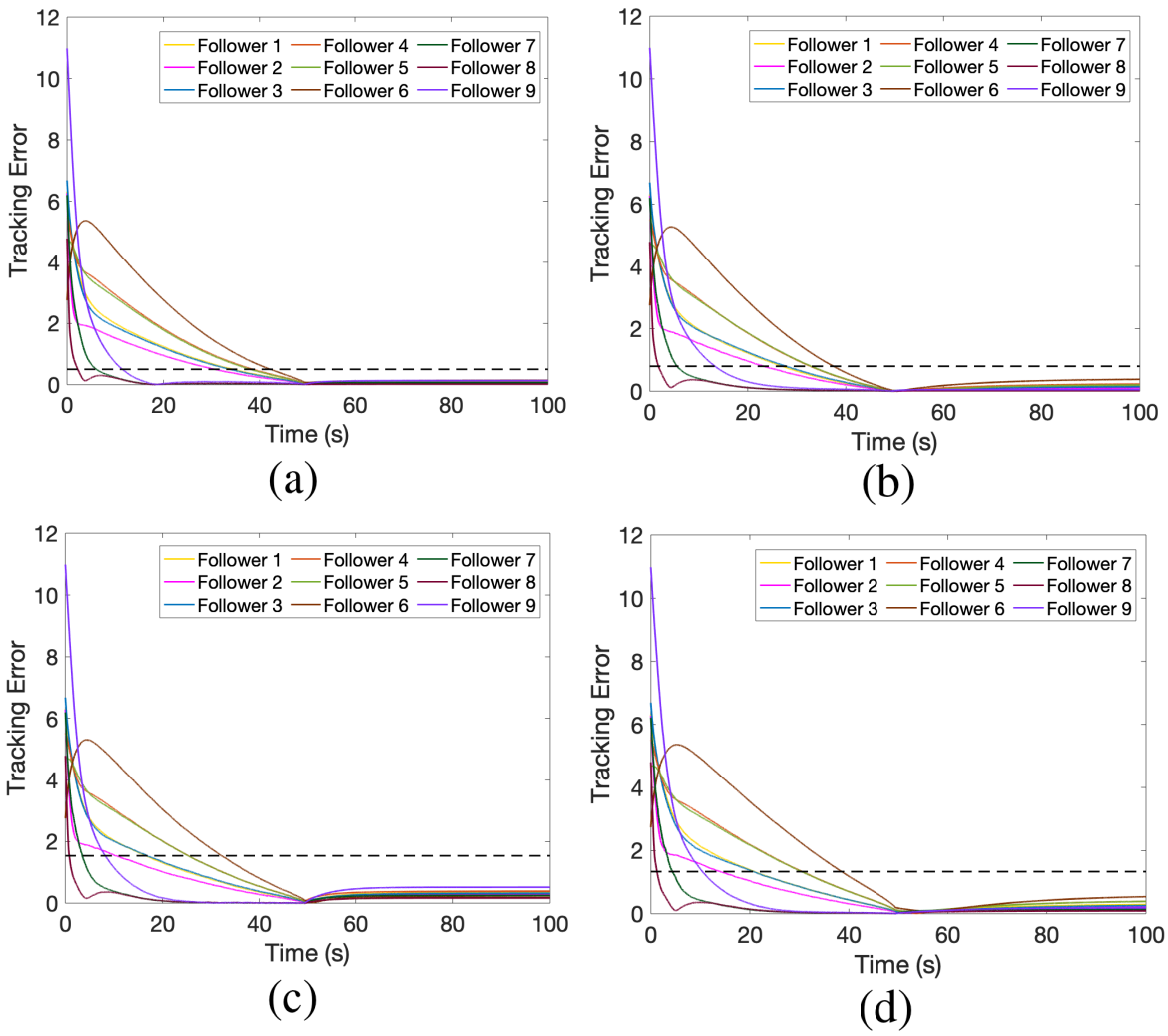

Figure 5.10: Tracking error of the followers for Example 1 (a), Example 2 (b), Example 3 (c), and Example 4 (d). The black dashed line denotes the computed bound for each example.

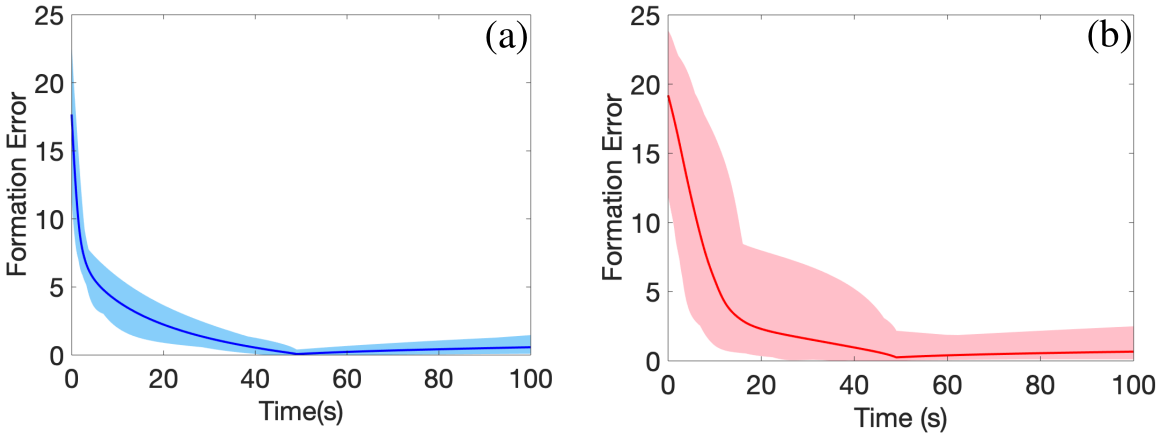

Figure 5.11: The performance of (a) the proposed controller and (b) the conventional method proposed in [1].

0.05. For each controller design, we choose the same interaction topology and the same parameters as shown in Section A. The initial states of the leaders are set as $[0, 0]$ and $[6, 0]$. The initial states of the followers are selected randomly from $[1, 11] \times [1, 11]$. 50 simulations are run for both controllers.

The performances of the proposed protocol and the conventional bearing-only protocol are demonstrated in Fig. 5.11(a) and (b), respectively. The formation error is defined as $\|p - p^*\|$. The blue and red zones display the 50 times simulation results of the protocols proposed in this chapter and the conventional strategy, and the blue and red solid lines represent the average values. It can be obtained that the formation error of the proposed protocol can converge to a small bound set under the exogenous disturbance and actuator faults with any initial state of the followers. However, under the conventional method, the formation tracking error becomes large if the initial positions of the followers are far away from the leaders. Hence, compared to the conventional controller, the proposed approach shows a better robust performance against the exogenous disturbances.

5.4.5 Experimental Validation

In this section, we conduct lab-based experiments to further verify the feasibility of the proposed method in real-world applications.

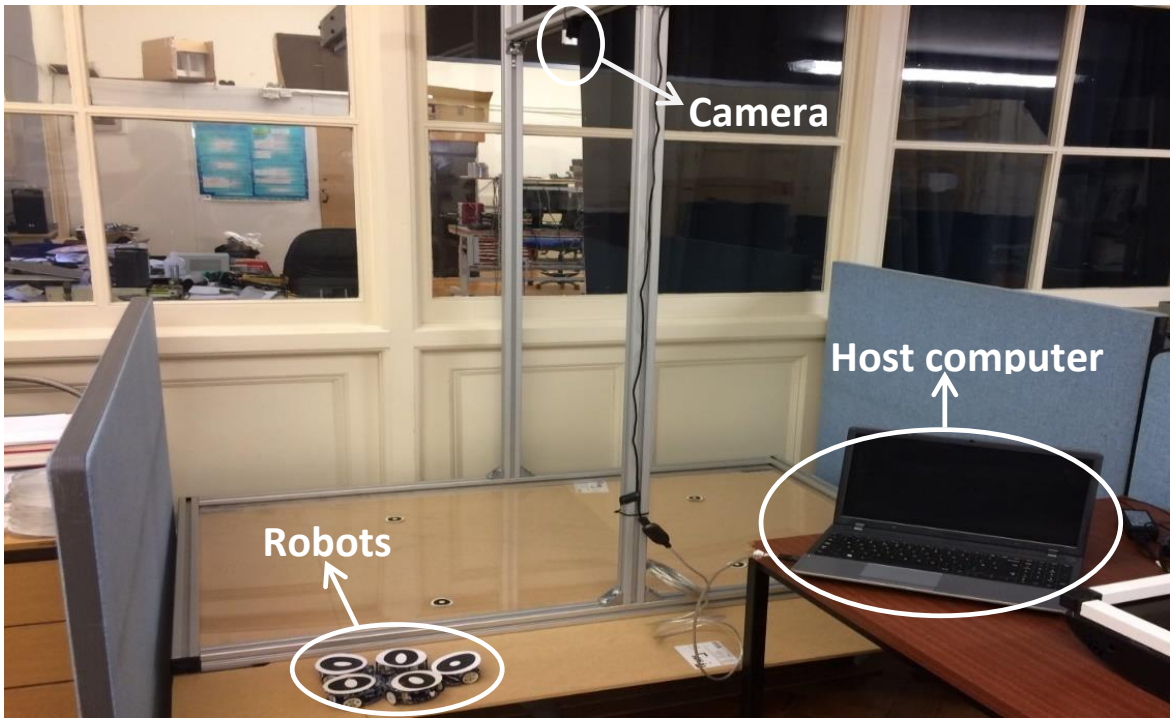

Figure 5.12: The experimental arena includes the overhead camera tracking system, the base station and the small-scale mobile robots.

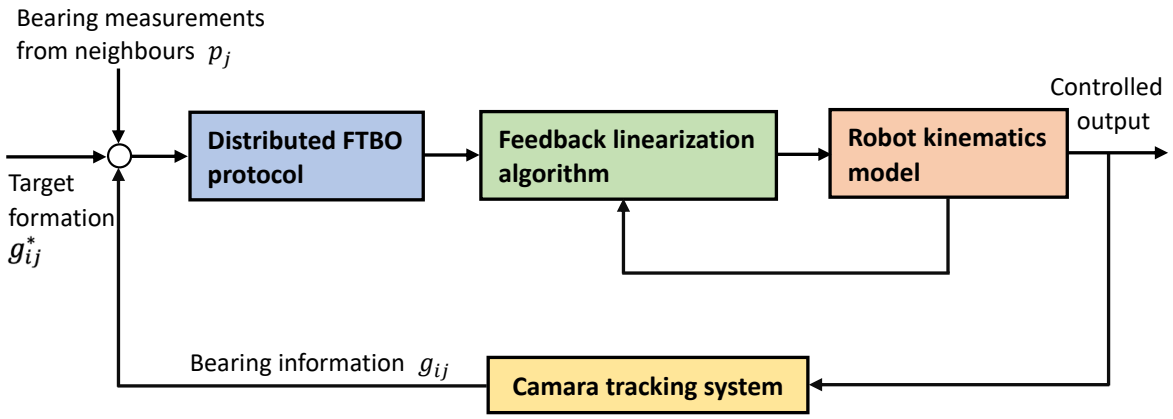

Figure 5.13: The control loop of the experiment. All the blocks are operated through the host computer shown in Fig. 5.12.

For the validation purpose, we use the wheeled mobile robot Mona [133] as the robotic platform. As shown in Fig. 5.12, the experimental platform includes a rectangular arena, a digital camera, and a laptop that operates the proposed control algorithm. The control architecture is shown in Fig. 5.13. The blue block denotes the controller module with the distributed FTBO protocol. The relative bearing between the neighbours is detected by the camera tracking system [134] and then transmitted to the controller module via the ROS (Robot Operating System) communication framework

in the host computer. Hence, we can get the velocities of each robot along x-axis and y-axis. After that, the linear and angular velocities of each robot can be acquired by the feedback linearisation algorithm [129]. Then, we can obtain the velocities of the wheels according to the kinematic model as the output. All the blocks shown in Fig. 5.13 are operated through the host computer shown in Fig. 5.12. The controlled output (velocities of the wheels) is transmitted to each follower by the RF (Radio Frequency) module attached on the Mona robot.

In the experiment, four mobile robots (including two leaders and two followers) aim to achieve a square formation in a given 2D arena. We choose $T = 30$ s as the desired settling time. In the beginning, the four robots were randomly placed in the arena. The positions of the mobile robots during the experiment are shown in Fig. 5.14. The trajectories and the formation tracking error are given in Fig. 5.15 and Fig. 5.16, respectively. We emphasise that although the camera tracking system may provide centralised measurements to all the robots, in view of a distributed implementation, each robot only used relative information from its neighbours. The experimental results verified that the designed coordination strategy fulfils the desired objectives in the presence of certain real disturbances such as communication delays and actuator noises.

To further explore the robustness of the FTBO algorithm when the leaders are not fixed, we execute a case study with four mobile robot followers and two virtual moving leaders in a 2D space. The trajectories of the virtual leaders are designed as

$$\dot{p}_i = \begin{bmatrix} \dot{p}_{ix}(t) \\ \dot{p}_{iy}(t) \end{bmatrix} = \begin{bmatrix} 0.02 \\ 0.02\sin(\frac{4\pi}{65}t) \end{bmatrix}, \quad i \in \mathcal{V}_l, \tag{5.61}$$

where $\mathcal{V}_l = \{1, 2\}$. We set the target formation of the followers as a square by bearing-only measurements in the presence of unknown exogenous disturbances with the boundary 0.06. The efficiency factor (ρ^*) and the output bias ($\bar{b}^*$) are selected as 0.5 and 0.05, and the parameters in the controller are chosen as $a = 5$, $b = 5$, and $h = 4$. The formation task is expected to be completed within the finite-time $T = 50$ s.

The movements of the followers under the proposed protocol with moving leaders are

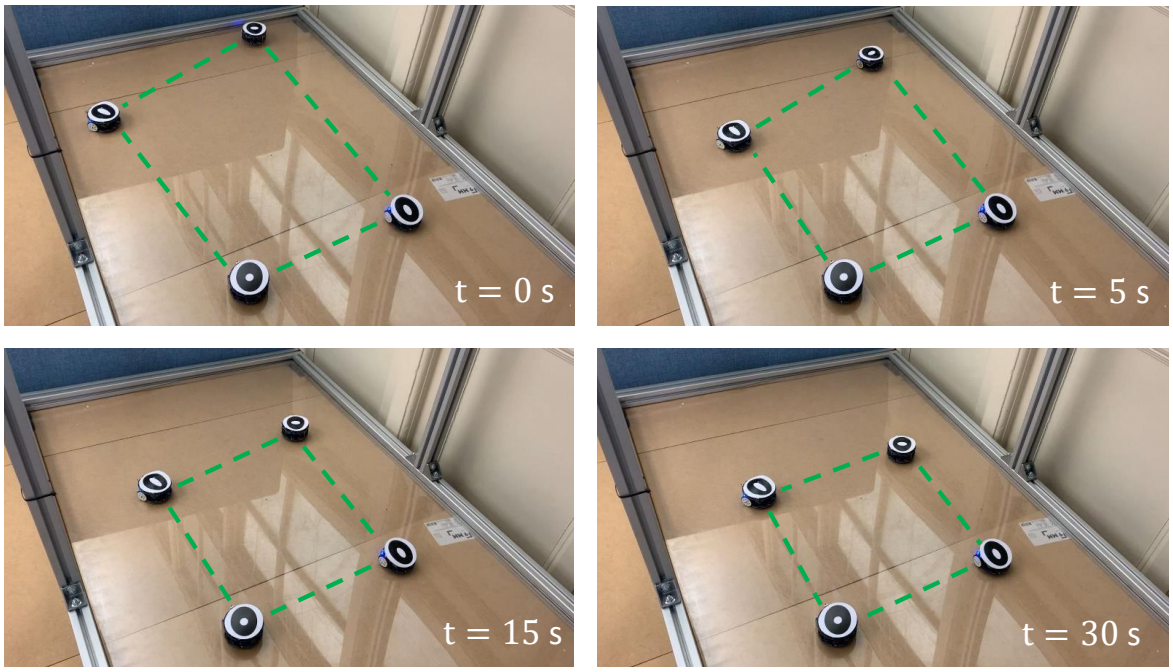

Figure 5.14: Progress of the formation tracking task being achieved by a group of four unmanned ground robots.

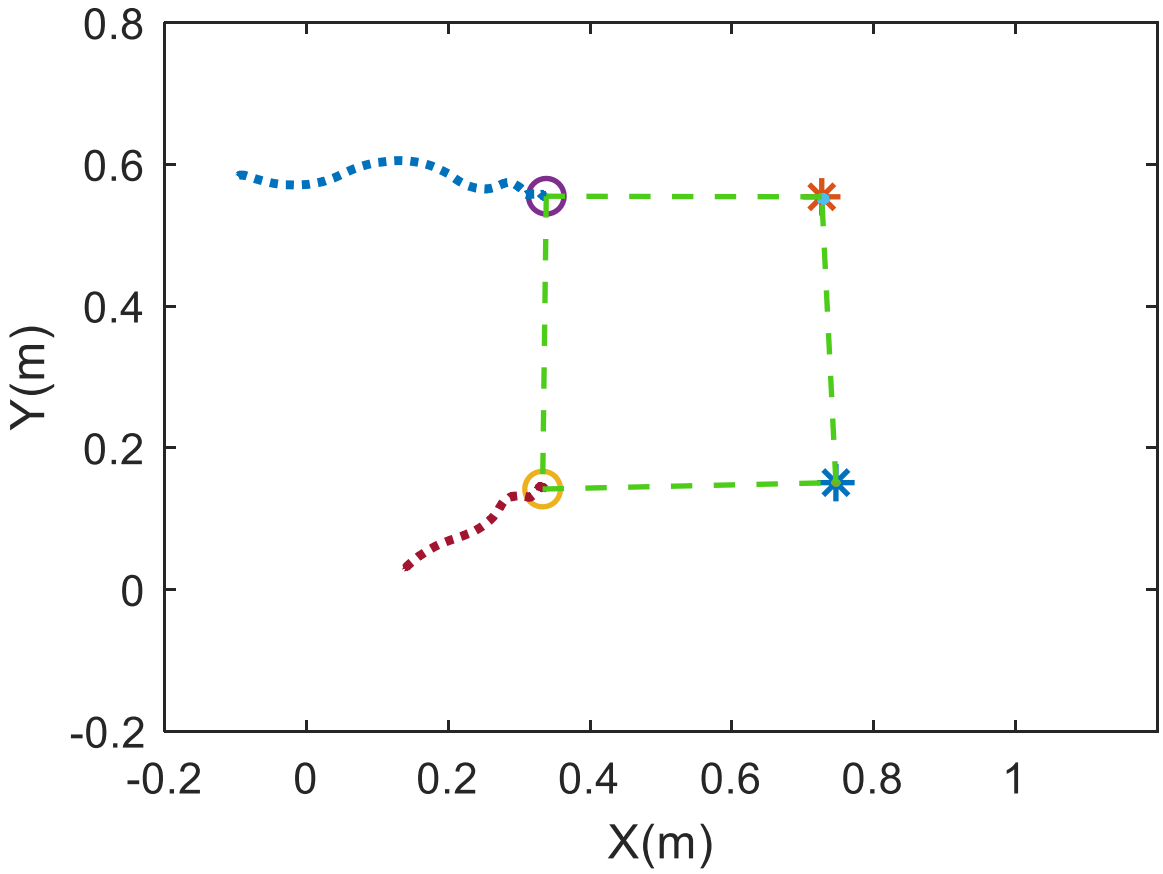

Figure 5.15: Trajectories of the robots in the experiment.

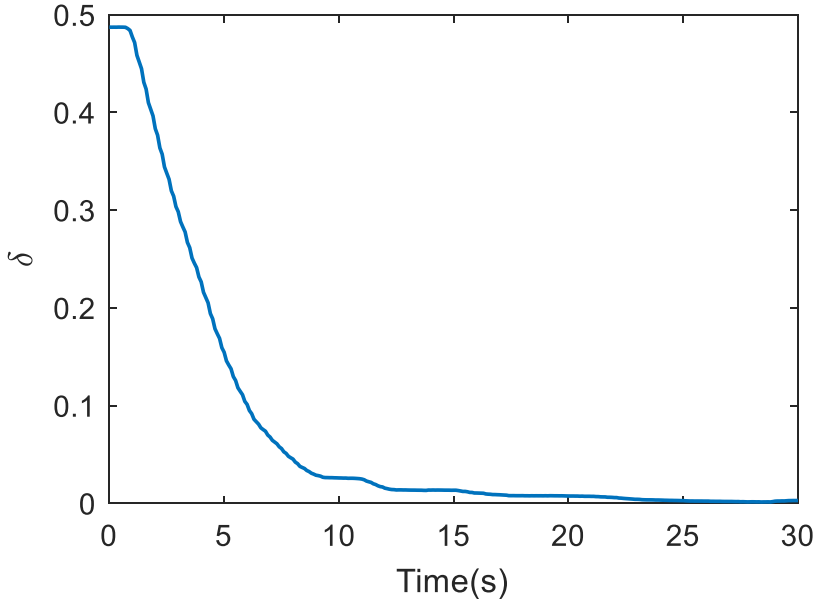

Figure 5.16: Time variation of the formation tracking error.

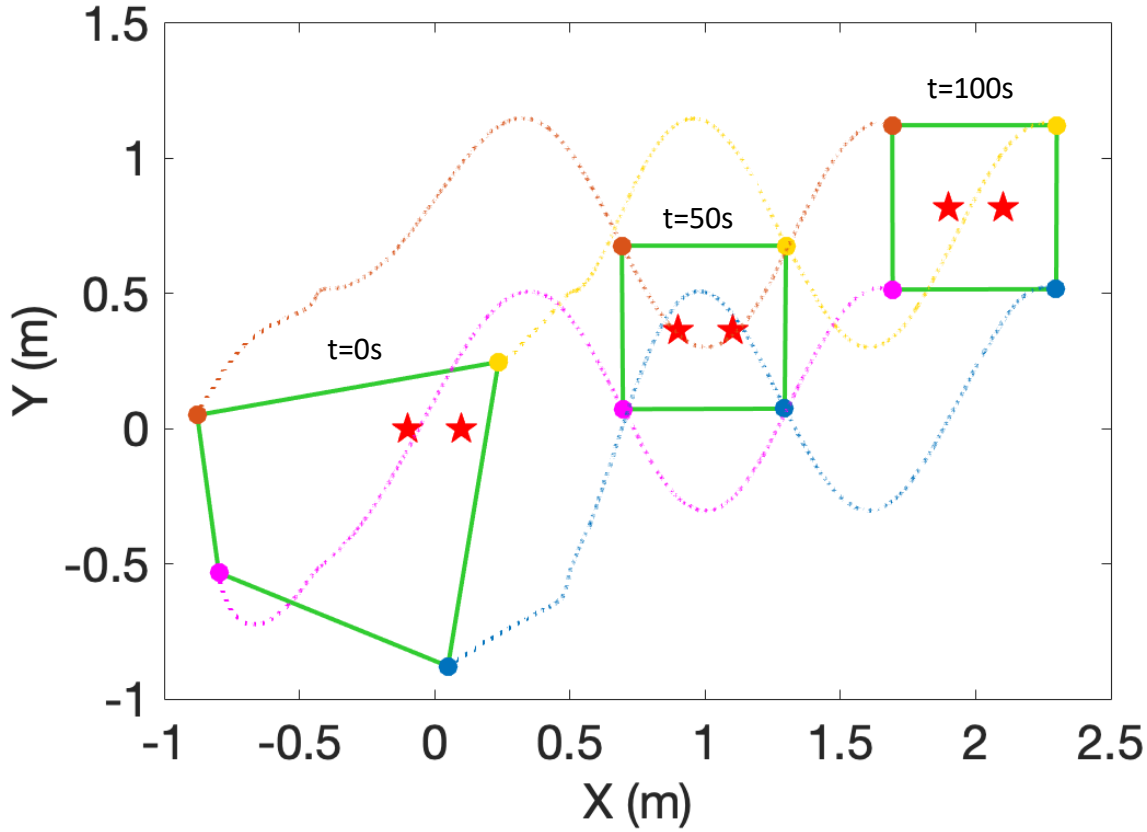

Figure 5.17: The trajectories of the followers with moving leaders.

illustrated in Fig. 5.17. The initial position of each robot is labelled by $t = 0$ s in Fig. 5.17, where the leaders are marked as two red stars. We use the dash curves with four different colours to denote the trajectories of four followers from 0 s to 100 s.

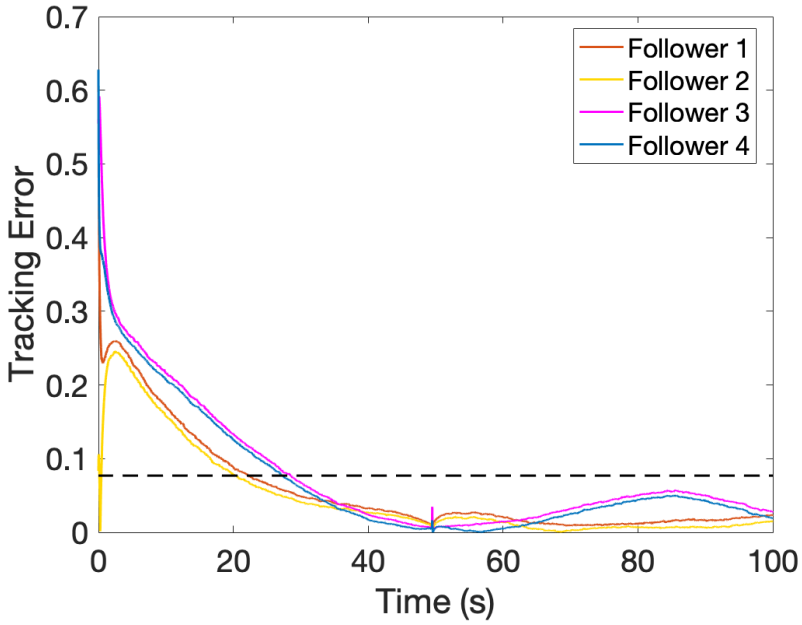

Figure 5.18: The formation tracking errors of the followers with moving leaders.

Fig. 5.18 displays that the tracking error of each follower during the formation task will converge to a bounded set in the finite-time. Hence, it can be obtained that the followers can converge to the target formation within a finite-time (labelled by $t = 50$ s in Fig. 5.17) when tracking the movements of the dynamic leaders, which validates the effectiveness of the proposed control design. It can be found that there exists a jump in the tracking error at $t = 50$ s, which is caused by the switching gain in the controller under the effect of the dynamic leaders. Based on that, the sudden change will influence the movement of the followers. Hence, the tracking error is affected by this sudden change and there exist a jump in Fig. 5.18.

5.5 Summary

In this chapter, the finite-time formation tracking problem with bearing-only measurements was addressed. A novel gradient-decent control protocol was proposed to let the multi-robot system achieve the target formation by measuring the relative bearings of their neighbours. Furthermore, the finite convergence time of the multi-robot network with exogenous disturbance was discussed and extended to the LTI system. Fault-tolerant analysis was also considered for these robots during the formation task. It was validated that the bound of the formation error could be guaranteed when

there were external disturbances and actuator failure in the robot dynamics. Finally, numerical simulations and practical experiments were provided to verify the obtained results. In the following chapter, the nonlinearity of the system will be considered when designing the bearing-only protocol.

Chapter 6

Formation-Containment Protocol and Application

6.1 Introduction

In the former chapters, we only consider the formation tasks for each robot. However, the robots should be assigned various goals for a complex project according to their function. In this chapter, we focus on the formation-containment issue in Objective 4. A novel distributed protocol is proposed to solve the formation-containment problem in a collaborative swarm system. Both single-integrator dynamics and double-integrator dynamics are considered in the control protocol design. For each robot, the controller only requires the relative state information from its neighbours, which ensures the asymptotic stability of the swarm when controlling large-scale robotic systems. The novelty of the control protocol for leaders is that it is robust in several conditions such as white noise perturbation, saturated input, etc., which has the potential to be used in extreme environments. The contributions of this chapter can be summarised as:

- A novel formation-containment control framework which only requires local relative state measurements is proposed.
- The convergence of the swarm system is guaranteed by the rigorous mathematical proof, and the feasibility of the proposed algorithm is analysed.
- Experiments using real robots were conducted to verify the effectiveness of the theoretical results.

The remainder of the chapter proceeds as follows. Section 6.2 illustrates the main problem of this chapter. Section 6.3 and 6.4 present the proposed formation-containment framework, from which the swarm system under the proposed coordinated algorithm is shown to satisfy asymptotically stable properties via a rigorous mathematical proof. Section 6.5 presents simulation results and Section 6.6 presents the experimental validation of the proposed strategy using laboratory-based small-scale mobile robots. Section 6.7 concludes the chapter.

6.2 Problem Description

Robots in the swarm system can be divided into leaders and followers, with each having different properties: i) the neighbours of a leader are only leaders, and ii) the neighbours of a follower can be leaders or other followers. The leaders are expected to form the desired formation and the followers are expected to converge into the convex hull formed by the leaders by a proper design. Due to the behavioural differences, the swarm system can be viewed as a heterogeneous swarm as described by Dorigo et al. [135]. The communication network among all the robots is described using Graph Theory. We use $\mathcal{G}_E$ to represent the interaction topology among the leaders.

Assume that there are $M(M < N)$ followers and $N - M$ leaders in the robot swarm. Let $\mathcal{V}_F = \{1, 2, ..., M\}$ and $\mathcal{V}_E = \{M + 1, M + 2, ..., N\}$ be the follower subscript set and leader subscript set respectively. Hence we have the follower's state $p_i(t)$ $(\forall i \in \mathcal{V}_F)$ and the leader's state $p_j(t)$ $(\forall j \in \mathcal{V}_E)$.

Definition 6.1. *[94] A swarm system is said to achieve containment if for any given bounded initial states and any $k \in \mathcal{V}_F$, there exists non-negative $\alpha_{k,j}(j \in \mathcal{V}_E)$ satisfying $\sum_{j=M+1}^{N} \alpha_{k,j} = 1$ such that*

$$\lim_{t\to\infty}(p_k(t) - \sum_{j=M+1}^{N} \alpha_{k,j} p_j(t)) = 0 \ . \tag{6.1}$$

Let the formation reference vector $h \in \mathbb{R}^{2(N-M)}$ denote the coordinate of the desired formation of leaders and $h^{\perp} \in \mathbb{R}^{2(N-M)}$ denote the coordinates of agents when the desired formation is rotated by 90°. The swarm system is said to achieve formation-containment if for any given bounded initial states, on condition that the agents of the

leaders globally converge to the desired formation, there exists non-negative $\alpha_{k,j}(j \in \mathcal{V}_E)$ satisfying $\sum_{j=M+1}^{N} \alpha_{k,j} = 1$ such that (6.1) holds.

6.3 Formation-Containment Protocol for Single Integrator Systems

6.3.1 Control Strategy

In this section, we aim to design the formation-containment control protocol for single-integrator systems. Consider N robots in the swarm system with single-integrator dynamics described by

$$\dot{p}_i(t) = u_i(t) \ , \tag{6.2}$$

where $p_i = [p_{i1}, p_{i2}]^\top \in \mathbb{R}^2$ is the coordinate for robot $i \in \{1, 2, ..., N\}$, and $u_i \in \mathbb{R}^2$ is the control input. In order to achieve formation-containment, inspired by [136], the control protocol for the leaders and followers is chosen as

$$u_i = \sum_{j \in \mathcal{N}_i} A_{ij}(p_j - p_i) \qquad i \in \mathcal{V}_E \ , \tag{6.3}$$

$$u_i = \sum_{j \in \mathcal{N}_i} w_{ij}(p_j - p_i) \qquad i \in \mathcal{V}_F \ , \tag{6.4}$$

where $\mathcal{N}_i$ represents the neighbors of agent i, w_{ij} is a non-negative gain and $A_{ij} \in \mathbb{R}^{2\times 2}$ are the constant control gain matrices with the form of

$$A_{ij} = \begin{bmatrix} a_{ij} & -b_{ij} \\ b_{ij} & a_{ij} \end{bmatrix}, \quad a_{ij}, b_{ij} \in \mathbb{R} \ . \tag{6.5}$$

In the formation control design process, we establish a formation matrix A which contains the formation information and the communication topology of the leaders. A is given by (6.6) as shown in the top of the next page, where A_{ij} is defined as zero matrices if $j \notin \mathcal{N}_i$. We note that A has a block Laplacian structure, hence the following vectors

$$\mathbf{1} = [1, 0, 1, 0, ..., 1, 0]^\top \in \mathbb{R}^{2(N-M)}$$

$$\mathbf{1}^\perp = [0, 1, 0, 1, ..., 0, 1]^\top \in \mathbb{R}^{2(N-M)}$$

satisfy $A\mathbf{1} = 0$ and $A\mathbf{1}^\perp = 0$.

$$A = \begin{bmatrix} -\sum_{j=2}^{N-M} A_{1j} & A_{12} & \dots & A_{1(N-M)} \\ A_{21} & -\sum_{j=1,j\neq 2}^{N-M} A_{2j} & \dots & A_{2(N-M)} \\ \vdots & \vdots & \ddots & \vdots \\ A_{(N-M)1} & A_{(N-M)2} & \dots & -\sum_{j=1}^{N-M-1} A_{(N-M)j} \end{bmatrix} \in \mathbb{R}^{2(N-M)\times 2(N-M)}, \tag{6.6}$$

Denote L as the Laplacian matrix corresponding to the interaction topology ($\mathcal{G}$) of the swarm system (6.2). L has the form

$$L = \begin{bmatrix} L_1 & L_2 \\ 0 & L_3 \end{bmatrix},$$

where $L_1 \in \mathbb{R}^{M\times M}$, $L_2 \in \mathbb{R}^{M\times(N-M)}$ and $L_3 \in \mathbb{R}^{(N-M)\times(N-M)}$, the following Lemma holds.

Lemma 6.1. *[128] Assume the interaction topology among leaders ($\mathcal{G}_E$) has a spanning tree and, for each follower, there exists at least one directed path from a leader, we have:*
(I) all eigenvalues of L_1 have positive real parts,
(II) each entry of $-L_1L_2$ is non-negative, and each row of $-L_1L_2$ has a sum of one.

Here, we present the following theorem to guarantee the convergence of a single-integrator system under the proposed formation-containment coordination.

Theorem 6.1. *Consider leaders and followers with single-integrator dynamics* (6.2) *and control protocol* (6.3) *and* (6.4). *Assume the interaction topology among leaders ($\mathcal{G}_E$) contains a spanning tree and, for each follower, there exists at least one directed path from a leader, then, for any $w_{ij} > 0$, the swarm system* (6.2) *achieves formation-containment if A_{ij} are selected such that*
(I) $\mathbf{1}$, $\mathbf{1}^\perp$, h and $h^\perp$ are linearly independent and $A\mathbf{1} = Ah = A\mathbf{1}^\perp = Ah^\perp = 0$,
(II) $Re\lambda(A) < 0$, where $\lambda(A)$ denotes the non-zero eigenvalues of A and $Re(\cdot)$ stands for the real part of the eigenvalue.

Proof. Let $\bar{L}_1 = L_1 \otimes I_2$ and $\bar{L}_2 = L_2 \otimes I_2$, where I_2 denotes the identity matrix with two dimensions. By using control protocol (6.3) and (6.4), the system can be written

as:

$$\begin{pmatrix} \dot{p}_F \\ \dot{p}_E \end{pmatrix} = \begin{bmatrix} -\bar{L}_1 & -\bar{L}_2 \\ 0 & A \end{bmatrix} \begin{pmatrix} p_F \\ p_E \end{pmatrix}, \tag{6.7}$$

where p_F and p_E are the states of followers and leaders, respectively.

On the one hand, for leaders, from (6.7), we have

$$\dot{p}_E = Ap_E \ , \tag{6.8}$$

the solution of (6.8) can be shown as

$$p_E(t) = e^{At}p_E(0) \ , \tag{6.9}$$

where $p_E(0)$ is the initial position of leaders.

Denote J as the Jordan form of A, the following case is given on condition that A has all Jordan blocks of order one. The general case follows similarly. Hence, we can obtain from (6.9) that

$$\begin{aligned} p_E(t) &= Qe^{Jt}Q^{-1}p_E(0) \\ &= \sum_{i=1}^{2(N-M)} r_i e^{\lambda_i t} q_i^\top p_E(0) \\ &= \sum_{i=1}^{2(N-M)} \left(q_i^\top p_E(0)\right) e^{\lambda_i t} r_i \ , \end{aligned} \tag{6.10}$$

where $r_i \in \mathbb{R}^{2(N-M)\times 1}$ and $q_i^\top \in \mathbb{R}^{1\times 2(N-M)}$ are the right and left eigenvectors of A respectively, and $\lambda_i (i = 1, 2, \cdots, 2(N-M))$ is the eigenvalues of A. From condition (I), we see that $\mathbf{1}$, $\mathbf{1}^\perp$, h and $h^\perp$ are four right eigenvectors respond to the four zero eigenvalues (denoted by λ_1, λ_2, λ_3 and λ_4, respectively). Furthermore, all the entries of the Jordan part of the four zero eigenvalues are zero. If we denote left eigenvectors of $\mathbf{1}$, $\mathbf{1}^\perp$, h and $h^\perp$ are $q_1^\top$, $q_2^\top$ $q_3^\top$ and $q_4^\top$, (6.10) can be written as

$$\begin{aligned} p_E(t) = &\sum_{i=5}^{2(N-M)} \left(q_i^\top p_E(0)\right) e^{\lambda_i t} r_i + \mathbf{1}q_1^\top p_E(0) \\ &+ \mathbf{1}^\perp q_2^\top p_E(0) + h{q_3}^\top p_E(0) + h^\perp {q_4}^\top p_E(0) \ . \end{aligned} \tag{6.11}$$

From condition (II), we know

$$\lim_{t\to\infty} e^{\lambda_i t} = 0 \quad \text{for any} \ \ i \geq 5 \ ,$$

so we let $t \to \infty$ in (6.11), then we have

$$\begin{aligned} p_E(t) \to \mathbf{1}q_1^\top p_E(0) + \mathbf{1}^\perp q_2^\top p_E(0) \\ + hq_3{}^\top p_E(0) + h^\perp q_4{}^\top p_E(0) \ , \end{aligned} \tag{6.12}$$

if we denote $c_1 = q_1^\top p_E(0)$, $c_2 = q_2^\top p_E(0)$, $c_3 = q_3^\top p_E(0)$ and $c_4 = q_4^\top p_E(0)$, they are four constants, so we can get

$$p_E(t) \to \mathbf{1}c_1 + \mathbf{1}^\perp c_2 + hc_3 + h^\perp c_4 \ , \tag{6.13}$$

that is to say, the leaders can converge to nothing but all translations, rotations, and non-negative scale factors of h, which also indicates that leaders can converge to the desired formation shape.

On the other hand, for followers, from (6.7), we have

$$\dot{p}_F = -\bar{L}_1 p_F - \bar{L}_2 p_E \ . \tag{6.14}$$

Since leaders globally converge to the desired formation, denoted by h_F, let $t \to \infty$ in (6.14), we obtain

$$\dot{p}_F = -\bar{L}_1 p_F - \bar{L}_2 h_F \ , \tag{6.15}$$

then, we solve (6.15) and have

$$\begin{aligned} p_F &= e^{-t\bar{L}_1}(p_F(0) - \int_0^t e^{s\bar{L}_1}\bar{L}_2 h_F \, \mathrm{d}s) \\ &= e^{-t\bar{L}_1}(p_F(0) + \bar{L}_1{}^{-1}\bar{L}_2 h_F) - \bar{L}_1{}^{-1}\bar{L}_2 h_F \ , \end{aligned} \tag{6.16}$$

where $p_F(0)$ is the initial position of the followers.

From Lemma 6.1 (I), all eigenvalues L_1 have positive real parts, that is to say, L_1 has no zero eigenvalue. Hence, L_1 is invertible and $\bar{L}_1$ is also invertible. We have

$$p_F = -\bar{L}_1{}^{-1}\bar{L}_2 h_F \ , \ \text{ when } \ t \to \infty \ . \tag{6.17}$$

By Lemma 6.1 (II), we can conclude that p_F satisfies Definition (6.1), and then the swarm system (6.2) achieves formation-containment. This completes the proof. □

Remark 6.1. *It can be seen that for each robot, the formation-containment protocol is fully distributed because the controller only requires the relative state information from*

its neighbours, which ensures the asymptotic stability of the swarm when controlling large-scale networked robots. One of the conditions of the proposed control strategy is the connectivity of the communication network. In the case when some robots are experiencing communication failures, if a proper network topology can be switched to connect all the robots, the robustness and stability of the whole swarm system can still be guaranteed as proved in Theorem 6.1. In the extreme situation where a robot loses communication with all the other robots, the remaining robots in the swarm will not be affected using the proposed coordination algorithm.

Remark 6.2. *From Theorem 6.1, we also indicate that for any $w_{ij} > 0$, the swarm system* (6.2) *achieves formation-containment if and only if leaders globally converge to the desired formation.*

Let $P = [h, h^{\perp}, \mathbf{1}, \mathbf{1}^{\perp}]$ and $USV^{\top} = P$ be the singular value decomposition (SVD) of P, where

$$U = [\overline{Q}, Q] \in \mathbb{R}^{2(N-M)\times 2(N-M)} \tag{6.18}$$

with $\overline{Q} \in \mathbb{R}^{2(N-M)\times 4}$ defined as the first 4 columns of U and $Q \in \mathbb{R}^{2(N-M)\times 2(N-M)-4}$ defined as the last $2(N-M)-4$ columns of U.

Lemma 6.2. *[137] Using Q in* (6.18)*, define*

$$\overline{A} = \overline{Q}AQ \in \mathbb{R}^{(2(N-M)-4)\times(2(N-M)-4)} \quad . \tag{6.19}$$

Matrices A and $\overline{A}$ have the same set of nonzero eigenvalues.

From Lemma 6.2, we can obtain that the projection operation in (6.19) removes the zero eigenvalues of A. By setting $a_{ij} = a_{ji}$ and $b_{ij} = -b_{ji}$ in (6.5) matrix A can be design symmetric. Hence, its eigenvalues are real and can be ordered, then A can be computed by solving the optimisation problem

$$\begin{aligned} A = \underset{a_{ij},\, b_{ij}}{\operatorname{argmax}} \quad & \lambda_1(-\overline{A}) \quad , \\ \text{subject to} \quad & AP = 0 \quad , \end{aligned} \tag{6.20}$$

where $\lambda_1(\cdot)$ denotes the smallest eigenvalue of a matrix.

From the Remark 6.2, in order to let the swarm system (6.2) achieve formation-containment, it is essential to design a proper A matrix that satisfies the conditions in Theorem 6.1. Motivated by [137], we can use the following algorithm to solve this issue.

Algorithm 2 Formation-containment gain design

1: Let $P = [h, h^{\perp}, \mathbf{1}, \mathbf{1}^{\perp}]$
2: Compute SVD of $USV^{\top} = P$
3: Define Q as the last $2n-4$ columns of U
4: Solve (6.20) using a SDP solver
5: **if** $j \in \mathcal{N}_i$ $(i \in \mathcal{V}_F)$ **then**
6: Set $w_{ij} = 1$
7: **else**
8: $w_{ij} = 0$
9: **end if**

Remark 6.3. *Even though obstacle avoidance is not considered in the proposed formation-containment coordination protocol design, the standard low-level obstacle avoidance algorithms can be easily integrated with the proposed framework during the real-world operation. Based on different scenarios and tasks, the low-level controller which is implemented in the robot can be changed, however, the proposed formation-containment coordination algorithm will remain the same.*

6.3.2 Robustness to Input Saturation

In real robotic systems, the velocity of each robot cannot exceed a certain value due to hardware constraints. Thus, any large control input will be saturated by a maximum allowed speed. This, however, does not affect the robots to accomplish the formation-containment task under the proposed control algorithm.

In order to prove that the control protocols (6.3) and (6.4) are robust to saturated inputs, the following Lemma is present here.

Lemma 6.3. *[138] Consider the family of switched system $\dot{x} = f_i(x)$, with $i = 1, 2 \cdots, N$. Let $V : \mathbb{R}^n \to \mathbb{R}$ be a positive definite, continuously differentiable, and radially unbounded function. If $\frac{\partial V}{\partial x} f_i(x) < 0$, $\forall x \neq 0$, $\forall i$ then the switched system is globally uniformly asymptotically stable.*

Lemma 6.3 can be extended to the following corollary,

Corollary 6.1. *[138] For a positive semi-definite V with the zero set of $Z := \{x \in \mathbb{R}^N : V(x) = 0\}$. In this case, If $\frac{\partial V}{\partial x} f_i(x) < 0$, $\forall x \notin Z$, $\forall i$, then all trajectories globally uniformly asymptotically converge to Z.*

Now, we present the theorem to show that the control protocols (6.3) and (6.4) are robust to saturated input

Theorem 6.2. *Consider the single-integrator system* (6.2)*, and assume that $u_{max} > 0$ is a real positive scalar. If the control input u_i of each robot is saturated such that $|u_i| \leq u_{max}$, then under the control laws* (6.3) *and* (6.4)*, the formation-containment can still be achieved globally.*

Proof. In order to model the saturated control input, we introduce the diagonal matrix $S \in \mathbb{R}^{2N \times 2N}$ with diagonal entries

$$(S)_{ii} = \begin{cases} 1 & \text{if } |u_i| \leq u_{max} \\ \dfrac{u_{max}}{|u_i|} & \text{if } |u_i| > u_{max} \end{cases} . \tag{6.21}$$

It can be seen that the diagonal entries of S are considered as functions that saturate any large control input to the maximum value u_{max}. The single-integrator systems under saturated input can be expressed in the vector form via

$$\begin{pmatrix} \dot{p}_F \\ \dot{p}_E \end{pmatrix} = S \begin{bmatrix} -\bar{L}_1 & -\bar{L}_2 \\ 0 & A \end{bmatrix} \begin{pmatrix} p_F \\ p_E \end{pmatrix} . \tag{6.22}$$

From [138], (6.22) should be understood as a family of switched dynamical systems, and the solution is well-defined in the Filippov sense. To verify the stability of the system, two cases are discussed in the following part. Let

$$S = \begin{bmatrix} S_F & 0 \\ 0 & S_E \end{bmatrix} , \tag{6.23}$$

where $S_F \in \mathbb{R}^{2M \times 2M}$ and $S_E \in \mathbb{R}^{2(N-M) \times 2(N-M)}$. Both S_F and S_E are diagonal matrices.

Part I (Leaders): The dynamics of the leaders can be described as

$$\dot{p}_E = S_E A p_E \ . \tag{6.24}$$

The Lyapunov function can be constructed by

$$V_E = -\frac{1}{2} p_E^\top A p_E \geq 0 \ , \tag{6.25}$$

V_E is a positive semi-definite scalar-valued function since A is negative semi-definite. Time derivative of V_E along the trajectory of (6.24) is

$$\begin{aligned} \dot{V}_E &= -p_E^\top A \dot{p}_E \\ &= -p_E^\top A S_E A p_E \\ &= -(S_E^{\frac{1}{2}} A p_E)^\top (S_E^{\frac{1}{2}} A p_E) = -\|S_E^{\frac{1}{2}} A p_E\|^2 \leq 0 \ , \end{aligned} \tag{6.26}$$

where $S_E^{\frac{1}{2}}$ is the diagonal matrix with entries given by the square root of diagonal elements of S_E. Note that all diagonal elements of S_E are strictly positive, hence $S_E^{\frac{1}{2}}$ is well-defined. The last step of (6.26) is according to the fact that A can be designed to be symmetric in Algorithm 1. Considering that V_E is a positive semi-definite, continuously differentiable and radially unbounded function. Then, based on Lemma 6.3, Corollary 6.1 and LaSalle's invariance principle, we can conclude that all trajectories of (6.24) converge to the zero set of V_E (i.e., the kernel of A). That is to say, the formation of the leaders can be achieved under input constraints. The proof of the leaders' part is completed.

Part II (followers): Since the leaders can converge to the desired formation h_F, if t is large enough, the dynamics of followers can be described as

$$\dot{p}_F = -S_F \bar{L}_1 p_F - S_F \bar{L}_2 h_F \ . \tag{6.27}$$

The Lyapunov function can be constructed by

$$V_F = \frac{1}{2} {p_F^*}^\top \bar{L}_1 p_F^* \geq 0 \ , \tag{6.28}$$

where $p_F^* = p_F + {\bar{L}_1}^{-1} \bar{L}_2 h_F$. V_F is a positive definite scalar-valued function since $\bar{L}_1$ is positive definite from Lemma 1 (i). Time derivative of V_F along the trajectory of

(6.27) is

$$\begin{aligned}\dot{V}_F &= {p_F^*}^\top \bar{L}_1 \dot{p}_F \\ &= (p_F + {\bar{L}_1}^{-1}\bar{L}_2 h_F)^\top \bar{L}_1(-S_F\bar{L}_1 p_F - S_F\bar{L}_2 h_F) \\ &= -p_F^\top \bar{L}_1 S_F \bar{L}_1 p_F - h_F^\top \bar{L}_2^\top S_F \bar{L}_2 h_F \\ &= -(S_F^{\frac{1}{2}}\bar{L}_1 p_F)^\top (S_F^{\frac{1}{2}}\bar{L}_1 p_F) - (S_F^{\frac{1}{2}}\bar{L}_2 h_F)^\top (S_F^{\frac{1}{2}}\bar{L}_2 h_F) \\ &= -\|S_F^{\frac{1}{2}}\bar{L}_1 p_F\|^2 - \|S_F^{\frac{1}{2}}\bar{L}_2 h_F\|^2 \leq 0 \ , \end{aligned} \tag{6.29}$$

where $S_F^{\frac{1}{2}}$ is the diagonal matrix with entries given by the square root of diagonal elements of S_F. Note that, all the diagonal elements of S_F are strictly positive. Hence, $S_F^{\frac{1}{2}}$ is well-defined. The last step of (6.29) is according to the fact that $\bar{L}_1$ is symmetric for undirected interaction among followers. Similar to the above analysis, all trajectories of (6.27) converge to the zero set of V_F applying Lemma 6.3, Corollary 6.1 and LaSalle's invariance principle. Hence, we can imply that

$$p_F = -{\bar{L}_1}^{-1}\bar{L}_2 h_F \ , \ \text{ when } \ t \to \infty \ . \tag{6.30}$$

By Lemma 6.1 (II), we can conclude that p_F satisfies Definition (6.1). Thus, the followers can converge to the hull convex formed by leaders. Combining Parts I and II, it can be concluded that the swarm system (6.2) achieves formation-containment under input saturation. This completes the proof. □

6.4 Formation-Containment Protocol for Double Integrator Systems

In this section, we extend the formation-containment protocol design with double-integrator systems in 2-dimensions

$$\begin{aligned}\dot{p}_i(t) &= v_i(t) \\ \dot{v}_i(t) &= u_i(t) \ , \end{aligned} \tag{6.31}$$

where $u_i(t)$ is the acceleration input to be designed. We can find that double-integrator systems (6.31) can be expressed in the following form

$$\begin{pmatrix} \dot{p}_i \\ \dot{v}_i \end{pmatrix} = \begin{bmatrix} 0 & I_2 \\ 0 & 0 \end{bmatrix} \begin{pmatrix} p_i \\ v_i \end{pmatrix} + \begin{pmatrix} 0 \\ I_2 \end{pmatrix} u_i \ . \tag{6.32}$$

Let $s_i = (p_i^\top, v_i^\top)^\top$, For the leaders and followers, our proposed formation-containment control protocol is

$$u_i = \sum_{j \in \mathcal{N}_i} \hat{A}_{ij}(s_j - s_i) \qquad i \in \mathcal{V}_E \ , \tag{6.33}$$

$$u_i = \sum_{j \in \mathcal{N}_i} w_{ij}[(p_j - p_i) + (v_j - v_i)] \qquad i \in \mathcal{V}_F \ , \tag{6.34}$$

where $\hat{A}_{ij} = [k_0 A_{ij} \ , \ k_1 A_{ij}]$, $k_0 \in \mathbb{R}$ and $k_1 \in \mathbb{R}$ are scalar control gains. w_{ij} is non-negative gain. The definition of A_{ij} is shown in (6.5).

Now, we present the following theorem to guarantee the convergence of double-integrator systems under the proposed formation-containment coordination.

Theorem 6.3. *Consider leaders and followers with double-integrator dynamics* (6.31) *and control protocol* (6.33) *and* (6.34)*. Assume the interaction topology among leaders* ($\mathcal{G}_E$) *contains a spanning tree and, for each follower, there exists at least one directed path from a leader, then, for any* $w_{ij} > 0$*, the swarm system* (6.31) *achieves formation-containment if* A *is that chosen by Algorithm 1, for all the non-zero eigenvalues of* A ($\lambda(A)$)*,* k_0*,* k_1 *are selected such that*

$$Re(k_1\lambda(A) + \Gamma) < 0, \tag{6.35}$$

where $\Gamma^2 = k_1^2\lambda^2(A) + 4k_0\lambda(A)$*.*

Proof. We put the control protocol (6.33) and (6.34) into (6.32).

On the one hand, for leaders, we have

$$\dot{S}_E = \begin{bmatrix} 0 & I_{2(N-M)} \\ k_0 A & k_1 A \end{bmatrix} S_E \ , \tag{6.36}$$

where, $S_E = [s_{M+1}^\top, \ldots, s_N^\top]^\top$. Let

$$\hat{A} = \begin{bmatrix} 0 & I_{2(N-M)} \\ k_0 A & k_1 A \end{bmatrix} \in \mathbb{R}^{4(N-M)\times 4(N-M)}.$$

Then, the proof can be divided into two steps. In step 1, we will find the eigenvectors of $\hat{A}$ corresponding to zero. In step 2, we will show that all non-zero eigenvalues of $\hat{A}$

have negative real parts.

Firstly, since

$$\text{rank}(\hat{A}) = \text{rank}(A) + \text{rank}(I_{2(N-M)}) = 4(N-M) - 4,$$

we have the matrix $\hat{A}$ have 4 zero eigenvalues. If we let

$$\hat{\mathbf{1}} = [\mathbf{1}^\top,\ 0]^\top,\ \hat{\mathbf{1}}^\perp = [\mathbf{1}^{\perp\top},\ 0]^\top,$$

$$\hat{h} = [h^\top,\ 0]^\top,\ \hat{h}^\perp = [h^{\perp\top},\ 0]^\top,$$

we can easily verify that $\hat{A}\hat{\mathbf{1}} = \hat{A}\hat{\mathbf{1}}^\perp = \hat{A}\hat{h} = \hat{A}\hat{h}^\perp = 0$. Hence we find the four eigenvectors corresponding to zero.

Secondly, since A is selected by Algorithm 1, we have $Re(\lambda(A)) < 0$, where $Re(\lambda(A))$ denotes the non-negative eigenvalues of A. Then, the characteristic equation of $\hat{A}$ is given by

$$\begin{aligned} &\det(\lambda^2 I_{2(N-M)} - k_1\lambda A - k_0 A) \\ &= \prod_{\mu\in eig(A)} |\lambda^2 - k_1\mu\lambda - k_0\mu| \\ &= 0\ . \end{aligned} \tag{6.37}$$

From (6.35) and (6.37), for all non-zero eigenvalues of $\hat{A}$, we have

$$Re(\lambda(\hat{A})) = \frac{Re(k_1\lambda(A) + \Gamma)}{2} < 0\ , \tag{6.38}$$

where $\Gamma^2 = k_1^2\lambda^2(A) + 4k_0\lambda(A)$.

Therefore, we can conclude that all of the non-eigenvalues of $\hat{A}$ have negative real parts. Hence, similar to the discussion in the leader case of Theorem 6.1, when $t \to \infty$, we obtain

$$S_E(t) \to \hat{\mathbf{1}}\hat{c}_1 + \hat{\mathbf{1}}^\perp\hat{c}_2 + \hat{h}\hat{c}_3 + \hat{h}^\perp\hat{c}_4\ , \tag{6.39}$$

which implies

$$p_E(t) \to \mathbf{1}\hat{c}_1 + \mathbf{1}^\perp\hat{c}_2 + h\hat{c}_3 + h^\perp\hat{c}_4\ , \tag{6.40}$$

where $\hat{c}_1$, $\hat{c}_2$, $\hat{c}_3$ and $\hat{c}_4$ are constants. That is to say, the leaders can converge to nothing but all translations, rotations, and non-negative scale factors of h, which also

indicates that leaders can converge to the desired formation shape.

On the other hand, for followers, we have

$$\dot{S}_F = \begin{bmatrix} 0 & I_{2M} \\ -\bar{L}_1 & -\bar{L}_1 \end{bmatrix} S_F + \begin{bmatrix} 0 & 0 \\ -\bar{L}_2 & -\bar{L}_2 \end{bmatrix} S_E \ , \tag{6.41}$$

where $S_F = [s_1^\top, \ldots, s_M^\top]^\top$. Let $t \to \infty$, similar to discussion in the follower case of Theorem 6.1, we conclude

$$S_F \to \begin{bmatrix} -\bar{L}_1{}^{-1}\bar{L}_2 & -\bar{L}_1{}^{-1}\bar{L}_2 \\ 0 & 0 \end{bmatrix} \hat{h}_F \ , \tag{6.42}$$

where $\hat{h}_F = [h_F^\top \ , \ 0]$ and h_F is the formation shaped by leaders. Then we can imply

$$p_F = -\bar{L}_1{}^{-1}\bar{L}_2 h_F \ , \ \text{ when } \ t \to \infty \ . \tag{6.43}$$

From Lemma 6.1 (ii), we can conclude that p_F satisfy Definition (6.1), and then the swarm system (6.31) achieve formation-containment. This completes the proof. □

Since the condition (6.35) is not easy to be verified, we have the following corollary.

Corollary 6.2. *In Theorem 6.3, if we can select the matrix A which satisfies $\lambda(A) \in \mathbb{R}$, where $\lambda(A)$ denote all non-zero eigenvalues of A. The chosen of k_0 and k_1 can be substituted by $k_0 > 0$ and $k_1 > 0$.*

Proof. Since $\lambda(A) \in \mathbb{R}$, we have $\Gamma^2 \in \mathbb{R}$.

On the one hand, in (6.37), if $k_1^2\lambda^2(A) + 4k_0\lambda(A) \leq 0$, we can obtain

$$Re(\lambda(\hat{A})) = \frac{k_1\lambda(A)}{2} < 0 \ .$$

On the other hand, in (6.37), if $k_1^2\lambda^2(A) + 4k_0\lambda(A) > 0$, we can imply that $\Gamma \in \mathbb{R}$. Let $\gamma = \sqrt{k_1^2\lambda^2(A) + 4k_0\lambda(A)}$, we have

$$\begin{aligned} Re(\lambda(\hat{A})) &= \frac{k_1\lambda(A) + \Gamma}{2} \\ &< \frac{k_1\lambda(A) + \gamma}{2} \\ &= \frac{4k_0\lambda(A)}{\gamma - k_1\lambda(A)} \ . \end{aligned}$$

Using this, combined with the selection of A, k_0 and k_1, we conclude that $Re(\lambda(\hat{A})) < 0$. The remaining proof is similar to Theorem 6.3, we omit here. □

Remark 6.4. *It can be seen that the formation matrix A in the control protocol plays a key role in both single and double integrator systems. Different from [12, 82], where both the relative formation reference signal and the relative state information are required in the real-time data transmission, the proposed control law only uses the relative state information. Hence, less data is used in the transmission resulting in reducing the communication cost in each robot.*

Remark 6.5. *The values of k_0 and k_1 reflect the convergence speed of velocity and acceleration, hence, if we select a larger set of k_0 and k_1, the formation-containment task will be completed faster. However, considering the energy costs and constraints of real-robot hardware, we cannot select arbitrary large values of k_0 and k_1. Therefore, there is a trade-off between control performance and input constraints.*

6.5 Simulation Results & Discussion

This section presents the observed results from simulation studies, followed by the results obtained from experiments using real robots.

6.5.1 Mission Description

Formation-containment control of a swarm robotic system has the potential to be applied in various applications such as automated farming and precision agriculture [135, 139]. As an example, Fig. 1.1 shows an agri-robotic scenario using two different types of robots in a swarm, which are deployed for a weed management task. The leader robots (which are quadrotors with their embedded sensory system, e.g. multispectral imaging camera) are deployed to form a formation around the boundary of the target area i.e. an area of interest. The follower robots (which are the ground robots directly interacting with plants) converge to the target area spanned by the leaders using inter-robot communication to complete the task, which may, for example, be the targeted application of insecticide. By developing and coordinating multiple sensing mobile platforms, the observed data can facilitate the practices of sustainable agricultural intensification.

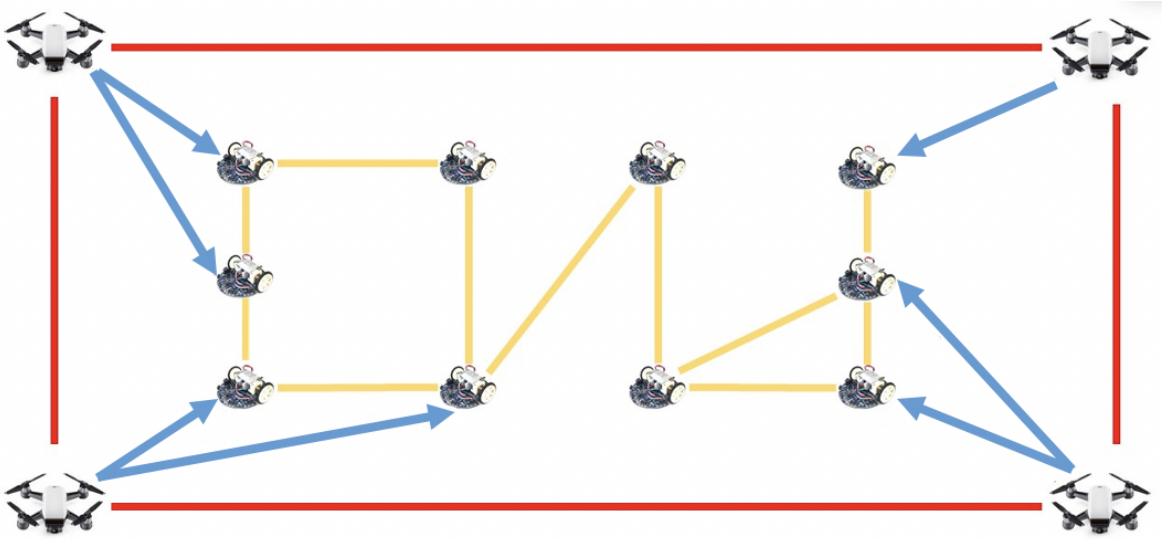

Figure 6.1: Interaction topology of the proposed swarm system. The four UAVs denote the leaders and the ten Mona robots denote the followers. The interactions among leaders and among followers are denoted by the red lines and yellow lines, respectively. The interactions between leaders and followers are denoted by blue arrows.

6.5.2 Results

In this section, we design a numerical simulation in the Matlab/Simulink environment to demonstrate the effectiveness of the theorem results obtained in the previous section.

We consider the double-integrator swarm system with four leaders and ten followers. Their dynamics are described by (6.31). The interaction topology among them is shown in Fig. 6.1. To test the robustness of the system, we add the white noise with an amplitude equal to 0.03 to the measured position of each robot. The input saturation is also considered in the simulation, where we set $\|u_{max}\| = 3$ for all the robots.

Initially, the desired formation of the four leader agents is chosen as a square. For simplicity, we set the final configuration of four agents as $(0, 0)$, $(1, 0)$, $(1, 1)$ and $(0, 1)$ to fix a square shape. Hence, h can then be defined as the following form $h = [0, 0, 1, 0, 1, 1, 0, 1]^\top$.

Then, the matrix A is generated as follows, utilising Algorithm 1

$$A = \begin{bmatrix} -2 & 0 & 1 & 1 & 0 & 0 & 1 & -1 \\ 0 & -2 & -1 & 1 & 0 & 0 & 1 & 1 \\ 1 & -1 & -2 & 0 & 1 & 1 & 0 & 0 \\ 1 & 1 & 0 & -2 & -1 & 1 & 0 & 0 \\ 0 & 0 & 1 & -1 & -2 & 0 & 1 & 1 \\ 0 & 0 & 1 & 1 & 0 & -2 & -1 & 1 \\ 1 & 1 & 0 & 0 & 1 & -1 & -2 & 0 \\ -1 & 1 & 0 & 0 & 1 & 1 & 0 & -2 \end{bmatrix}.$$

Finally, for followers, we set the interaction that has $0-1$ weight in the final step of Algorithm 1. It is straightforward to verify that all nonzero eigenvalues of A are real. Hence, by Corollary (6.2), we set the control gain for $k_0 = k_1 = \frac{1}{10}$. The swarm system (6.31) will achieve the formation-containment by the control protocol (6.33) and (6.34).

Fig. 6.2 shows the trajectory snapshots of leaders and followers with the interaction topology in Fig. 6.1 at different time instants $t \in \{0, 20, 50, 100\}$ s. The positions of followers are denoted by circles, and the positions of leaders are denoted by square, triangle, diamond, and asterisk, respectively. Moreover, the convex hull formed by leaders is marked by the red solid line. Fig. 6.2(a) shows the initial state of leaders and followers. From (a) to (b) in Fig. 6.2, it can be seen that the positions of the followers converged to the convex hull which was formed by the leaders. Fig. 6.2 (b)-(d) show the leaders converged to the desired formation and, simultaneously, the followers still stayed in the convex hull formed by the leaders. Finally, the swarm system achieved formation-containment at $t = 100$ s. The states and control inputs of the robots are shown in Fig. 6.3, where the solid lines denote leaders, and the dashed lines denote followers. It can be seen that the velocity and acceleration of each robot converge to zero, and all the robots complete the formation-containment task within t =80 s. Furthermore, the results of the simulation reveal that our control protocol is robust in several situations like white noise perturbation and input constraints.

Next, we analyse how different cases in followers and leaders affected the result of

the formation-containment. Two metrics which are i) time to achieve formation-containment (denoted by T) and ii) the average distance between followers to the barycentre in followers (denoted by d) were investigated. We assumed there are four leaders in the swarm system with the interaction shown in Fig. 6.1, and the interaction topology between followers is a ring. The variables are the number of followers and the interaction between leaders and followers. For each case, we repeated the experiments 50 times and the initial position of the robots was randomly selected for each run.

A. Number of followers (N): Assuming all leaders can transmit information to two followers and every follower can receive information from at least one leader. The only difference is the number of followers. We can indicate from Fig. 6.4 (a) that the value of T increased as an increase in N. Also, as shown in Fig. 6.4 (b), the value of d was also raised as an increase in N, however, with a different trend.

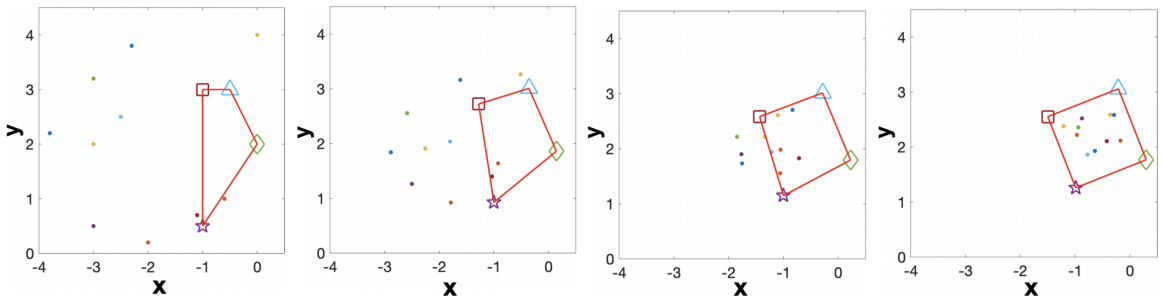

(a) $t = 0$ s (b) $t = 20$ s (c) $t = 50$ s (d) $t = 100$ s

Figure 6.2: Trajectory snapshots of leaders (denoted by square, triangle, diamond, and asterisk, respectively) and followers (denoted by ten nodes) in the swarm system at different time instants, $t \in \{0, 20, 50, 100\}$ s.

B. Leaders can transmit information to how many followers (N_l): Assuming there are four followers and every follower can receive information from at least one leader. The only difference is that leaders can transmit information to how many followers. We can see from Fig. 6.5 (a) that the value of T was decreased as an increase in N_l. However, the change in the value of d had no strong relationship with the various N_l.

C. How many followers can receive information from leaders (N_f): Assuming there are four followers and all leaders can transmit information to one follower. The only difference is that the number of followers can receive information from the leaders. We

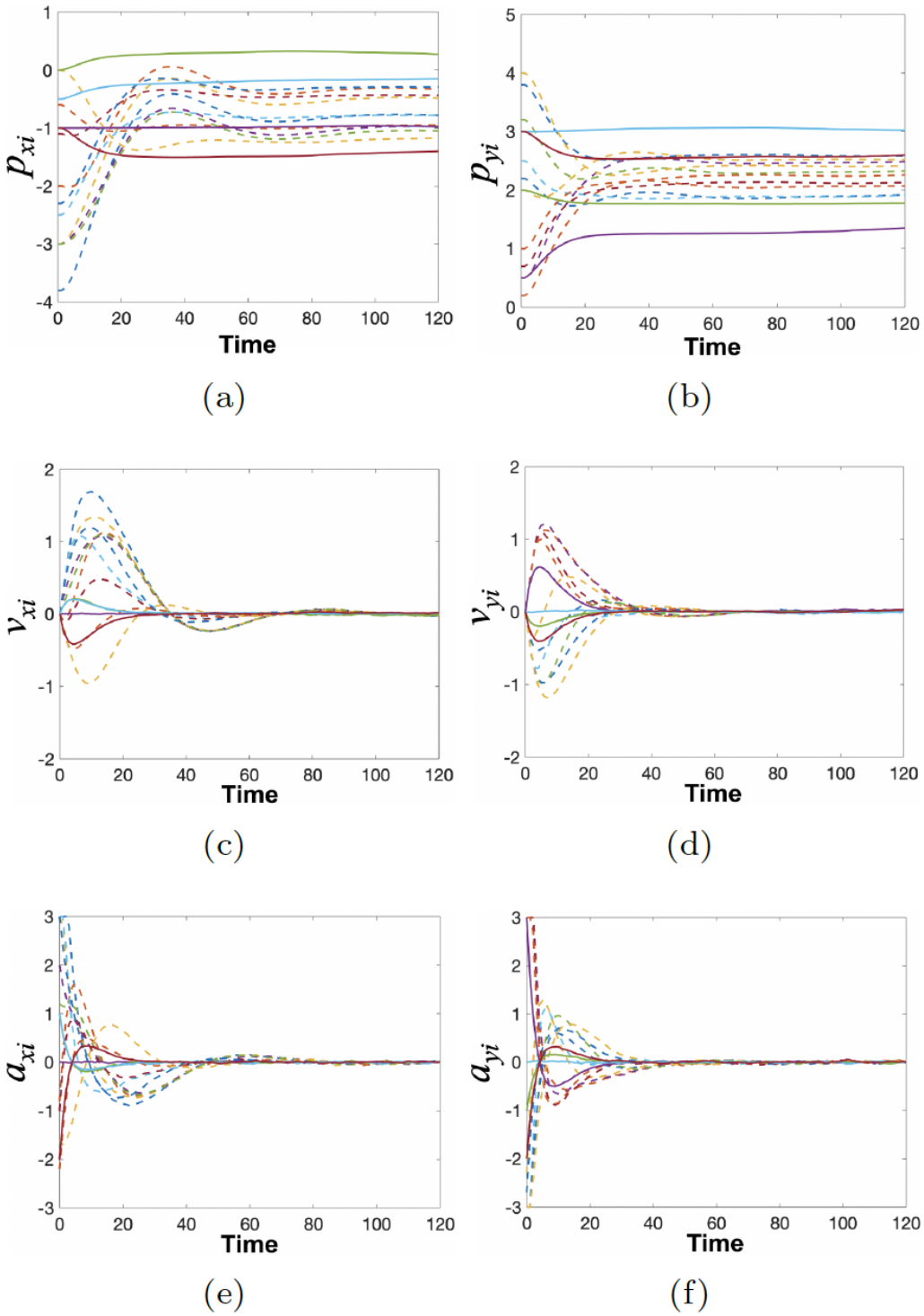

Figure 6.3: (a) and (b) show the time variation of position in x-axis (p_{x_i}) and y-axis (p_{y_i}) of i^{th} robot, respectively. (c) and (d) show the time variation of velocity in x-axis (v_{x_i}) and y-axis (v_{y_i}) of i^{th} robot, respectively. (e) and (f) show the time variation of acceleration (control input) in x-axis (a_{x_i}) and y-axis (a_{y_i}) with saturated input equals to 3 of i^{th} robot, respectively. The solid lines denote leaders, and the dashed lines denote followers.

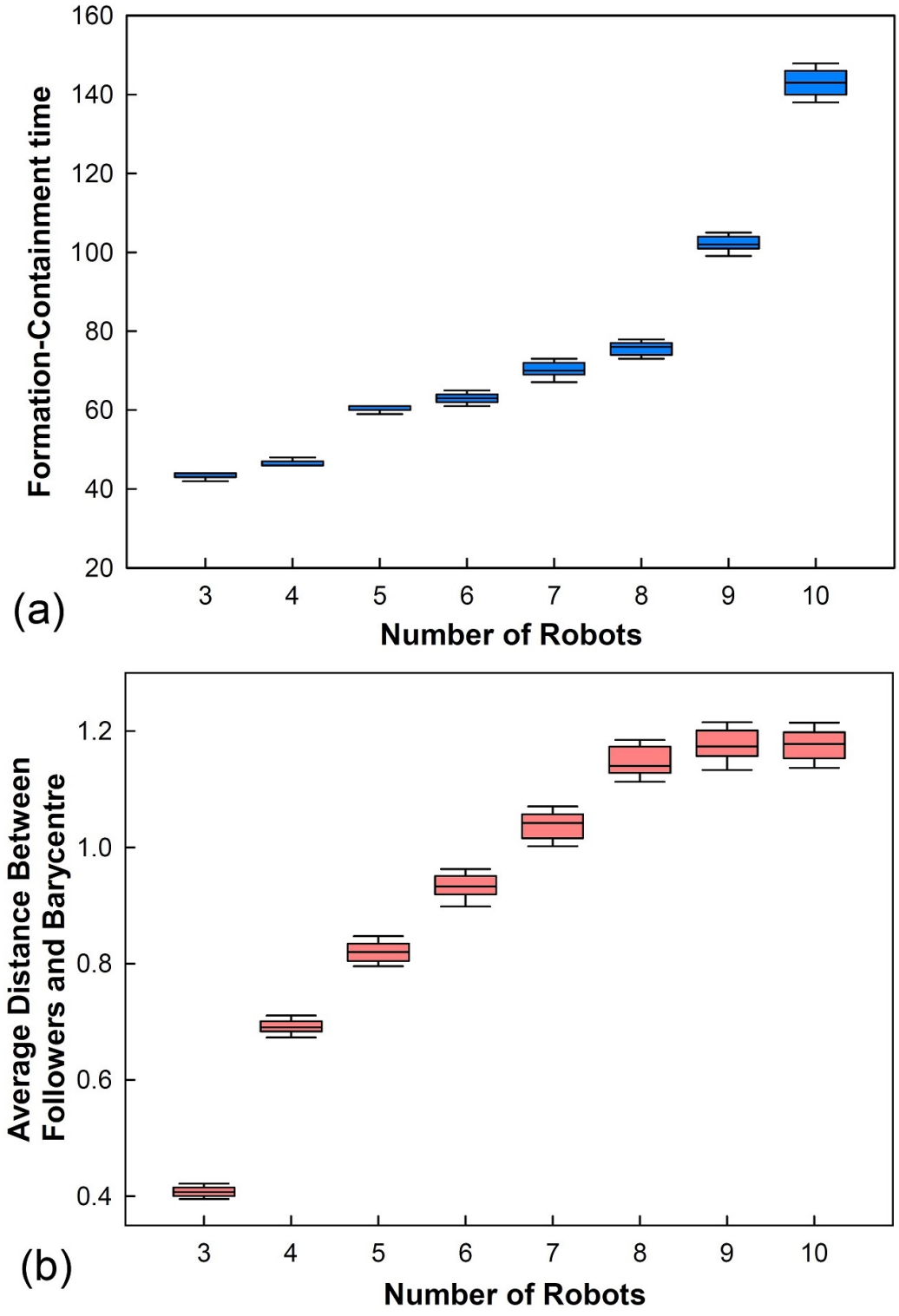

Figure 6.4: (a) Time of formation-containment achievement, T, and (b) average distance between followers and barycentre, d, for number of followers, $N \in \{3, 4, 5, 6, 7, 8, 9, 10\}$ robots.

can observe from Fig. 6.5 (b) that the value of T decreased as N_f increased. However, the value of d increased as N_f increased.

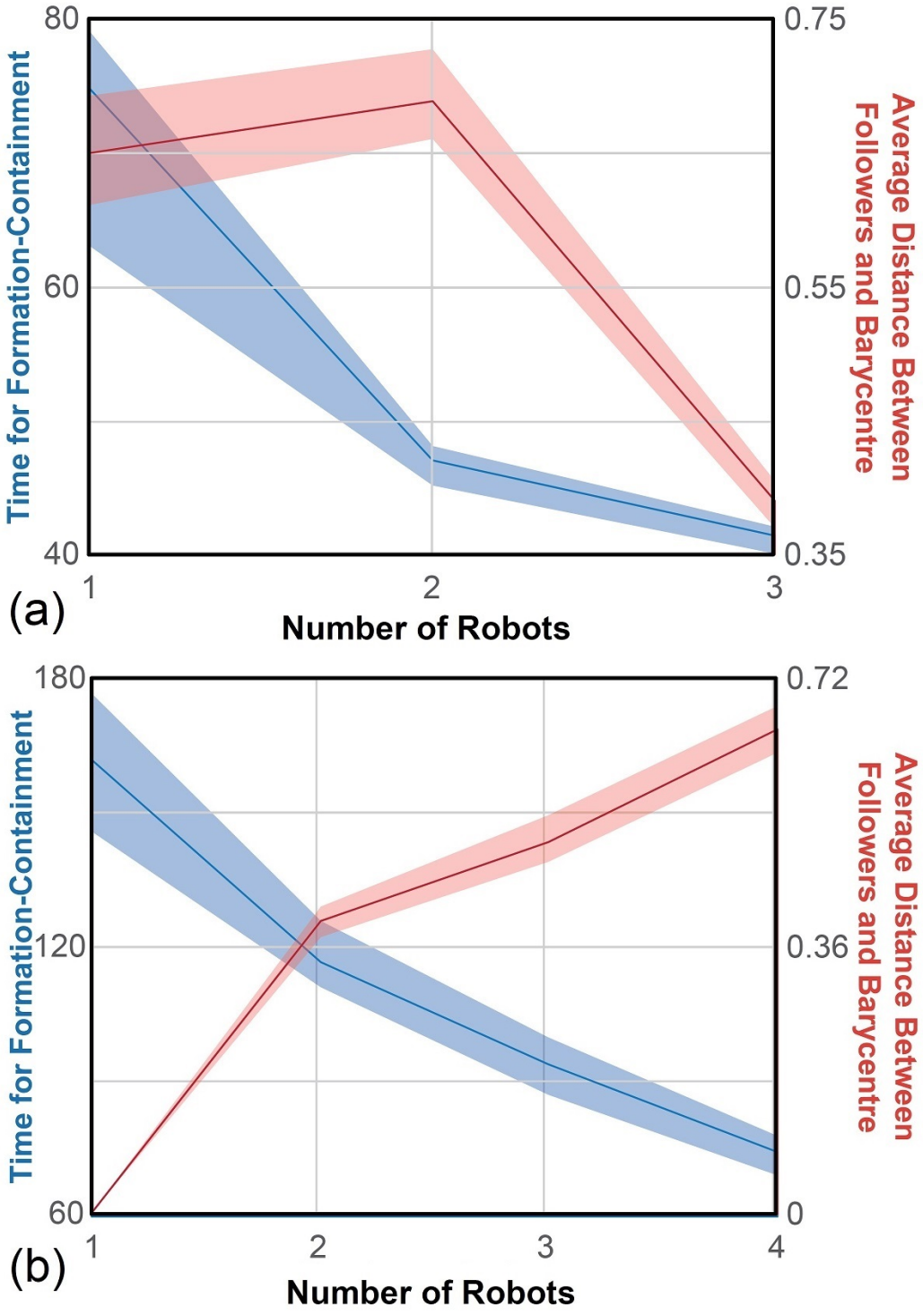

Figure 6.5: Time of formation-containment achievement, T, and average distance between followers and barycentre, d, for (a) the leaders link to $N_l \in \{1, 2, 3\}$ followers and (b) followers number ($N_f \in \{1, 2, 3, 4\}$) which directly linked to the leaders. The average values of T and d from 50 simulations are indicated by the blue and red colour lines, respectively. The shaded area indicates all the obtained results (between minimum and maximum).

Therefore, we can see that the time for formation-containment can be affected by both the number of followers and the interactions between leaders and followers. The convergence speed slows down when the number of robots increases or the interaction becomes sparse. Hence, the required time for formation-containment will be prolonged. However, the average distance between followers and barycentre is affected mostly by the interaction, which increases as the interaction becomes sparse. In fact, the trend of the red line in Fig. 6.5(a) is mainly due to the interaction since the interaction will become sparse in ring topology as the number of robots increases. If we change to another topology, the performance will be different.

6.5.3 Comparisons

In contrast to the formation tracking problems solved in [140] where there exists only one leader in the swarm system, in this work, we deal with the case when there exist multiple leaders, which brings more challenges to the control system design. Similar containment control problems are discussed in [2, 82], however, for each robot, it requires not only the relative state information from its neighbours, but also the relative formation reference signal which cannot be measured by the distance sensors directly, such that the control scheme is not fully distributed and scalable. On the contrary, the proposed control protocol only requires relative position measurements, which provides more feasibility in real-world implementation.

In order to show the superior coordination performance under the proposed algorithm, a comparison between the proposed formation-containment protocol and the adaptive controller recently developed in [2] is made. For both controllers, we adopted the same dynamics and conditions as shown in Section 6.6. The initial state of each robot was selected randomly. We repeated experiments 50 times for each controller, where we used $\|p - p^*\|$ (p is the position vector of every robot, and p^* is the final state vector of every robot) to define the tracking error. The performance analysis is illustrated in Fig. 6.6, wherein (a), the yellow area represents the observed results from 50 times experiments of our controller and the solid yellow line is the mean value. In Fig. 6.6 (b), the blue area represents results from 50 times experiments of the controller proposed in [2] and the solid blue line is the mean value. It can be seen that the convergence

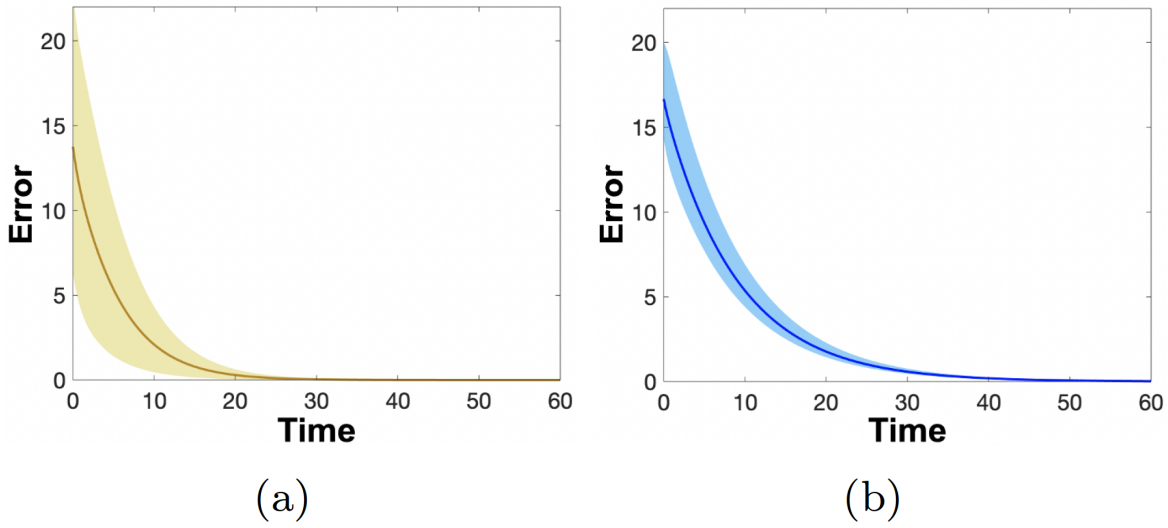

Figure 6.6: Controller performances of (a) the proposed protocol in this work and (b) the protocol proposed in [2]. The shaded area represents the observed results from 50 times experiments and lines represent the mean value.

time of the proposed protocol in this work is shorter than [2]. Such advantages reveal that our protocol is more efficient in completing formation-containment tasks.

6.6 Real-robot Experiments

6.6.1 Experimental Setup

To investigate the performance of the proposed formation scenario, we used a collection of real robots, namely *Mona* robots which are an open-source swarm robotic platform [141]. Fig. 6.7 (a) shows a Mona robot and its various modules. The robot is based on Arduino AVR architecture with ATMEGA-328 micro-controller. It is actuated with two wheels (with 3.2 mm diameter), which are differentially-driven using two gear-head micro DC motors [142]. The main controller uses PWM (pulse-width modulation) to control the rotational speed of the left and right motors independently. We developed an arena with an overhead camera as shown in Fig. 6.7 (b). In the experimental setup, we used a low-cost Microsoft LifeCam Studio Webcam as the swarm localisation platform. The position of each robot was continuously tracked by an open-source tracking software developed in [143] with a sampling time of 0.1 s. A time delay of 0.05 s and a tracking error of ± 0.005 m can be observed during the experiments due to the processing speed of the host computer and the quality of the camera. Hence, the

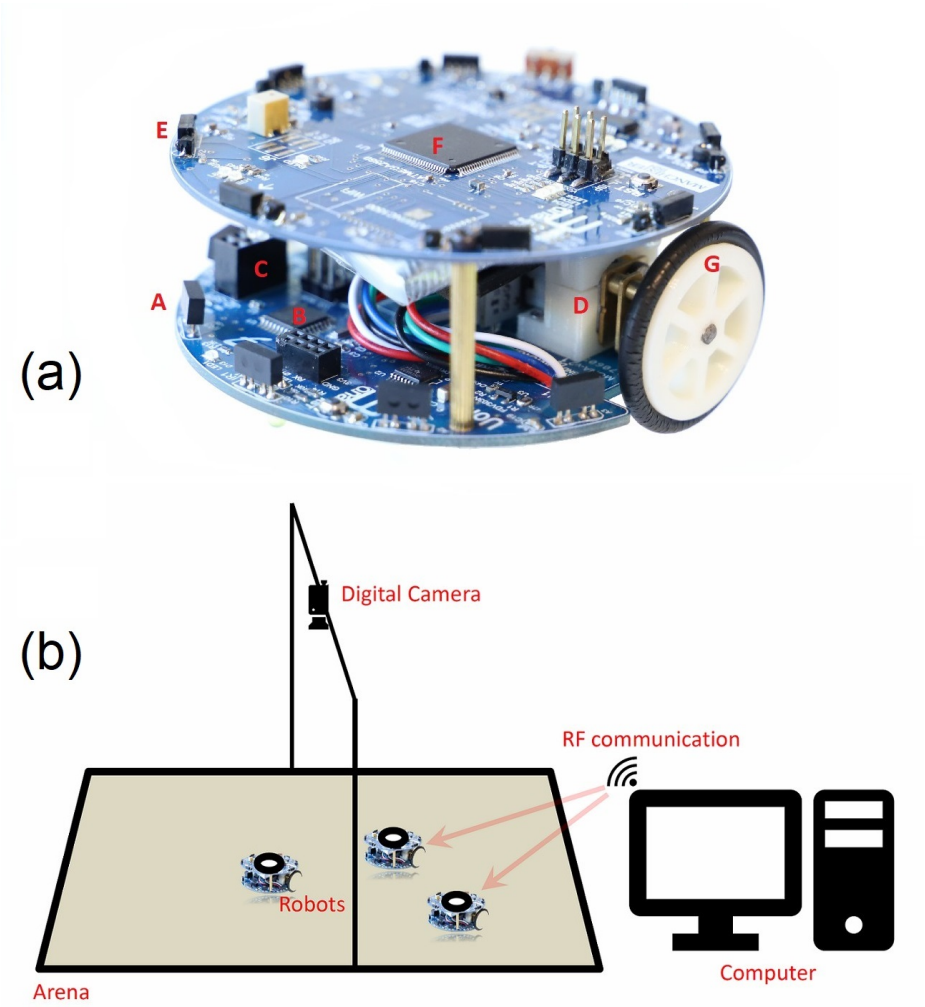

Figure 6.7: (a) Mona Robot, an open-source swarm robotic platform. A) infrared proximity sensors, B) main AVR processor, C) SPI port for RF transceiver. D) gear-head DC micro-motor, E) local IR communication transmitters and encoders, F) communication modules processor, G) 32 mm wheels. (b) Arena configuration includes a PC that tracks the position of robots using a digital camera and sends motion commands to the robots using RF communication.

robustness of the swarm system subjected to certain communication delays, actuator noises and inaccuracies of the camera tracking system can be verified via the experiments. The control algorithm generates the next position for each robot and transmits this information to them using an RF (radio frequency) module, which is connected to the robots using a serial port. The generated position command contains two bytes for the rotational speeds of the left and right motors. The main controller (microcontroller) of the robots receives this command and translates it to two PWM signals associated with the left and right motors. Details on motion control and kinematics of the robot were presented in [141]. All the mobile robots used in the experiments

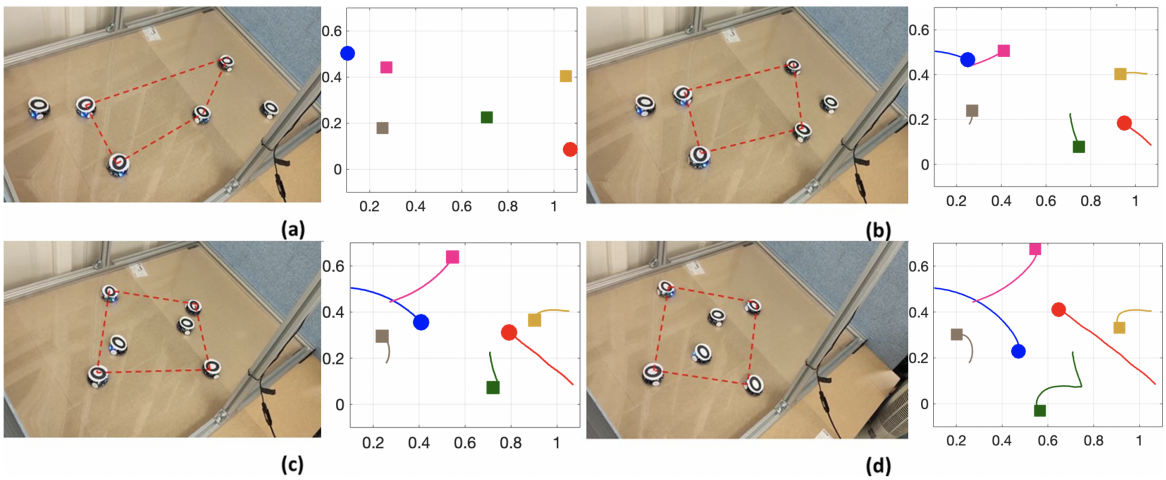

Figure 6.8: Selected snapshots of the experiments and the trace with six robots at (a) t=0 s, (b) t=10 s, (c) t=20 s and (d) t=40 s. The leaders are linked with red dashed lines.

have the same physical and hardware configuration. The dynamic model in terms of the global coordinates can be described as follows

$$\begin{aligned} \dot{p}_{xi} &= v_i \cos\theta_i \quad , \\ \dot{p}_{yi} &= v_i \sin\theta_i \quad , \\ \dot{\theta}_i &= \omega_i \quad , \end{aligned} \tag{6.44}$$

where (p_{xi}, p_{yi}) denotes the position of the i^{th} robot and θ_i is the orientation. v_i and ω_i represent the linear and angular velocities of the i^{th} robot respectively. In order to deal with the nonlinear dynamics that appeared in the robot model, the feedback linearisation technique [144] was used to transfer the dynamics of the robots (6.44) to single-integrator systems, such that the algorithm proposed in the previous section can be directly applied on the feedback linearised dynamics.

6.6.2 Results with Real Mobile Robots

In the real-robot experiment, six Mona robots (4 leaders and 2 followers) were utilised. The goal of these experiments was to make the robots move and then observe the trajectory they followed to achieve the final position. Analysis of this trajectory allowed the functionality of the proposed formation-containment to be verified.

We utilised six robots, where the four leaders are linked by the red dashed lines as

shown in Fig. 6.8, which illustrates the trajectories of the four leaders and two followers. In Fig. 6.8 (a), the robots are positioned at randomly selected initial states. From Fig. 6.8 (b) to (c), it was observed that the robots started to move toward the desired position. The leaders accomplished their formation control in a square, and the followers moved toward the convex hull spanned by the leaders. In Fig. 6.8 (d), the formation-containment task is seen to be complete. We can see from Fig. 6.8 that the leaders formed a square arrangement, that was set as the desired formation, gradually. At the same time, the followers entered the convex hull formed by the leaders, demonstrating that formation-containment was accomplished. Hence, it is clear from these figures that the robots were able to achieve the formation-containment by the control protocol proposed in this study.

In this set of experiment, because time delays and tracking errors existed in the camera tracking systems, the trace of the robots was not as smooth as might be expected (especially the yellow trace). One of the reasons was that the robots were driven by two motors, there also existed some tracking error between the desired speed and real speed. Furthermore, since the moment they receive the command via the RF (radio frequency) module may be delayed because of the wireless connection, and there also exists disturbances (such as friction and the internal interrupts of the robots), further deviation of the tracking was observed. On the other hand, due to the fact that the robots could not be treated as particles (points) in the real-world environment, we activated the collision avoidance function of the robots using artificial potential field methods. The robots changed their route when they discovered their distance between other robots was smaller than the threshold. Despite all of this, the robustness of the control system was shown to overcome these difficulties. Hence, the task was completed, and the effectiveness of the proposed controller was validated.

According to the results, the control protocol was successfully applied to real robots allowing them to achieve formation-containment. The proposed technique has significant potential to perform more complex behaviours to assist humans in dealing with challenging tasks in real-world scenarios.

6.7 Summary

In conclusion, a novel formation-containment control protocol design was proposed that makes the leaders converge to the desired formation, and the followers move to the convex hull spanned by the leaders. Simulations were performed to verify the control design algorithm and analysed some of the factors that affected the formation-containment performance. Finally, we applied our theorem to a real-world scenario by performing an experiment using multiple mobile robots. It can be seen that the proposed coordination framework can be used in precision agriculture applications where the leaders act as markers, indicating an area of interest and the followers are robots that interact with the plants. In the future, the nonlinear dynamics of the robot and time delay of the sensors will be taken into consideration when designing the distributed protocol. Furthermore, robust adaptive control techniques [145] will also be exploited to guarantee reliable performance.

Chapter 7

Conclusion and Future Work

7.1 Conclusion

The ultimate goal of the thesis is to explore novel formation strategies to swarm robotics and find the potential real-world applications by implementing the proposed algorithms.

First of all, a mixed formation strategy based on edge and bearing measurements is designed for networked MRS. We combined the edge-based and bearing-based approaches in the controller to maximise the advantages of both methods. Depending on the sensing-ability of the robotic platform, this mixed control method can provide an efficient solution to maximise the tracking performance. The robustness of the mixed controller is also discussed for both leaderless and leader-follower cases by Lyapunov method. The effectiveness of the theoretical results is illustrated with numerical simulation case studies.

Furthermore, we design a bearing-only collision-free formation coordination strategy for networked heterogeneous robots. In contrast to traditional position-based coordination strategies, the bearing-only coordinated movements of the robots only rely on the neighbouring bearing information. This feature can be utilised to reduce the sensing requirements in the hardware implementation. The robots can converge to the target formation within a prespecified settling time under the proposed GD protocol. The bound of the tracking can be ensured in the case of exogenous disturbances and

actuator faults. We also extend the result to LTI systems. Both Numerical simulations and lab-based experiments are presented to validate the effectiveness of these proposed algorithms.

Additionally, we also address the bearing-only formation tracking problem nonlinear MRS. A novel formation protocol is designed for the follower robots based on bearing measurements to form the desired formation configuration. We add a compensation term in the controller to tackle the unknown nonlinear elements in the system. The formation tracking error will converge to zero exponentially under the proposed bearing-only algorithm by Lyapunov method. After that, we extend the stability analysis of the proposed strategy on moving leaders, and the formation tracking error is able to be guaranteed in a bounded set. Simulation case studies are provided to verify the effectiveness of the theoretical results.

Moreover, we propose an SDP-based robust formation-containment coordination for swarm robotics that makes the leaders converge to the desired formation, and the followers move to the convex hull spanned by the leaders. In contrast to conventional consensus-based formation control methods, the relative formation reference signal is not required in real-time data transmission, which provides greater feasibility for implementation on hardware platforms. We provided the robustness analysis of the protocol with input saturation. The effectiveness of the proposed formation-containment control algorithm is demonstrated with both numerical simulations and experiments using real robots that utilise the miniature mobile robot, Mona.

To sum up, this thesis proposes several formation protocols for MRS. Some potential future research is listed on the next section.

7.2 Future Work

Some possible future work is displayed below

- In this thesis, the bearing-only formation protocols are only designed for followers. The performance of the bearing-based controller will be further explored if

the input of the leaders is considered.

- It can be seen that the continuation of the protocol proposed in Chapter 6 can not be guaranteed during the formation. How to modify the bearing-only protocol to ensure the continuity of the controller will be investigated in the future. Moreover, the safety of the robots is also significant when designing the protocol. Hence, the collision-free bearing-only strategy will be considered in the future.

- The FTBO protocol is only discussed for single-integrator systems. How to design an FTBO formation algorithm for nonlinear MAS will be taken into consideration. Moreover, we will also focus on fixed-time bearing-only formation protocol for nonlinear MAS in the future.

- Learning-based training (such as radial basis function neural network, reinforcement learning, etc.) can be implemented to evaluate the uncertainty in the system. Hence, combining bearing-only protocol with a learning-based algorithm is also an interesting direction in the future.

Bibliography

[1] Z. Li, H. Tnunay, S. Zhao, W. Meng, S. Q. Xie, and Z. Ding, "Bearing-only formation control with prespecified convergence time," *IEEE Transactions on Cybernetics*, vol. 52, no. 1, pp. 620–629, 2022.

[2] J. Hu, P. Bhowmick, and A. Lanzon, "Two-layer distributed formation-containment control strategy for linear swarm systems: Algorithm and experiments," *International Journal of Robust and Nonlinear Control*, vol. 30, no. 16, pp. 6433–6453, 2020.

[3] M. Schranz, G. A. Di Caro, T. Schmickl, W. Elmenreich, F. Arvin, A. Şekercioğlu, and M. Sende, "Swarm intelligence and cyber-physical systems: Concepts, challenges and future trends," *Swarm and Evolutionary Computation*, vol. 60, p. 100762, 2020.

[4] F. Arvin, A. E. Turgut, T. Krajník, and S. Yue, "Investigation of cue-based aggregation in static and dynamic environments with a mobile robot swarm," *Adaptive Behavior*, vol. 24, no. 2, pp. 102–118, 2016.

[5] S. O. Obute, P. Kilby, M. R. Dogar, and J. H. Boyle, "Swarm foraging under communication and vision uncertainties," *IEEE Transactions on Automation Science and Engineering*, vol. 19, no. 3, pp. 1446–1457, 2022.

[6] S. Mai, N. Traichel, and S. Mostaghim, "Driving swarm: A swarm robotics framework for intelligent navigation in a self-organized world," in *2022 International Conference on Robotics and Automation (ICRA)*, pp. 01–07, IEEE, 2022.

[7] K. M. Cabral, J. Silveira, P. T. Jardine, and S. N. Givigi, "Auction-based solution for the ordering problem in robotic self-assembly," in *2023 IEEE International Systems Conference (SysCon)*, pp. 1–8, IEEE, 2023.

[8] J. Hu, A. E. Turgut, T. Krajník, B. Lennox, and F. Arvin, "Occlusion-based coordination protocol design for autonomous robotic shepherding tasks," *IEEE Transactions on Cognitive and Developmental Systems*, vol. 14, no. 1, pp. 126–135, 2022.

[9] S. H. Alsamhi, A. V. Shvetsov, S. V. Shvetsova, A. Hawbani, M. Guizani, M. A. Alhartomi, and O. Ma, "Blockchain-empowered security and energy efficiency of drone swarm consensus for environment exploration," *IEEE Transactions on Green Communications and Networking*, vol. 7, no. 1, pp. 328–338, 2022.

[10] M. Kondoyanni, D. Loukatos, C. Maraveas, C. Drosos, and K. G. Arvanitis, "Bio-inspired robots and structures toward fostering the modernization of agriculture," *Biomimetics*, vol. 7, no. 2, p. 69, 2022.

[11] O. Spykman, A. Emberger-Klein, A. Gabriel, and M. Gandorfer, "Autonomous agriculture in public perception-german consumer segments' view of crop robots," *Computers and Electronics in Agriculture*, vol. 202, p. 107385, 2022.

[12] J. Hu, P. Bhowmick, and A. Lanzon, "Distributed adaptive time-varying group formation tracking for multiagent systems with multiple leaders on directed graphs," *IEEE Transactions on Control of Network Systems*, vol. 7, no. 1, pp. 140–150, 2020.

[13] J. Hu, P. Bhowmick, I. Jang, F. Arvin, and A. Lanzon, "A decentralized cluster formation containment framework for multirobot systems," *IEEE Transactions on Robotics*, vol. 37, no. 6, pp. 1936–1955, 2021.

[14] Y. Bian, C. Du, M. Hu, S. E. Li, H. Liu, and C. Li, "Fuel economy optimization for platooning vehicle swarms via distributed economic model predictive control," *IEEE Transactions on Automation Science and Engineering*, vol. 19, no. 4, pp. 2711–2723, 2021.

[15] R. Yang, L. Liu, and G. Feng, "An overview of recent advances in distributed coordination of multi-agent systems," *Unmanned Systems*, vol. 10, no. 03, pp. 307–325, 2022.

[16] Y. Ding, X. Wang, Y. Cong, and H. Li, "Scalability analysis of algebraic graph-based multi-uavs formation control," *IEEE Access*, vol. 7, pp. 129719–129733, 2019.

[17] Y.-Y. Dong, C.-x. Dong, W. Liu, H. Chen, and G.-q. Zhao, "2-d doa estimation for l-shaped array with array aperture and snapshots extension techniques," *IEEE Signal Processing Letters*, vol. 24, no. 4, pp. 495–499, 2017.

[18] M. Ye, B. D. Anderson, and C. Yu, "Multiagent self-localization using bearing only measurements," in *52nd IEEE Conference on Decision and Control*, pp. 2157–2162, IEEE, 2013.

[19] E. Montijano, E. Cristofalo, D. Zhou, M. Schwager, and C. Saguees, "Vision-based distributed formation control without an external positioning system," *IEEE Transactions on Robotics*, vol. 32, no. 2, pp. 339–351, 2016.

[20] F. Schiano, A. Franchi, D. Zelazo, and P. R. Giordano, "A rigidity-based decentralized bearing formation controller for groups of quadrotor uavs," in *2016 IEEE/RSJ International Conference on Intelligent Robots and Systems (IROS)*, pp. 5099–5106, IEEE, 2016.

[21] B. Tian, L. Liu, H. Lu, Z. Zuo, Q. Zong, and Y. Zhang, "Multivariable finite time attitude control for quadrotor uav: Theory and experimentation," *IEEE Transactions on Industrial Electronics*, vol. 65, no. 3, pp. 2567–2577, 2017.

[22] B. Ning, Q.-L. Han, Z. Zuo, L. Ding, Q. Lu, and X. Ge, "Fixed-time and prescribed-time consensus control of multiagent systems and its applications: A survey of recent trends and methodologies," *IEEE Transactions on Industrial Informatics*, vol. 19, no. 2, pp. 1121–1135, 2022.

[23] S. Wang, J. Xiao, X. Hu, H. Luo, T. Chen, and Z. Zuo, "Distributed finite-time average consensus over unbalanced digraphs via broadcast mode," *IEEE Transactions on Network Science and Engineering*, 2023.

[24] J. Wang, C. Bi, D. Wang, Q. Kuang, and C. Wang, "Finite-time distributed event-triggered formation control for quadrotor uavs with experimentation," *ISA transactions*, vol. 126, pp. 585–596, 2022.

[25] B. Tian, H. Lu, Z. Zuo, Q. Zong, and Y. Zhang, "Multivariable finite-time output feedback trajectory tracking control of quadrotor helicopters," *International Journal of Robust and Nonlinear Control*, vol. 28, no. 1, pp. 281–295, 2018.

[26] Z. Zuo and L. Tie, "A new class of finite-time nonlinear consensus protocols for multi-agent systems," *International Journal of Control*, vol. 87, no. 2, pp. 363–370, 2014.

[27] Y. Liu, H. Li, R. Lu, Z. Zuo, and X. Li, "An overview of finite/fixed-time control and its application in engineering systems," *IEEE/CAA Journal of Automatica Sinica*, vol. 9, no. 12, pp. 2106–2120, 2022.

[28] X. Fang, Q. Zhong, F. Liu, Z. Ding, and T. Yang, "Fixed-time nonsingular terminal sliding mode control for a class of nonlinear systems with mismatched disturbances and its applications," *Nonlinear Dynamics*, pp. 1–13, 2023.

[29] H. Hu, W. Yang, and Z. Ding, "Feedback control for stochastic finite-time/fixed-time synchronization of stochastic coupled nonlinear systems," *Control Theory and Technology*, pp. 1–11, 2023.

[30] F. Mei, H. Wang, Y. Yao, J. Fu, X. Yuan, and W. Yu, "Robust second-order finite-time formation control of heterogeneous multi-agent systems on directed communication graphs," *IET Control Theory & Applications*, vol. 14, no. 6, pp. 816–823, 2020.

[31] J. Hu, H. Niu, J. Carrasco, B. Lennox, and F. Arvin, "Fault-tolerant cooperative navigation of networked uav swarms for forest fire monitoring," *Aerospace Science and Technology*, vol. 123, p. 107494, 2022.

[32] J. A. Fax and R. M. Murray, "Information flow and cooperative control of vehicle formations," *IEEE transactions on automatic control*, vol. 49, no. 9, pp. 1465–1476, 2004.

[33] N. Moshtagh, N. Michael, A. Jadbabaie, and K. Daniilidis, "Vision-based, distributed control laws for motion coordination of nonholonomic robots," *IEEE Transactions on Robotics*, vol. 25, no. 4, pp. 851–860, 2009.

[34] Y.-P. Tian and Q. Wang, "Global stabilization of rigid formations in the plane," *Automatica*, vol. 49, no. 5, pp. 1436–1441, 2013.

[35] Z. Lin, L. Wang, Z. Han, and M. Fu, "Distributed formation control of multi-agent systems using complex laplacian," *IEEE Transactions on Automatic Control*, vol. 59, no. 7, pp. 1765–1777, 2014.

[36] Z. Han, L. Wang, Z. Lin, and R. Zheng, "Formation control with size scaling via a complex laplacian-based approach," *IEEE transactions on cybernetics*, vol. 46, no. 10, pp. 2348–2359, 2015.

[37] H. Liu, Z. Lin, M. Cao, X. Wang, and J. Lü, "Coordinate-free formation control of multi-agent systems using rooted graphs," *Systems & Control Letters*, vol. 119, pp. 8–15, 2018.

[38] X. Dong, B. Yu, Z. Shi, and Y. Zhong, "Time-varying formation control for unmanned aerial vehicles: Theories and applications," *IEEE Transactions on Control Systems Technology*, vol. 23, no. 1, pp. 340–348, 2014.

[39] X. Dong and G. Hu, "Time-varying formation tracking for linear multiagent systems with multiple leaders," *IEEE Transactions on Automatic Control*, vol. 62, no. 7, pp. 3658–3664, 2017.

[40] X. Dong, Y. Li, C. Lu, G. Hu, Q. Li, and Z. Ren, "Time-varying formation tracking for uav swarm systems with switching directed topologies," *IEEE Transactions on Neural Networks and Learning Systems*, vol. 30, no. 12, pp. 3674–3685, 2018.

[41] P. Rao and X. Li, "Cooperative formation of self-propelled vehicles with directed communications," *IEEE Transactions on Circuits and Systems II: Express Briefs*, vol. 67, no. 2, pp. 315–319, 2019.

[42] C. J. Stamouli, C. P. Bechlioulis, and K. J. Kyriakopoulos, "Multi-agent formation control based on distributed estimation with prescribed performance," *IEEE Robotics and Automation Letters*, vol. 5, no. 2, pp. 2929–2934, 2020.

[43] J. Hu, P. Bhowmick, F. Arvin, A. Lanzon, and B. Lennox, "Cooperative control of heterogeneous connected vehicle platoons: An adaptive leader-following approach," *IEEE Robotics and Automation Letters*, vol. 5, no. 2, pp. 977–984, 2020.

[44] Y. Xie, L. Han, X. Dong, Q. Li, and Z. Ren, "Bio-inspired adaptive formation tracking control for swarm systems with application to uav swarm systems," *Neurocomputing*, vol. 453, pp. 272–285, 2021.

[45] L. Krick, M. E. Broucke, and B. A. Francis, "Stabilisation of infinitesimally rigid formations of multi-robot networks," *International Journal of control*, vol. 82, no. 3, pp. 423–439, 2009.

[46] Y. H. Choi and D. Kim, "Distance-based formation control with goal assignment for global asymptotic stability of multi-robot systems," *IEEE Robotics and Automation Letters*, vol. 6, no. 2, pp. 2020–2027, 2021.

[47] D. V. Dimarogonas and K. H. Johansson, "Further results on the stability of distance-based multi-robot formations," in *2009 American Control Conference*, pp. 2972–2977, IEEE, 2009.

[48] J. Chen, Z. Shi, and Y. Zhong, "Robust formation tracking for uncertain multi-agent systems with unknown leader input," *IET Control Theory & Applications*, vol. 14, no. 4, pp. 646–653, 2020.

[49] H. Liu, Y. Wang, and F. L. Lewis, "Robust distributed formation controller design for a group of unmanned underwater vehicles," *IEEE Transactions on Systems, Man, and Cybernetics: Systems*, vol. 51, no. 2, pp. 1215–1223, 2021.

[50] J. Hu, B. Lennox, and F. Arvin, "Robust formation control for networked robotic systems using negative imaginary dynamics," *Automatica*, vol. 140, p. 110235, 2022.

[51] Y. Lu, R. Su, C. Zhang, and L. Qiao, "Event-triggered adaptive formation keeping and interception scheme for autonomous surface vehicles under malicious attacks," *IEEE Transactions on Industrial Informatics*, vol. 18, no. 6, pp. 3947–3957, 2021.

[52] M. A. Kamel, X. Yu, and Y. Zhang, "Real-time fault-tolerant formation control of multiple wmrs based on hybrid ga–pso algorithm," *IEEE Transactions on Automation Science and Engineering*, vol. 18, no. 3, pp. 1263–1276, 2021.

[53] G. Guo, P. Li, and L.-Y. Hao, "Adaptive fault-tolerant control of platoons with guaranteed traffic flow stability," *IEEE Transactions on Vehicular Technology*, vol. 69, no. 7, pp. 6916–6927, 2020.

[54] L. Sauter and P. Palmer, "Onboard semianalytic approach to collision-free formation reconfiguration," *IEEE Transactions on Aerospace and Electronic Systems*, vol. 48, no. 3, pp. 2638–2652, 2012.

[55] H. A. Poonawala, A. C. Satici, H. Eckert, and M. W. Spong, "Collision-free formation control with decentralized connectivity preservation for nonholonomic-wheeled mobile robots," *IEEE Transactions on control of Network Systems*, vol. 2, no. 2, pp. 122–130, 2014.

[56] Y. Liu, P. Shi, and C.-C. Lim, "Collision-free formation control for multi-agent systems with dynamic mapping," *IEEE Transactions on Circuits and Systems II: Express Briefs*, vol. 67, no. 10, pp. 1984–1988, 2019.

[57] S. S.-D. Xu, H.-C. Huang, Y.-C. Kung, and S.-K. Lin, "Collision-free fuzzy formation control of swarm robotic cyber-physical systems using a robust orthogonal firefly algorithm," *IEEE Access*, vol. 7, pp. 9205–9214, 2019.

[58] S. A. Ajwad, E. Moulay, M. Defoort, T. Ménard, and P. Coirault, "Collision-free formation tracking of multi-agent systems under communication constraints," *IEEE Control Systems Letters*, vol. 5, no. 4, pp. 1345–1350, 2020.

[59] X. Ge, Q.-L. Han, J. Wang, and X.-M. Zhang, "A scalable adaptive approach to multi-vehicle formation control with obstacle avoidance," *IEEE/CAA Journal of Automatica Sinica*, vol. 9, no. 6, pp. 990–1004, 2021.

[60] Z. Sui, Z. Pu, J. Yi, and S. Wu, "Formation control with collision avoidance through deep reinforcement learning using model-guided demonstration," *IEEE Transactions on Neural Networks and Learning Systems*, vol. 32, no. 6, pp. 2358–2372, 2020.

[61] Z. Enjiao, Z. Zenan, and Z. Xin, "Finite-time control of formation system for multiple flight vehicles subject to actuator saturation," *Journal of Systems Engineering and Electronics*, vol. 31, no. 5, pp. 1019–1030, 2020.

[62] K. Gao, Y. Liu, Y. Zhou, Y. Zhao, and P. Huang, "Practical fixed-time affine formation for multi-agent systems with time-based generators," *IEEE Transactions on Circuits and Systems II: Express Briefs*, vol. 69, no. 11, pp. 4433–4437, 2022.

[63] Y. Hua, X. Dong, L. Han, Q. Li, and Z. Ren, "Finite-time time-varying formation tracking for high-order multiagent systems with mismatched disturbances," *IEEE Transactions on Systems, Man, and Cybernetics: Systems*, vol. 50, no. 10, pp. 3795–3803, 2018.

[64] T. Xiong and Z. Gu, "Observer-based adaptive fixed-time formation control for multi-agent systems with unknown uncertainties," *Neurocomputing*, vol. 423, pp. 506–517, 2021.

[65] C. Wang, H. Tnunay, Z. Zuo, B. Lennox, and Z. Ding, "Fixed-time formation control of multirobot systems: Design and experiments," *IEEE Transactions on Industrial Electronics*, vol. 66, no. 8, pp. 6292–6301, 2018.

[66] Y. Li, J. Yang, and K. Zhang, "Distributed finite-time cooperative control for quadrotor formation," *IEEE Access*, vol. 7, pp. 66753–66763, 2019.

[67] J. Lan, Y.-J. Liu, T. Xu, S. Tong, and L. Liu, "Adaptive fuzzy fast finite-time formation control for second-order mass based on capability boundaries of agents," *IEEE Transactions on Fuzzy Systems*, vol. 30, no. 9, pp. 3905–3917, 2021.

[68] F. Mehdifar, F. Hashemzadeh, M. Baradarannia, and M. de Queiroz, "Finite-time rigidity-based formation maneuvering of multiagent systems using distributed finite-time velocity estimators," *IEEE transactions on cybernetics*, vol. 49, no. 12, pp. 4473–4484, 2018.

[69] L. Yu and M. Fu, "A robust finite-time output feedback control scheme for marine surface vehicles formation," *IEEE Access*, vol. 6, pp. 41291–41301, 2018.

[70] S.-L. Dai, K. Lu, and J. Fu, "Adaptive finite-time tracking control of nonholonomic multirobot formation systems with limited field-of-view sensors," *IEEE Transactions on Cybernetics*, vol. 52, no. 10, pp. 10695–10708, 2021.

[71] Q. Wang, X. Dong, B. Wang, Y. Hua, and Z. Ren, "Finite-time observer-based h_∞ fault-tolerant output formation tracking control for heterogeneous nonlinear multi-agent systems," *IEEE Transactions on Network Science and Engineering*, vol. 10, no. 4, pp. 1822–1834, 2023.

[72] H.-Q. Hou, Y.-J. Liu, J. Lan, and L. Liu, "Adaptive fuzzy fixed time time-varying formation control for heterogeneous multiagent systems with full state constraints," *IEEE Transactions on Fuzzy Systems*, vol. 31, no. 4, pp. 1152–1162, 2022.

[73] W. Shang, G. Jing, D. Zhang, T. Chen, and Q. Liang, "Adaptive fixed time nonsingular terminal sliding-mode control for quadrotor formation with obstacle and inter-quadrotor avoidance," *IEEE Access*, vol. 9, pp. 60640–60657, 2021.

[74] H. Xu, G. Cui, Q. Ma, Z. Li, and W. Hao, "Fixed-time disturbance observer-based distributed formation control for multiple quavs," *IEEE Transactions on Circuits and Systems II: Express Briefs*, vol. 70, no. 6, pp. 2181–2185, 2023.

[75] H. B. Abebe, C.-L. Hwang, B.-S. Chen, F. Wu, and C. Jan, "Recurrent neural network with fractional learning-based fixed-time formation tracking constrained control for a group of quadrotors," *IEEE Access*, vol. 9, pp. 81399–81411, 2021.

[76] Z. Gao and G. Guo, "Fixed-time leader-follower formation control of autonomous underwater vehicles with event-triggered intermittent communications," *IEEE access*, vol. 6, pp. 27902–27911, 2018.

[77] S. Chang, Y. Wang, Z. Zuo, and H. Yang, "Fixed-time formation control for wheeled mobile robots with prescribed performance," *IEEE Transactions on Control Systems Technology*, vol. 30, no. 2, pp. 844–851, 2021.

[78] T.-F. Ding, K.-T. Xu, M.-F. Ge, J. H. Park, and C.-D. Liang, "Fast fixed-time output multi-formation tracking of networked autonomous surface vehicles: A

mathematical induction method," *IEEE Transactions on Vehicular Technology*, vol. 72, no. 5, pp. 5769–5781, 2023.

[79] M. Ji, G. Ferrari-Trecate, M. Egerstedt, and A. Buffa, "Containment control in mobile networks," *IEEE Transactions on Automatic Control*, vol. 53, no. 8, pp. 1972–1975, 2008.

[80] Y. Cao, D. Stuart, W. Ren, and Z. Meng, "Distributed containment control for multiple autonomous vehicles with double-integrator dynamics: algorithms and experiments," *IEEE Transactions on Control Systems Technology*, vol. 19, no. 4, pp. 929–938, 2010.

[81] Z. Li, W. Ren, X. Liu, and M. Fu, "Distributed containment control of multi-agent systems with general linear dynamics in the presence of multiple leaders," *International Journal of Robust and Nonlinear Control*, vol. 23, no. 5, pp. 534–547, 2013.

[82] X. Dong, Z. Shi, G. Lu, and Y. Zhong, "Output containment analysis and design for high-order linear time-invariant swarm systems," *International Journal of Robust and Nonlinear Control*, vol. 25, no. 6, pp. 900–913, 2015.

[83] X. Dong, J. Xi, G. Lu, and Y. Zhong, "Containment analysis and design for high-order linear time-invariant singular swarm systems with time delays," *International Journal of Robust and Nonlinear Control*, vol. 24, no. 7, pp. 1189–1204, 2014.

[84] T. Li, W. Bai, Q. Liu, Y. Long, and C. P. Chen, "Distributed fault-tolerant containment control protocols for the discrete-time multiagent systems via reinforcement learning method," *IEEE Transactions on Neural Networks and Learning Systems*, 2021.

[85] X. Zhou, H. Hou, W. Liang, I. Kevin, K. Wang, and Q. Jin, "Intelligent containment control with double constraints for cloud-based collaborative manufacturing," *IEEE Transactions on Industrial Informatics*, 2022.

[86] D. Yao, C. Dou, D. Yue, and X. Xie, "Event-triggered practical fixed-time fuzzy

containment control for stochastic multiagent systems," *IEEE Transactions on Fuzzy Systems*, vol. 30, no. 8, pp. 3052–3062, 2021.

[87] Z. Li, J. Wu, X. Zhan, T. Han, and H. Yan, "Distributed adaptive predefined-time bipartite containment algorithm for nonlinear multi-agent systems with actuator faults," *IEEE Transactions on Circuits and Systems II: Express Briefs*, 2022.

[88] L. Zhang, S. Liu, and C. Hua, "Distributed bipartite containment control of high-order nonlinear multi-agent systems with time-varying powers," *IEEE Transactions on Circuits and Systems I: Regular Papers*, vol. 70, no. 3, pp. 1371–1380, 2022.

[89] H. Sun, R. Xia, and A. Yu, "Fully distributed containment control for second-order nonlinear multi-agent systems with external disturbances," *IEEE Transactions on Circuits and Systems II: Express Briefs*, vol. 69, no. 4, pp. 2126–2130, 2020.

[90] Y. Liu, H. Zhang, Z. Shi, and Z. Gao, "Neural-network-based finite-time bipartite containment control for fractional-order multi-agent systems," *IEEE Transactions on Neural Networks and Learning Systems*, 2022.

[91] X. Dong, *Formation and containment control for high-order linear swarm systems*. Springer, 2015.

[92] G. Ferrari-Trecate, M. Egerstedt, A. Buffa, and M. Ji, "Laplacian sheep: A hybrid, stop-go policy for leader-based containment control," in *International Workshop on Hybrid Systems: Computation and Control*, pp. 212–226, Springer, 2006.

[93] H. Liu, L. Cheng, M. Tan, Z. Hou, Z. Cao, and M. Wang, "Containment control with multiple interacting leaders under switching topologies," in *Proceedings of the 32nd Chinese Control Conference*, pp. 7093–7098, IEEE, 2013.

[94] X. Dong, Z. Shi, G. Lu, and Y. Zhong, "Formation-containment analysis and design for high-order linear time-invariant swarm systems," *International Journal of Robust and Nonlinear Control*, vol. 25, no. 17, pp. 3439–3456, 2015.

[95] X. Dong, Z. Shi, Z. Ren, and Y. Zhong, "Output formation-containment control for high-order swarm systems with directed topologies," in *The 27th Chinese control and decision conference (2015 CCDC)*, pp. 36–43, IEEE, 2015.

[96] Y. Wang, Y. Song, and W. Ren, "Distributed adaptive finite-time approach for formation–containment control of networked nonlinear systems under directed topology," *IEEE transactions on neural networks and learning systems*, vol. 29, no. 7, pp. 3164–3175, 2017.

[97] Y. Lu, X. Dong, Q. Li, J. Lü, and Z. Ren, "Time-varying group formation-containment tracking control for general linear multiagent systems with unknown inputs," *IEEE Transactions on Cybernetics*, vol. 52, no. 10, pp. 11055–11067, 2021.

[98] Q. Sun, X. Wang, and Y.-H. Chen, "Satellite formation-containment control emphasis on collision avoidance and uncertainty suppression," *IEEE Transactions on Cybernetics*, 2022.

[99] S. Zuo, Y. Song, F. L. Lewis, and A. Davoudi, "Time-varying output formation containment of general linear homogeneous and heterogeneous multiagent systems," *IEEE Transactions on Control of Network Systems*, vol. 6, no. 2, pp. 537–548, 2018.

[100] M. Cheng, H. Liu, Y. Wan, K. P. Valavanis, and F. L. Lewis, "Data-driven optimal formation-containment control for a group of spacecrafts subject to switching topologies," *IEEE Transactions on Aerospace and Electronic Systems*, 2023.

[101] X. Zhang, J. Wu, X. Zhan, T. Han, and H. Yan, "Observer-based adaptive time-varying formation-containment tracking for multiagent system with bounded unknown input," *IEEE Transactions on Systems, Man, and Cybernetics: Systems*, vol. 53, no. 3, pp. 1479–1491, 2022.

[102] W. Xiao, H. Ma, L. Zhou, and H. Li, "Adaptive fuzzy fixed-time formation-containment control for euler-lagrange systems," *IEEE Transactions on Fuzzy Systems*, 2023.

[103] Z. Liu, C. West, B. Lennox, and F. Arvin, "Local bearing estimation for a swarm of low-cost miniature robots," *Sensors*, vol. 20, no. 11, p. 3308, 2020.

[104] Z. Tang, R. Cunha, T. Hamel, and C. Silvestre, "Formation control of a leader–follower structure in three dimensional space using bearing measurements," *Automatica*, vol. 128, p. 109567, 2021.

[105] Z. Tang, R. Cunha, T. Hamel, and C. Silvestre, "Relaxed bearing rigidity and bearing formation control under persistence of excitation," *Automatica*, vol. 141, p. 110289, 2022.

[106] Z. Lin, T. Han, R. Zheng, and M. Fu, "Distributed localization for 2-d sensor networks with bearing-only measurements under switching topologies," *IEEE Transactions on Signal Processing*, vol. 64, no. 23, pp. 6345–6359, 2016.

[107] R. Tron, J. Thomas, G. Loianno, K. Daniilidis, and V. Kumar, "A distributed optimization framework for localization and formation control: Applications to vision-based measurements," *IEEE Control Systems Magazine*, vol. 36, no. 4, pp. 22–44, 2016.

[108] G. Mao, B. Fidan, and B. D. Anderson, "Wireless sensor network localization techniques," *Computer Networks*, vol. 51, no. 10, pp. 2529–2553, 2007.

[109] M. Basiri, A. N. Bishop, and P. Jensfelt, "Distributed control of triangular formations with angle-only constraints," *Systems & Control Letters*, vol. 59, no. 2, pp. 147–154, 2010.

[110] X. Li, C. Wen, X. Fang, and J. Wang, "Adaptive bearing-only formation tracking control for nonholonomic multiagent systems," *IEEE Transactions on Cybernetics*, vol. 52, no. 8, pp. 7552–7562, 2022.

[111] S. Li, X. Wang, S. Wang, and Y. Zhang, "Distributed bearing-only formation control for uav-uwsv heterogeneous system," *Drones*, vol. 7, no. 2, p. 124, 2023.

[112] S. Zhao and D. Zelazo, "Localizability and distributed protocols for bearing-based network localization in arbitrary dimensions," *Automatica*, vol. 69, pp. 334–341, 2016.

[113] R. Tron, J. Thomas, G. Loianno, K. Daniilidis, and V. Kumar, "Bearing-only formation control with auxiliary distance measurements, leaders, and collision avoidance," in *2016 IEEE 55th Conference on Decision and Control (CDC)*, pp. 1806–1813, IEEE, 2016.

[114] S. Zhao, Z. Li, and Z. Ding, "Bearing-only formation tracking control of multiagent systems," *IEEE Transactions on Automatic Control*, vol. 64, no. 11, pp. 4541–4554, 2019.

[115] Y.-B. Bae, H.-S. Ahn, and Y.-H. Lim, "Leader-follower bearing-based formation system with exogenous disturbance," in *2019 IEEE 13th International Symposium on Applied Computational Intelligence and Informatics (SACI)*, pp. 000039–000044, IEEE, 2019.

[116] Y.-B. Bae, S.-H. Kwon, Y.-H. Lim, and H.-S. Ahn, "Distributed bearing-based formation control and network localization with exogenous disturbances," *International Journal of Robust and Nonlinear Control*, vol. 32, no. 11, pp. 6556–6573, 2022.

[117] J. Zhao, X. Li, X. Yu, and H. Wang, "Finite-time cooperative control for bearing-defined leader-following formation of multiple double-integrators," *IEEE Transactions on Cybernetics*, vol. 52, no. 12, pp. 13363–13372, 2021.

[118] M. H. Trinh, D. Mukherjee, D. Zelazo, and H.-S. Ahn, "Finite-time bearing-only formation control," in *2017 IEEE 56th Annual Conference on Decision and Control (CDC)*, pp. 1578–1583, IEEE, 2017.

[119] M. H. Trinh and H.-S. Ahn, "Finite-time bearing-based maneuver of acyclic leader-follower formations," *IEEE Control Systems Letters*, vol. 6, pp. 1004–1009, 2021.

[120] S. Zhao, F. Lin, K. Peng, B. M. Chen, and T. H. Lee, "Finite-time stabilisation of cyclic formations using bearing-only measurements," *International Journal of Control*, vol. 87, no. 4, pp. 715–727, 2014.

[121] Q. Van Tran, M. H. Trinh, D. Zelazo, D. Mukherjee, and H.-S. Ahn, "Finite-time bearing-only formation control via distributed global orientation estimation,"

IEEE Transactions on Control of Network Systems, vol. 6, no. 2, pp. 702–712, 2018.

[122] K. Chen, G. Qi, Y. Li, and A. Sheng, "Finite-time target localization and multicircular circumnavigation with bearing-only measurements," *Journal of the Franklin Institute*, vol. 360, no. 9, pp. 6338–6356, 2023.

[123] X. Li, Y. Zhu, X. Zhao, and J. Lu, "Bearing-based prescribed time formation tracking for second-order multi-agent systems," *IEEE Transactions on Circuits and Systems II: Express Briefs*, vol. 69, no. 7, pp. 3259–3263, 2022.

[124] R. A. Horn and C. R. Johnson, *Matrix analysis*. Cambridge university press, 2012.

[125] C. Godsil and G. F. Royle, *Algebraic graph theory*, vol. 207. Springer Science & Business Media, 2001.

[126] S. Zhao and D. Zelazo, "Bearing rigidity and almost global bearing-only formation stabilization," *IEEE Transactions on Automatic Control*, vol. 61, no. 5, pp. 1255–1268, 2015.

[127] Z. Ding, "Nonlinear and adaptive control systems," *IET CONTROL ENGINEERING SERIES*, 2013.

[128] Z. Meng, W. Ren, and Z. You, "Distributed finite-time attitude containment control for multiple rigid bodies," *Automatica*, vol. 46, no. 12, pp. 2092–2099, 2010.

[129] H. Khalil, *Nonlinear Systems*. Prentice Hall, 2002.

[130] K. Shojaei, A. M. Shahri, and B. Tabibian, "Design and implementation of an inverse dynamics controller for uncertain nonholonomic robotic systems," *Journal of Intelligent & Robotic Systems*, vol. 71, no. 1, pp. 65–83, 2013.

[131] K. Shojaei and M. Abdolmaleki, "Output feedback control of a tractor with n-trailer with a guaranteed performance," *Mechanical Systems and Signal Processing*, vol. 142, p. 106746, 2020.

[132] M. Zhai, Q. Sun, B. Wang, Z. Liu, and H. Zhang, "Cooperative fault-estimation-based event-triggered fault-tolerant voltage restoration in islanded ac microgrids," *IEEE Transactions on Automation Science and Engineering*, vol. 20, no. 3, pp. 1829–1837, 2023.

[133] F. Arvin, J. Espinosa, B. Bird, A. West, S. Watson, and B. Lennox, "Mona: an affordable open-source mobile robot for education and research," *Journal of Intelligent & Robotic Systems*, vol. 94, no. 3, pp. 761–775, 2019.

[134] T. Krajník, M. Nitsche, J. Faigl, T. Duckett, M. Mejail, and L. Přeučil, "External localization system for mobile robotics," in *2013 16th International Conference on Advanced Robotics (ICAR)*, pp. 1–6, IEEE, 2013.

[135] M. Dorigo, G. Theraulaz, and V. Trianni, "Reflections on the future of swarm robotics," *Science Robotics*, vol. 5, p. eabe4385, 2020.

[136] K. Fathian, D. I. Rachinskii, T. H. Summers, M. W. Spong, and N. R. Gans, "Distributed formation control under arbitrarily changing topology," in *2017 American Control Conference (ACC)*, pp. 271–278, IEEE, 2017.

[137] K. Fathian, S. Safaoui, T. H. Summers, and N. R. Gans, "Robust distributed planar formation control for higher order holonomic and nonholonomic agents," *IEEE Transactions on Robotics*, vol. 37, no. 1, pp. 185–205, 2021.

[138] D. Liberzon, *Switching in systems and control*. Springer Science & Business Media, 2003.

[139] B. D. Grieve, T. Duckett, M. Collison, L. Boyd, J. West, H. Yin, F. Arvin, and S. Pearson, "The challenges posed by global broadacre crops in delivering smart agri-robotic solutions: A fundamental rethink is required," *Global Food Security*, vol. 23, pp. 116–124, 2019.

[140] Y. Hong, G. Chen, and L. Bushnell, "Distributed observers design for leader-following control of multi-agent networks," *Automatica*, vol. 44, no. 3, pp. 846–850, 2008.

[141] F. Arvin, J. Espinosa, B. Bird, A. West, S. Watson, and B. Lennox, "Mona: an affordable open-source mobile robot for education and research," *Journal of Intelligent & Robotic Systems*, vol. 94, no. 3-4, pp. 761–775, 2019.

[142] F. Arvin and M. Bekravi, "Encoderless position estimation and error correction techniques for miniature mobile robots," *Turkish Journal of Electrical Engineering & Computer Sciences*, vol. 21, no. 6, pp. 1631–1645, 2013.

[143] T. Krajník, M. Nitsche, J. Faigl, P. Vaněk, M. Saska, L. Přeučil, T. Duckett, and M. Mejail, "A practical multirobot localization system," *Journal of Intelligent & Robotic Systems*, vol. 76, no. 3-4, pp. 539–562, 2014.

[144] S. G. Tzafestas, *Introduction to mobile robot control*. Elsevier, 2013.

[145] J. Hu and P. Bhowmick, "A consensus-based robust secondary voltage and frequency control scheme for islanded microgrids," *International Journal of Electrical Power & Energy Systems*, vol. 116, p. 105575, 2020.

Appendix A

Extension of the FTBO protocol to the LTI Systems with Exogenous Disturbance

Considering that some robotic platforms may have general linear dynamics (e.g., after implementing geometry-based robust feedback linearisation techniques), in this appendix, we aim to extend the results obtained from the previous subsections to solve the robust formation coordination problem with exogenous disturbance and bearing measurement for LTI systems.

Suppose the leaders are fixed ($\dot{p}_i = 0$, $\forall i \in \mathcal{V}_l$), and the dynamics of the followers can be described by

$$\dot{p}_i(t) = A_i p_i(t) + u_i(t) + \omega_i(t), \quad i \in \mathcal{V}_f, \tag{A.1}$$

where $A_i \in \mathbb{R}^{d\times d}$, and $\omega_i \in \mathbb{R}^d$ is the exogenous disturbance of robot $i \in \mathcal{V}_f$.

Under the protocol (5.2), the dynamic of (A.1) can be written in compact form as

$$\dot{p} = \begin{bmatrix} 0 & 0 \\ 0 & A \end{bmatrix} p + (a + b\frac{\dot{\mu}}{\mu}) \begin{bmatrix} 0 & 0 \\ 0 & I_{dn_f} \end{bmatrix} \bar{H}^\top (g^* - g) + \omega, \tag{A.2}$$

where $A = \text{diag}\{A_{n_l+1}, \cdots, A_n\} \in \mathbb{R}^{n_f \times n_f}$.

Let $p = [p_l^\top, p_f^\top]^\top$, where $p_l = \text{col}(p_1, \cdots, p_{n_l})$ and $p_f = \text{col}(p_{n_l+1}, \cdots, p_n)$ denote the positions of leaders and followers. We have the following corollary.

Corollary A.1. *Consider the LTI system with the exogenous disturbance. Under Assumption 5.1-5.4, if A_i is negative semi-definite, and $p_i^{*\top} A_i = 0$ for each follower robot $i \in \mathcal{V}_f$, the formation error δ converge to the bound set $\mathcal{S}$*

$$\mathcal{S} = \left\{ \delta : \|\delta\|^2 \leq \frac{4\gamma^2 F^2 K}{a\lambda_{\min}(\mathcal{B}_{ff})} \right\}.$$

in finite time by protocol (6.1)*, where $K = 2n\boldsymbol{s}_0$, and $\gamma \geq \sqrt{aK/\lambda_{min}(\mathcal{B}_{ff})}$.*

Proof. The Lyapunov function can be constructed as $V = \frac{1}{2}\|\delta\|^2$. The derivative of V can be expressed as

$$\begin{aligned} \dot{V} =& \delta^\top \dot{p} \\ =& -(a + b\frac{\dot{\mu}}{\mu})(p - p^*)^\top \bar{H}^\top (g - g^*) + \delta^\top \omega \\ &+ (p - p^*)^\top \begin{bmatrix} 0 & 0 \\ 0 & A \end{bmatrix} p. \end{aligned} \tag{A.3}$$

From (5.37), since A_i is negative semi-definite and $p_i^{*\top} A_i = 0$ for each follower robot $i \in \mathcal{V}_f$, we have

$$\begin{aligned} \dot{V} \leq& -(a + b\frac{\dot{\mu}}{\mu})\frac{\lambda_{\min}(\mathcal{B}_{ff})}{2\text{max}_k\|e_k\|}\|\delta\|^2 + \delta^\top \omega + \sum_{i=n_l+1}^{n} p_i^{*\top} A_i p_i \\ &+ p_f^\top A p_f \\ \leq& -(a + b\frac{\dot{\mu}}{\mu})\frac{\lambda_{\min}(\mathcal{B}_{ff})}{2\text{max}_k\|e_k\|}\|\delta\|^2 + \delta^\top \omega. \end{aligned} \tag{A.4}$$

Following similar steps in Theorem 5.2, we can imply that the formation error δ converges to the bound set $\mathcal{S}$ in finite time by protocol (5.2). This completes the proof. □

Appendix B

Bearing-Only Formation Control for Nonlinear Systems

B.1 Introduction

It is noticeable that the dynamics of the robots are linear in the former chapters. However, the movement of the robot is complex in practical scenarios. In this chapter, we aim to deal with the nonlinearity in Objective 3. A cooperative bearing-only formation protocol is designed to deal with the heterogeneous MRS with nonlinear dynamics. The robots can only measure the bearing information from their neighbors while the position or distance measures are inaccessible. Moreover, the heterogeneous nonlinear function is included in the system. The stability of the proposed strategy can be guaranteed via Lyapunov techniques. Furthermore, we also discuss the robustness of the controller for moving leaders, which is more practical in real applications. Finally, the simulations are presented to verify the effectiveness of the proposed algorithm. The contribution of this chapter can be summarised as:

- A cooperative bearing-only formation strategy is proposed for nonlinear heterogeneous multi-robot networks. Compared with traditional position-based and distance-based coordination methods, the coordinated movement of each robot merely requires the relative bearings from their neighbours, which significantly reduces the sensing requirements.

- A novel compensation term based on bearing measurements is introduced in the proposed controller. The compensation function is able to eliminate the effect of the unknown nonlinear dynamics in the system without position and distance measurements. Different from the works presented in [114], the dynamics of the agents considered in this work could be nonlinear and heterogeneous.

- Moreover, the nonzero velocities of the leader are also considered in this research. The formation error can be guaranteed in a bounded set under the proposed protocol for moving leaders.

The rest of the chapter proceeds as follows. In Section B.2, the preliminaries and the problem description are introduced. In Section B.3, the cooperative bearing-only formation scheme is proposed and the stability analysis of the controller is presented by Lyapunov method. The proposed results are extended to deal with moving leaders. Simulation results are shown in Section B.4 to verify the feasibility of the proposed algorithm. Section B.5 concludes the chapter.

B.2 Problem Descriptions

In this chapter, we mainly focus on nonlinear heterogeneous MRS. Let $\mathcal{V}_l$ and $\mathcal{V}_f$ be the set of leaders and followers. Suppose the leaders are fixed ($\dot{p}_i(t) = 0,\ \forall i \in \mathcal{V}_l$), the dynamics of the ith follower robot can be written as

$$\dot{p}_i = \psi_i(p_i(t)) + u_i(t), \quad \forall i \in \mathcal{V}_f \tag{B.1}$$

where $\psi_i(\cdot) \in \mathbb{R}^p$ denotes the unknown nonlinear continuous function for each robot. We can imply that the nonlinear MRS is heterogeneous since ψ_i is different for each robot. $u_i(t) \in \mathbb{R}^p$ represents the control input for the ith robot generated by bearing measurements. The main problem of the work can be expressed as

Problem: Design the cooperative formation strategies for each follower robot merely based on bearing vectors $\{g_{ij}\}_{j\in\mathcal{N}_i}$ such that all the robots will converge to the target formation.

To deal with the problem, we propose the following assumptions

Assumption B.1. *The unknown nonlinear function $\psi_i(\cdot)$ is upper-bounded by a continuous function $\tilde{\psi}(t)$ which is known. That is to say, $\|\psi_i(\cdot)\| \leq \tilde{\psi}(t)$.*

Assumption B.2. *The formation scale $\boldsymbol{s}(t)$ is upper-bounded. In another words, $\boldsymbol{s}(t) \leq \boldsymbol{s}_0$, $\forall\ t \geq 0$.*

Assumption B.3. *The desired formation is unique. i.e., $\lambda_{min}(\mathcal{B}_{ff}) > 0$, where $\lambda_{min}(\mathcal{B}_{ff})$ denotes the minimum eigenvalue of $\mathcal{B}_{ff}$.*

Assumption B.4. *There is no collision between each robot during the formation task. i.e., $\|e_k\| > \sigma$, $\forall k \in \{1, 2, \cdots, m\}$, where σ is a positive constant.*

Assumption B.4 ensures that the bearing vectors generated by each pair of the neighbour are always well defined during the formation framework [114, 126].

B.3 Main Results

B.3.1 Bearing-Only Formation Protocol for Followers

In this section, we present a novel formation algorithm to solve the problem proposed in Section B.2. The controller of the ith follower robot is designed as

$$u_i(t) = \sum_{j \in \mathcal{N}_i} (a\xi_{ij} + b\Psi_i(\xi_{ij})), \tag{B.2}$$

where $\xi_{ij} = \xi_k = g_{ij} - g_{ij}^*$ denotes the bearing error of the kth undirected edge (i, j), a and b are controller gains which should be defined later, and

$$\Psi_i(\xi_{ij}) = \begin{cases} \dfrac{\xi_{ij}}{\|\xi_{ij}\|^2}\tilde{\psi}^2(t), & \text{when } \xi_{ij} \neq 0 \\ 0, & \text{when } \xi_{ij} = 0. \end{cases}$$

Denote $\delta_i = p_i - p_i^*$ as the formation error of the ith robot, and $\delta = [\delta_1^T, \cdots, \delta_n^T]^T$. Let $\xi = [\xi_1^T, \cdots, \xi_m^T]^T$. We have the following main result

Theorem B.1. *Under Assumption 1-4, the formation tracking error of the nonlinear heterogeneous MRS* (B.1) *converges to zero exponentially for the fixed leaders by implementing the controller* (B.2) *if the control gains a and b are selected to satisfy*

$$ab > \frac{2n^2\boldsymbol{s}_0}{m\sigma\lambda_{min}(\mathcal{B}_{ff})}. \tag{B.3}$$

Proof. It is obvious that $\delta_i = 0,\ \forall i \in \mathcal{V}_l$ since the leaders are stationary. Hence, we can rewritten the formation error as $\delta = [0, \delta_f^T]^T$, where $\delta_f = [\delta_{n_l+1}^T, \cdots, \delta_n^T]^T$. Let $\Gamma = \begin{bmatrix} 0 & 0 \\ 0 & I_{pn_f} \end{bmatrix}$, it can be obtained that

$$\delta^T \Gamma = \delta^T \tag{B.4}$$

and

$$\begin{aligned} \delta^T \mathcal{B} \delta &= \delta_f^T \mathcal{B}_{ff} \delta_f \\ &\geq \lambda_{\min}(\mathcal{B}_{ff}) \delta_f^T \delta_f \\ &= \lambda_{\min}(\mathcal{B}_{ff}) \delta^T \delta. \end{aligned} \tag{B.5}$$

Substituting the formation protocol (B.2) to the nonlinear heterogeneous MRS (B.1), then we present the compact form of (B.1) as

$$\dot{p} = -\Gamma \tilde{H}^T (a\xi + b\Psi(\xi)) + \psi(p). \tag{B.6}$$

where $\psi(p) = [0, \psi_{n_l+1}^T(p_{n_l+1}), \cdots, \psi_n^T(p_n)]^T$, and

$$\Psi(\xi) = \tilde{\psi}^2(t) \left[\frac{\xi_1^T}{\|\xi_1\|^2}, \cdots, \frac{\xi_m^T}{\|\xi_m\|^2} \right]^T.$$

Choosing the Lyapunov candidate as

$$V = \frac{1}{2} \delta^T \delta. \tag{B.7}$$

The derivation of V can be expressed as

$$\begin{aligned} \dot{V} &= \delta^T \dot{p} \\ &= -\delta^T \Gamma \tilde{H}^T (a\xi + b\Psi(\xi)) + \delta^T \psi(p) \\ &= -a\delta^T \tilde{H}^T \xi - b\delta^T \tilde{H}^T \Psi(\xi) + \delta^T \psi(p) \\ &\leq -a p^T \tilde{H}^T \xi + \Omega \\ &\leq -\frac{a\delta^T \mathcal{B} \delta}{2 \max_k \|e_k\|} + \Omega \\ &\leq -\frac{a\lambda_{\min}(\mathcal{B}_{ff})}{\max_k \|e_k\|} V + \Omega, \end{aligned} \tag{B.8}$$

where

$$\Omega = -b\delta^T \tilde{H}^T \Psi(\xi) + \delta^T \psi(p).$$

On the one hand, according to the definition of $\mathbf{s}(t)$, we can imply that

$$\begin{aligned} n^2\mathbf{s}(t)^2 &= n\sum_{k=1}^{n}\|p_k-\bar{p}\|^2 \\ &\geq (\|p_i-\bar{p}\|+\sum_{k\in\mathcal{V},k\neq i}^{n}\|p_k-\bar{p}\|)^2 \\ &\geq \|p_i-\bar{p}\|^2. \end{aligned} \tag{B.9}$$

Combining with Assumption B.2, it can be observed that

$$\begin{aligned} \|e_k\| &= \|p_i-p_j\| \\ &= \|(p_i-\bar{p})-(p_j-\bar{p})\| \\ &\leq \|p_i-\bar{p}\|+\|p_j-\bar{p}\| \\ &\leq 2n\mathbf{s}(t)\leq 2n\mathbf{s}_0\,. \end{aligned} \tag{B.10}$$

On the other hand, from Assumption B.1 and B.4, together with the average inequality, we have

$$\begin{aligned} \Omega &= -b(e-e^*)^T\Psi(\xi)+\delta^T\psi(p) \\ &= -b\sum_{k=1}^{m}\frac{e_k^Tg_k-e_k^Tg_k^*}{\|g_k-g_k^*\|^2}\tilde{\psi}^2(t)+b\sum_{k=1}^{m}\frac{e_k^{*^T}g_k-e_k^{*^T}g_k^*}{\|g_k-g_k^*\|^2}\tilde{\psi}^2(t) \\ &+\delta^T\psi(p) \\ &= -b\sum_{k=1}^{m}\frac{\|e_k\|(1-g_k^Tg_k^*)}{\|g_k-g_k^*\|^2}\tilde{\psi}^2(t)+b\sum_{k=1}^{m}\frac{\|e_k^*\|(g_k^Tg_k^*-1)}{\|g_k-g_k^*\|^2}\tilde{\psi}^2(t) \\ &+\delta^T\psi(p) \\ &\leq -b\sum_{k=1}^{m}\frac{\|e_k\|}{2}\tilde{\psi}^2(t)+\delta^T\psi(p) \\ &\leq -b\sum_{k=1}^{m}\frac{\|e_k\|}{2}\tilde{\psi}^2(t)+\frac{n}{2bm\sigma}\delta^Te+\frac{bm\sigma}{2n}\|\psi(p)\|^2 \\ &\leq \frac{n}{2bm\sigma}\delta^T\delta-b\sum_{k=1}^{m}\frac{\|e_k\|-\sigma}{2}\tilde{\psi}^2(t)\leq\frac{n}{bm\sigma}V. \end{aligned} \tag{B.11}$$

Substituting (B.10) and (B.11) into (B.8), from (B.3), we have

$$\dot{V}\leq-\tilde{a}V<0, \tag{B.12}$$

where

$$\tilde{a}=\frac{abm\sigma\lambda_{\min}(\mathcal{B}_{ff})-2n^2\mathbf{s}_0}{2bmn\sigma\mathbf{s}_0}>0.$$

That is to say, the formation error will converge to zero exponentially under the control strategy (B.2) with the exponential convergence rate equal to $\tilde{a}$. This completes the proof. □

B.3.2 Convergence Analysis for Moving Leaders

In this section, the performance of the proposed controller (B.2) is considered if the leaders are not fixed. Suppose the trajectories of the leaders are described as $\dot{p}_i = v(t),\ \forall i \in \mathcal{V}_l$, where $v(t)$ is the velocities of each leader which is bounded, i.e., $\|v\| \leq \tilde{v}$, where $\tilde{v}$ is a known positive constant. Then, it is easily to find that $\dot{p}_i^* = v,\ \forall i \in V$ [112]. The stability analysis of the proposed controller under moving leaders is shown in the following theorem

Theorem B.2. *Under Assumption B.1-B.4, the formation error of the nonlinear heterogeneous MRS* (B.1) *converges to the bounded set*

$$\mathcal{S} = \left\{ \delta : \|\delta\|^2 \leq \frac{4b^2m^2\sigma^2\tilde{v}^2}{n} \right\}.$$

for the moving leaders with the velocity v by implementing the controller (B.2) *if the control gains a and b are selected to satisfy*

$$ab > \frac{4n^2\boldsymbol{s}_0}{m\sigma\lambda_{min}(\mathcal{B}_{ff})}. \tag{B.13}$$

Proof. Selecting the Lyapunov function as (B.7), similar to the analysis in Theorem B.1, we can get

$$\begin{aligned} \dot{V} &= \delta^T(\dot{p} - \mathbf{1}_n \otimes v) \\ &\leq -\frac{a\lambda_{\min}(\mathcal{B}_{ff})}{\max_k \|e_k\|}V + \Omega - \delta^T v \\ &\leq -\tilde{a}V - \delta^T v \\ &\leq -\frac{n}{bm\sigma}V - \delta^T v, \end{aligned} \tag{B.14}$$

where the last inequity of (B.14) can be obtained from (B.13).

From average inequality, we have

$$\begin{aligned} -\delta^T(\mathbf{1}_n \otimes v) &\leq \frac{n}{4bm\sigma}\|\delta\|^2 + \frac{bm\sigma}{n}\|\mathbf{1}_n \otimes v\|^2 \\ &= \frac{n}{2bm\sigma}V + bm\sigma\|v\|^2 \\ &\leq \frac{n}{2bm\sigma}V + bm\sigma\tilde{v}^2. \end{aligned} \tag{B.15}$$

Combining (B.14) and (B.15), we can get

$$\dot{V} \leq -\frac{n}{2bm\sigma}V + bm\sigma\tilde{v}^2. \tag{B.16}$$

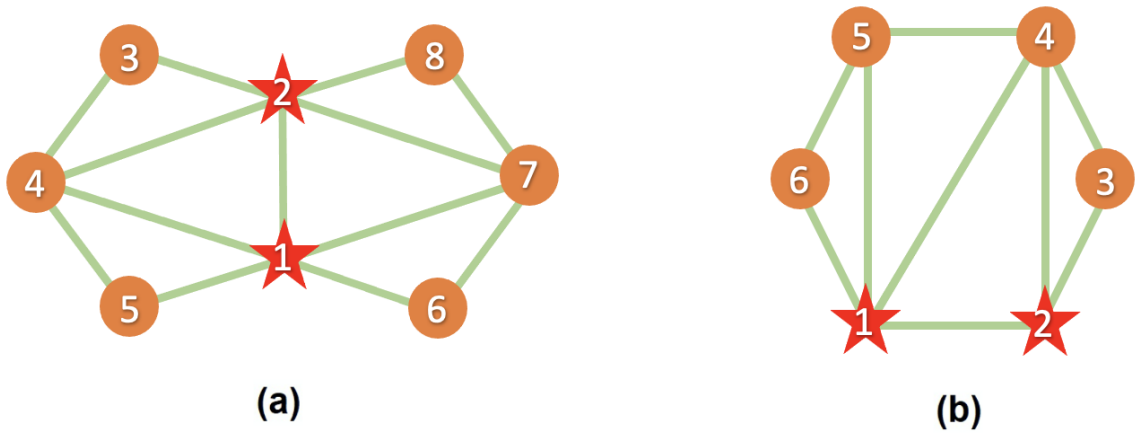

Figure B.1: Interaction topology of the MRS for (a) Case 1: Fixed leaders, and (b) Case 2: Moving leaders.

Define the bounded set $\mathcal{S}$ as

$$\mathcal{S} = \left\{ \delta : \|\delta\|^2 \leq \frac{4b^2 m^2 \sigma^2 \tilde{v}^2}{n} \right\}.$$

Denote $\bar{\mathcal{S}}$ as supplementary set of $\mathcal{S}$. if $e \in \bar{\mathcal{S}}$, it can be observed that

$$\dot{V} \leq 0. \tag{B.17}$$

That is to say, when $t \to \infty$, it holds that

$$\|e\|^2 \leq \frac{4b^2 m^2 \sigma^2 \tilde{v}^2}{n} \tag{B.18}$$

Hence, the formation tracking error will converge to the bounded set $\mathcal{S}$. This completes the proof. □

B.4 Simulation Results

In this section, the simulation case studies are presented to verify the theoretical results for both fixed and moving leaders.

B.4.1 Case Study on Fixed Leaders

We first design the simulation to validate the proposed bearing-only formation protocol (B.2) on fixed leaders. Eight mobile robots, with two leaders and six followers, are applied to this case study. The interaction topology among the robots is appeared in

Fig. B.1 (a). The leaders are represented by two red stars labelled 1 and 2, and the followers are denoted by six orange circles labelled from 3 to 8. The communications between each robot are denoted by green solid lines. These robots aim to attain a target formation as two pentagons together in 2D space. In robot dynamics, the nonlinear function for the ith follower robot is defined as

$$\psi_i(p_i(t)) = \begin{bmatrix} \frac{0.5\sin(ip_{i1}(t))}{t+1} \\ \frac{0.5\sin(ip_{i2}(t))}{t+1} \end{bmatrix}, \ i \in \mathcal{V}_f, \tag{B.19}$$

where $p_i(t) = [p_{i1}(t), p_{i2}(t)]^T$. It is easy to find that $\|\psi_i(p_i(t))\| \leq 1/(t+1)$, which satisfies Assumption 1. The MRS is heterogeneous since $\psi_i(p_i(t))$ is different for each follower. According to the condition in Theorem B.1, we select the control gains as $a = 10$, and $b = 2$.

By implementing the bearing-only controller (B.2), the trajectories of the follower robots are elucidated in Fig. B.2. We set the positions of the leaders (represented by two red stars) as $(3, 0)$ and $(6, 0)$. The initial states of the followers (represented by six circles with different colours) are chosen as $(15.9, 2)$, $(10, 2)$, $(-5, 1)$, $(-5.9, 3)$, $(4, -9)$, and $(14, -8)$. It can be observed that all the robots are able to form the target formation under the proposed protocol. Fig. B.3 reveals the time variation of the formation errors. We can conclude that all the formation errors of the followers will converge to zero during the formation task. Based on these results, the bearing-only formation task can be accomplished by the proposed strategy (B.2).

B.4.2 Case Study on Moving Leaders

In this section, we further verify the performance of the proposed protocol for moving leaders. Six robots, with two leaders and four followers, are used in this task. Fig. B.1 (b) displays the interaction topology between each robot. The velocities of the leaders are set as

$$\dot{p}_i(t) = \begin{bmatrix} 0.1 \\ 0.1\sin(\frac{\pi}{80}t) + 0.01\cos^5(\frac{\pi}{50}t) \end{bmatrix}, \quad i \in \mathcal{V}_l, \tag{B.20}$$

where $\mathcal{V}_l = \{1, 2\}$. The nonlinear function $\psi_i(p_i(t))$ is chosen as (B.19). The control gains are set as $a = 15$, and $b = 1$, which satisfy the condition in Theorem B.2.

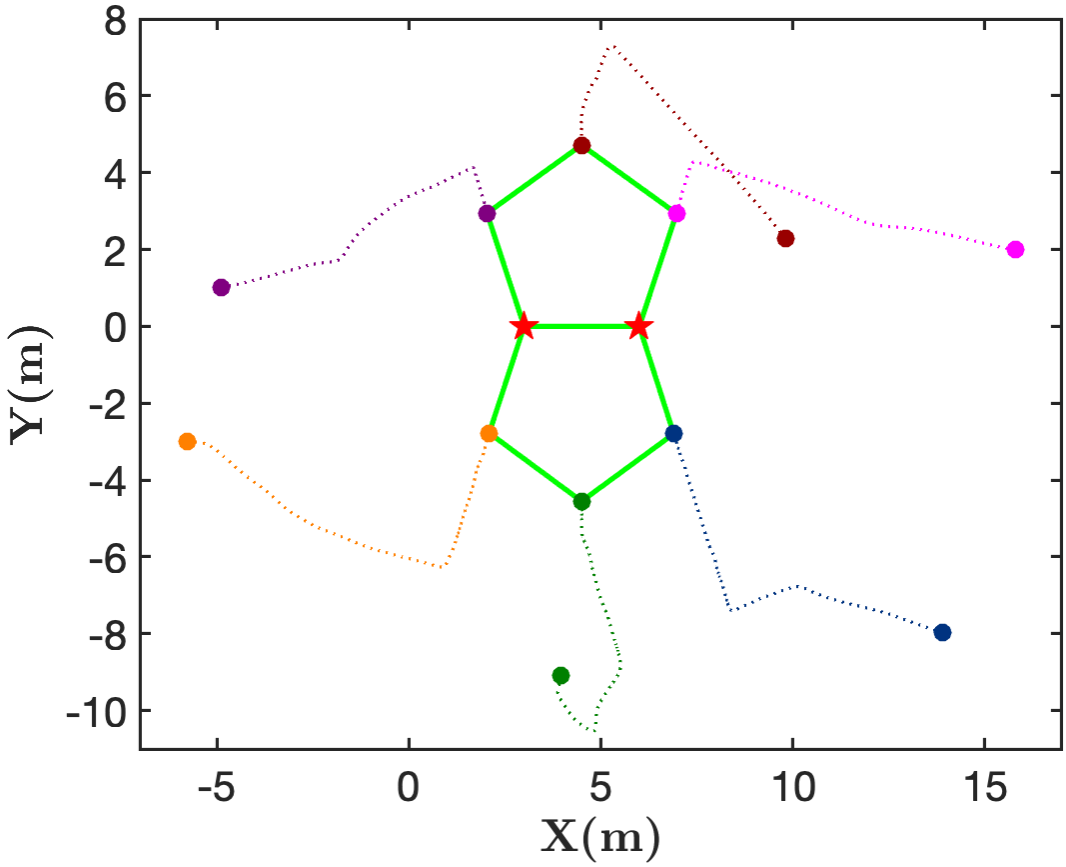

Figure B.2: Trajectories of the followers for fixed leaders (labelled by red stars).

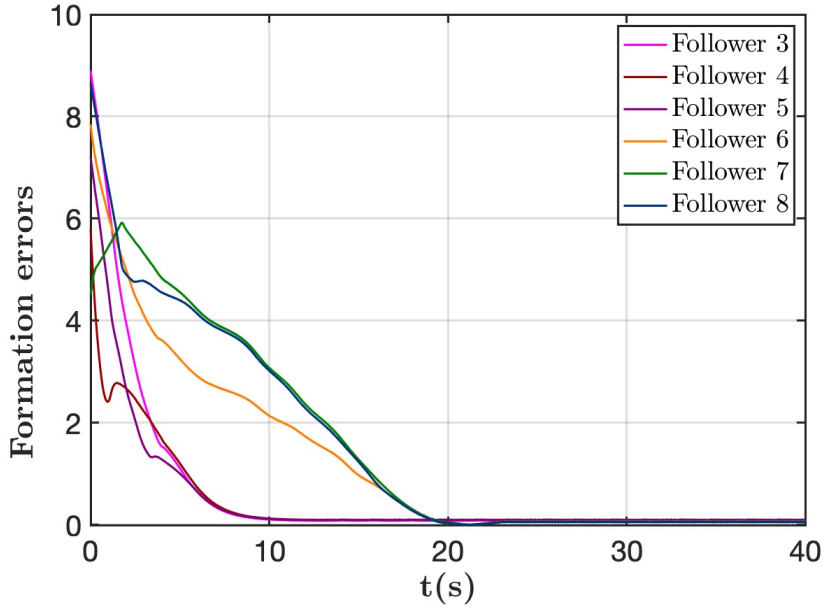

Figure B.3: Formation errors of the followers for fixed leaders.

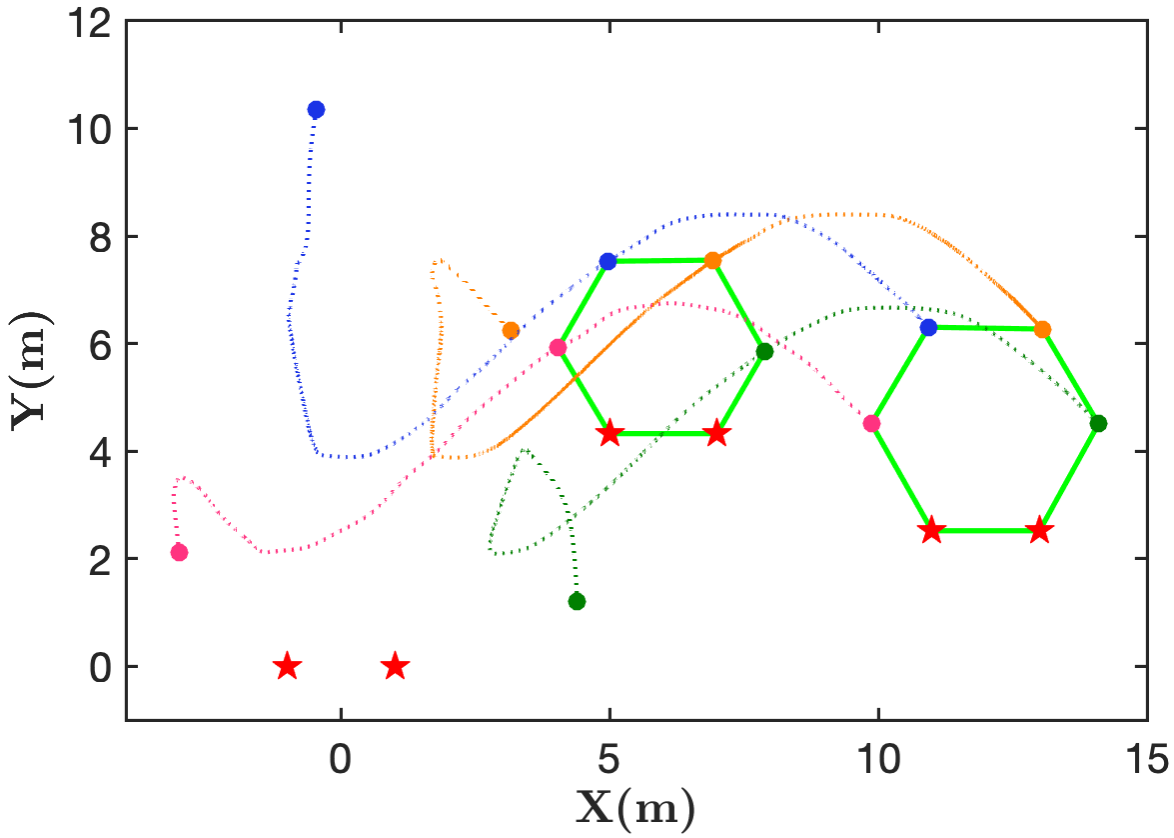

Figure B.4: Trajectories of the followers for moving leaders (labelled by red stars).

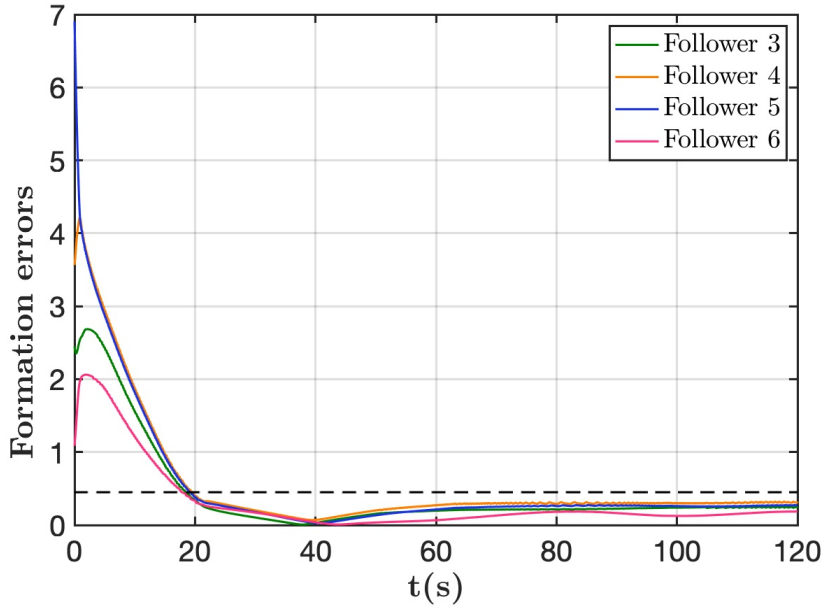

Figure B.5: Formation errors of the followers for moving leaders.

We select the initial positions of the leaders as $(-1, 0)$ and $(1, 0)$. Fig. B.4 demonstrates the movement of each robot under the controller (B.2). Two red stars denote the moving leaders. The trajectories of the followers are represented by four dash lines with various colours. From Fig. B.5, we can obtain that all the formation errors of the followers will converge to a bounded set (the boundary is denoted by a black dashed line). To sum up, the formation error can be guaranteed in a bounded set by implementing the proposed bearing-only formation protocol, which validates the feasibility of the theoretical result.

B.5 Summary

In this chapter, the bearing-only formation tracking problem is addressed for heterogeneous nonlinear MRS. We propose a novel formation protocol for the follower robots based on bearing measurements to form the desired formation configuration. A compensation term is included in the controller to deal with the unknown nonlinear items in the system. By using the Lyapunov method, the formation tracking error will converge to zero exponentially under the proposed bearing-only algorithm. Furthermore, we extend the stability analysis of the proposed strategy on moving leaders, and the formation tracking error is able to be guaranteed in a bounded set. Simulation case studies are provided to verify the effectiveness of the theoretical results. In the next chapter, we will move on formation-containment problem with different types of robots.